

Study of the sensitivity of UAP forecasts to meteorological input

Deliverable 6.2 Integrated Systems for Forecasting Urban Air Pollution and Population Exposure (FUMAPEX)

Viel Ødegaard (ed.)¹⁾, Alessio D'Allura³⁾, Alexander Baklanov⁶⁾, J. Jaime Diéguez⁵⁾, Barbara Fay²⁾, Sandro Finardi³⁾, Hubert Glaab²⁾, Steen C. Hoe⁷⁾, Millán Millán⁵⁾, Alexander Mahura^{6,8)}, Lina Neunhäuserer²⁾, Jose Luis Palau⁵⁾, Gorka Perez⁵⁾, Leiv Håvard Slørdal⁴⁾, Ariel Stein⁵⁾, Jens Havskov Sørensen⁶⁾

1) Research and Development Department,
Norwegian Meteorological Institute,
PO Box 43, Blindern
N-0313 Oslo, Norway

2) German Weather Service (DWD)

3) ARIANET Consulting

4) Norwegian Institute for Air Research (NILU)

5) Centro De Estudios Ambientales Del Mediterraneo (CEAM)

6) Danish Meteorological Institute (DMI)

7) Danish Emergency Management Agency (DEMA)

8) Ecole Centrale de Nantes (ECN)

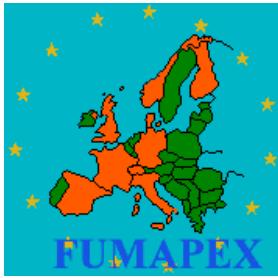


Title Study of the sensitivity of UAP forecasts to meteorological input	Date August 22 nd 2005
Section Meteorology	Report no. 13/2005
Author(s) Viel Ødegaard (ed.), Alessio D'Allura, Alexander Baklanov, J. Jaime Diéguez, Barbara Fay, Sandro Finardi, Hubert Glaab, Steen C. Hoe, Millán Millán, Alexander Mahura, Lina Neunhäuserer, Jose Luis Palau, Gorka Perez, Leiv Håvard Slørdal, Ariel Stein, Jens Havskov Sørensen	Classification <input checked="" type="checkbox"/> Free <input type="checkbox"/> Restricted
	ISSN 1503-8025
Client(s) European Commission FP5 EESD programme Key Action City of Tomorrow	e-ISSN 1503-8025
Client's reference EVK4-CT-2002-00097	
Abstract NWP models are increasingly used as providers of meteorological data for urban air quality (UAQ) models. UAQ forecasts are used as a decision making tool for local authorities. The near-surface wind and temperature fields are the main forcing of UAP models, directly and indirectly in defining the turbulence regime and parameters. Attempts to improve the input of temperature, wind and turbulence parameters in the boundary layer are evaluated in terms of their effect on the UAP forecasts. The sensitivity of the UAQ forecasts to NWP model horizontal resolution is examined in the simulations of the FUMAPEX target cities Turin, Valencia, Oslo, Helsinki and Copenhagen. The studies show that increasing the horizontal resolution of the NWP model leads to sharper gradients and more extreme values in wind speed. In complex terrain the increased horizontal resolution also increases the vertical velocity along the terrain following model layers and might lead to break up of inversions. The effect of increasing the vertical resolution of the model, near-surface conditions, the physiographic description of urban areas (roughness, albedo, emissivity, soil moisture and heat capacity) and anthropogenic heat source into a NWP model shown to increase the mechanical and the thermal turbulence respectively. Choice of parameterization schemes for the planetary boundary layer shows only limited impact on the error level in strong wintertime inversion. The deterioration of the forecasts due to the forecasts length required to initiate actions in urban areas is shown to be insignificant compared to other sources of error.	
Keywords high resolution NWP, urban meteorology, urban air pollution (UAP), air quality (AQ) modelling	

Disiplinary signature	Responsible signature
_____	_____

TABLE OF CONTENT

1.	Introduction.....	2
2.	Target city Turin.....	4
2.1	Description of the verification period (July 19 th - 23 rd 1999 ozone episode).....	5
2.2	Sensitivity to horizontal resolution of NWP and UAQ models.....	7
2.3	Sensitivity to forecast length.....	12
3.	Target area Castellón - UAQ forecast.....	19
3.1	Sensitivity to horizontal resolution in NWP and UAQ models.....	25
3.2	Sensitivity to forecast length.....	32
4.	Target area Castellón - trajectory model simulations.....	33
4.1	Sensitivity to vertical and horizontal resolution in NWP model.....	34
4.2	Sensitivity to forecast length.....	37
5.	Target city Oslo - UAQIFS experiments.....	39
5.1	Vertical resolution.....	43
5.2	Forecast length.....	46
5.3	Planetary boundary layer parameterizations.....	50
5.4	Conclusion.....	54
6.	Target city Oslo - trajectory model simulations.....	55
6.1	Sensitivity of LM trajectories to horizontal and vertical resolution in LM.....	55
6.2	Sensitivity of Lagrangian Particle Dispersion Model (LPDM) to horizontal and vertical resolution in LM.....	57
7.	Target city Helsinki - trajectory model simulations.....	64
7.1	Sensitivity of trajectories to horizontal and vertical resolution in LM.....	64
7.2	Sensitivity of trajectories surface data and land surface parameterizations.....	65
7.3	Sensitivity of LPDM to surface data and land surface parameterizations.....	67
8.	Target city Copenhagen - emergency model simulations.....	72
8.1	Sensitivity to the DMI-HIRLAM resolution.....	72
8.2	Sensitivity to forecast duration.....	75
8.3	Sensitivity to urban features.....	78
8.4	Sensitivity of dispersion models (DERMA and ARGOS) to meteorological input....	80
8.5	Evaluation of land surface scheme modifications on atmospheric transport and deposition patterns in Copenhagen metropolitan area.....	90
9.	Summary and Conclusions.....	91
9.1	Summary horizontal resolution experiments.....	91
9.2	Summary vertical resolution experiments.....	92
9.3	Summary forecast length experiments.....	92
9.4	Summary planetary boundary layer parameterization experiments.....	93
9.5	Summary surface data and land surface parameterization experiments.....	93
9.6	Conclusions.....	93
	References.....	97



FUMAPEX

**Integrated Systems for Forecasting Urban Meteorology,
Air Pollution and Population Exposure**

Study of the sensitivity of UAP forecasts to meteorological input

Viel Ødegaard (ed.)¹⁾, Alessio D'Allura³⁾, Alexander Baklanov⁶⁾, J. Jaime Diéguez⁵⁾, Barbara Fay²⁾, Sandro Finardi³⁾, Hubert Glaab²⁾, Steen C. Hoe⁷⁾, Millán Millán⁵⁾, Alexander Mahura^{6,8)}, Lina Neunhäuserer²⁾, Jose Luis Palau⁵⁾, Gorka Perez⁵⁾, Leiv Håvard Slørdal⁴⁾, Ariel Stein⁵⁾, Jens Havskov Sørensen⁶⁾

1) Research and Development Department,
Norwegian Meteorological Institute,
PO Box 43, Blindern
N-0313 Oslo, Norway

2) German Weather Service (DWD)

3) ARIANET Consulting

4) Norwegian Institute for Air Research (NILU)

5) Centro De Estudios Ambientales Del Mediterraneo (CEAM)

6) Danish Meteorological Institute (DMI)

7) Danish Emergency Management Agency (DEMA)

8) Ecole Centrale de Nantes (ECN)

WP6: Evaluation of the sensitivity of urban air quality forecasts to uncertainties in the meteorological input.

Deliverable 6.2, May 2005

1. INTRODUCTION

NWP models are increasingly used as providers of meteorological data for urban air quality (UAQ) models. As these kinds of models have developed along separate lines the efforts to bring them together face challenges on several fields. The NWP models provide meteorological descriptions of the planetary boundary layer on an increasingly higher resolution and more sophisticated parameterizations of the turbulent transport. However most operational NWP models still have coarse resolution compared to the variation in the urban air quality fields. Also the particular urban features remain to be described in most models (Baklanov et al., 2002).

The near-surface wind and temperature fields are the main forcing of UAP models, directly and indirectly in defining the turbulence regime and parameters. Attempts to improve the input of temperature, wind and turbulence parameters in the boundary layer are for a number of models and cases evaluated in terms of their effect on the UAP forecasts. The meteorological parameters in use in UAQ models within FUMAPEX are documented by Sokhi et al. (2003) in FUMAPEX D2.1-2.2.

The UAQ fields have a horizontal structure that is significantly more detailed than the resolution of most operational NWP models. Thus the problem of forecasting of UAQ is partly a problem of scale. The sensitivity of the UAQ forecasts to NWP model horizontal resolution is examined in the simulations of the FUMAPEX target cities Turin, Valencia, Oslo, Helsinki and Copenhagen, and described in section 2.1, 3.1, 4.1, 6.1, 6.2, 7.1 and 8.1.

Over the whole of Europe, low wind speeds and stable atmospheric stratification cause pollution episodes. Stable atmospheric conditions mean that temperature gradients can be very strong near the surface, and can only be resolved with a high vertical resolution of the NWP models. The effect of increasing the vertical resolution of the model is studied in the simulations of FUMAPEX target cities Valencia, Oslo and Helsinki and described in sections 5.1 and 7.1.

The near-surface conditions in the NWP models are to some extent varying with the choice of planetary boundary layer (PBL) parameterization scheme. The challenges of modelling the meteorological conditions are however dependent on the physical properties of the urban area in question. Episodes in Nordic winter time inversion, complex orography or Southern European heat islands all have their particular boundary layer problems (Berge et al. 2000, Kukkonen et al., Millán et al. 1997, 2000). The schemes typically calculate the vertical heat profile and the Richardson number, and determine the stability regime on the basis of this. Vertical exchange coefficients for heat, moisture and momentum, turbulence length scales and diagnosis of 2m temperature and 10m winds are further results of the parameterization schemes. The results from tests with three different schemes and a modification to one of them are shown in section 5.3.

Urban areas are relative small compared to the domains of synoptic scale models. However in mesoscale models used in UAQIFS a large part of the area might be of the urban type. The physiographic description of urban areas is usually limited for NWP purposes, both in terms of resolution and in terms of surface parameters like roughness, albedo, emissivity, soil moisture and heat capacity. Urbanised external parameters as well as an anthropogenic heat source into a NWP model are investigated in a sensitivity study for target cities Helsinki and Copenhagen in sections 7.2, 7.3 and 8.3.

The UAQ forecasts are intended to be used as a decision making tool for local authorities in order to reduce the pollution levels or protect the population of the cities against high

pollution levels. However human processes in urban areas are heavy to manage. For the present about 24 hours is required to implement actions like limitations on road traffic. There is a question of how much is lost in forecast quality by using longer range forecasts compared to the shortest ranges. The results presented in sections 2.2, 3.2, 4.2, 5.2 and 8.2 for the target cities Turin, Castellon, Oslo and Copenhagen respectively, shed light on this issue.

2. TARGET CITY TURIN

The UAQIFS that is being built in Torino (Slørddal, 2003) is based on the meteorological model RAMS (Regional Atmospheric Modelling System) Version 4.4 (Pielke et al., 1992; Cotton et al., 2003) and on the chemical transport model FARM (Calori and Silibello, 2004). RAMS is a prognostic, non-hydrostatic model with a sigma terrain following coordinate system (also called z^*) and an Arakawa-C horizontal grid. FARM is an Eulerian model that accounts for transport and diffusion, transformation of chemical species by gas- and aerosol-phase chemistry, dry and wet removal of atmospheric pollutants. FARM model can be configured with the different gas-phase chemical mechanisms: SAPRC-90 is being used for the described application. The cited meteorological and air quality models are connected by the interface module GAP/SurfPRO (Calori et al., 2005; Finardi, 2005) for the estimation of atmospheric turbulence and dispersion parameters.

The forecasting modelling system configuration is based on three nested domains, to describe atmospheric motions, sources influence and air pollution processes at all the different scales potentially affecting the target urban area: a “background” domain (1088x1088 km² with 16 km horizontal resolution) devoted to optimise the connection with the larger scale driving meteorological model and to describe long range influence of pollutant sources located outside the target domains (Figure 2.1), a regional domain, including all Piemonte Region (208x272 km² with 4 km resolution) and a metropolitan domain, focused on the city of Turin (52x52 km² with 1 km resolution). This multi-scale modelling approach, applied to both meteorological and air quality models, should allow describing air pollution processes dominated by scales larger than the city scale, like photochemical smog. Moreover, due to the peculiar geographic location of Torino city, at the western limit of the Po river valley, clustered between the Alps and a hilly region, a proper meteorological downscaling is important to obtain a reliable description of local and urban scale meteorology.

Boundary and initial values for the meteorological model RAMS are built from ECMWF forecasts and ECMWF soil temperature and humidity analysis with 0.5 degrees space resolution and 6 hours time resolution. The boundary conditions for the air quality model have been obtained by EMEP simulation fields, while initial concentration fields have been built by objective analysis of EMEP background fields and local observations over Piemonte Region.

The emissions for the three nested domains are prepared from different inventories: the high-resolution Piemonte and Lombardia Regions inventories, the Italian national inventory and the European scale EMEP inventory. Hourly emission rates of the desired species are then estimated through the use of a pre-processing system allowing a flexible space disaggregation, time modulation and non-methanic hydrocarbon (NMVOC) speciation of inventory data related to point, line and area sources.

The geographic data used are GTOPO30 30” DTM and USGS GLCC 30” (Grid 1) + CORINE 250m Land Cover (Grid 2-3). CORINE data are necessary to describe local surface features that are very roughly represented by GLCC class distribution. Higher resolution topographic data (5”x7.5” \approx 250m) are available over Italy but they were not used because GTOPO30 has a resolution very similar to the target resolution (1 km) and contains sufficient topographic details.

The forecasting system simulations have been extended for 72 hours to emulate operational conditions.

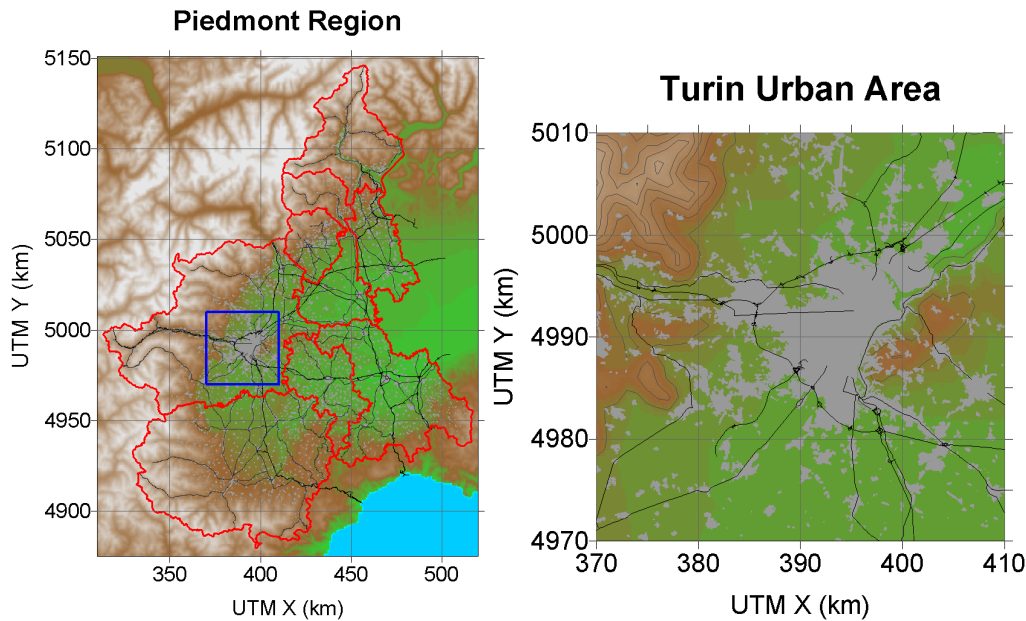


Figure 2.1 Torino UAQIFS computational domains

2.1. Description of the verification period (July 19th –23rd 1999 ozone episode)

Air Quality conditions

The chosen verification period is a photochemical pollution episode occurred during July 1999 (19-23/07/1999), when exceedance of the O₃ hourly concentration limit 180 µg/m³ have been recorded in some monitoring stations of the Torino urban area network (Figure 2.2). During this period 43 cases of exceedance for O₃ were recorded, representing 8% of all the exceedance recorded in the six considered stations during the whole year.

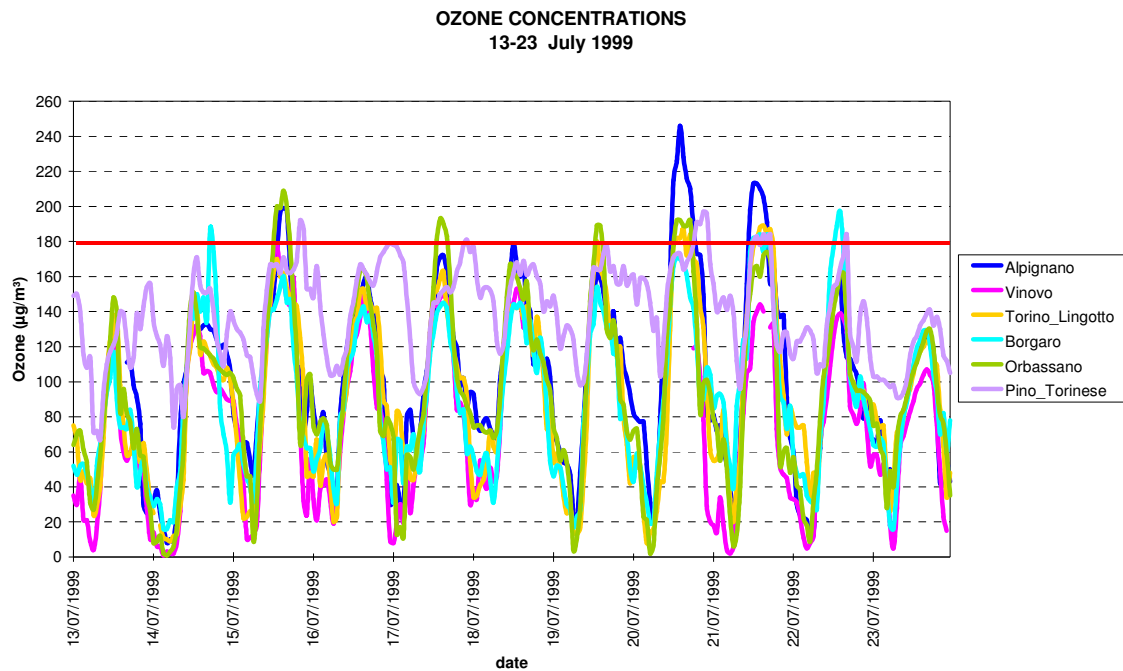


Figure 2.2 Ozone concentrations measured by the monitoring stations of the Torino urban area network during July 1999.

Mesoscale and local circulation

During the period July 19th – 22nd 1999, in the Mediterranean area the synoptic and meso-scale meteorology is dominated by a high pressure ridge (Figure 2.3) which favours weak horizontal pressure gradients and weak wind conditions (Figure 2.4). The weather is fair and surface temperature is increasing over the period, reaching maximum values over 30°C (D1.2, Valkama and Kukkonen, 2003). The described condition lasts until June 23rd, when a through moving over northern Europe influences the sub-alpine and Mediterranean regions. The surface wind speed remains low until July 21st while an increase is observed on July 22nd when katabatic wind reaches Turin metropolitan area during the afternoon, causing a quick drop of relative humidity (Figure 2.4).

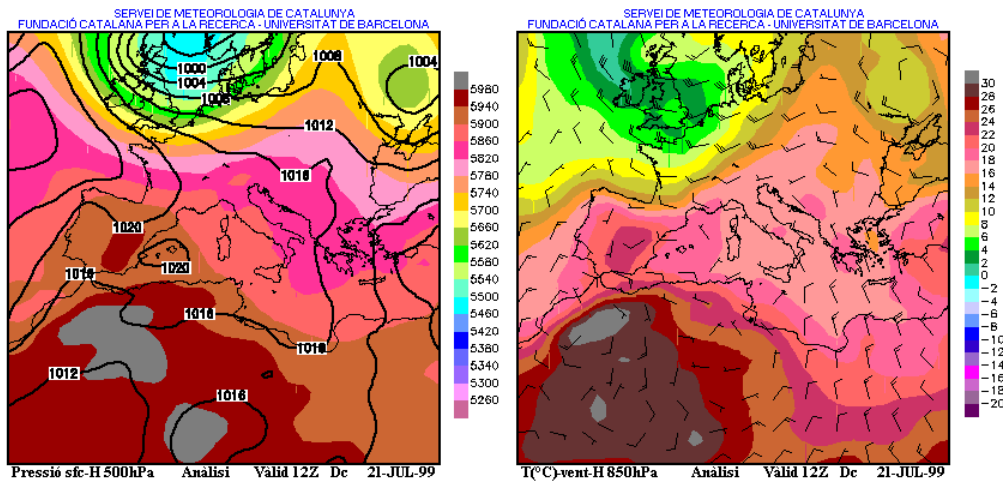
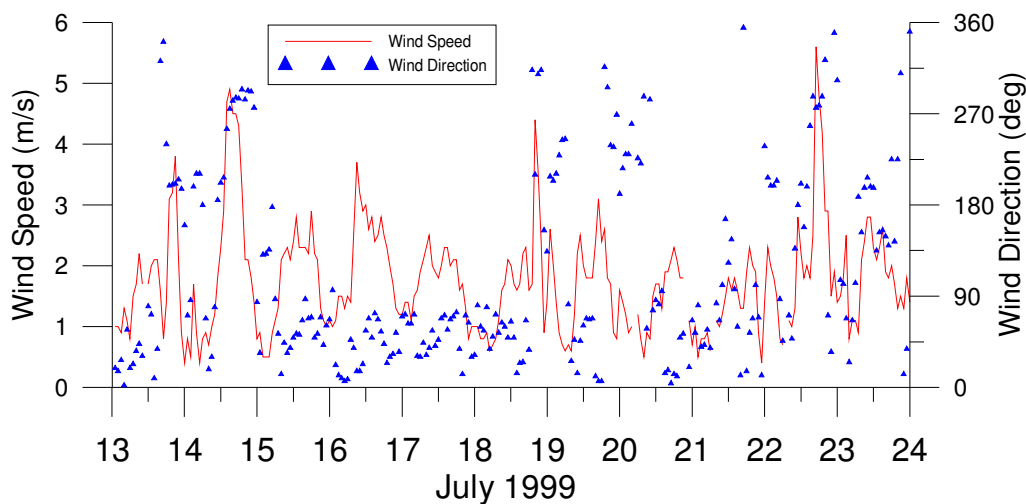


Figure 2.3 Meteorological analysis charts for July 21st, 1999 (Surface pressure and 500 hPa level, left, and temperature and wind vectors at 850 hPa level, right)



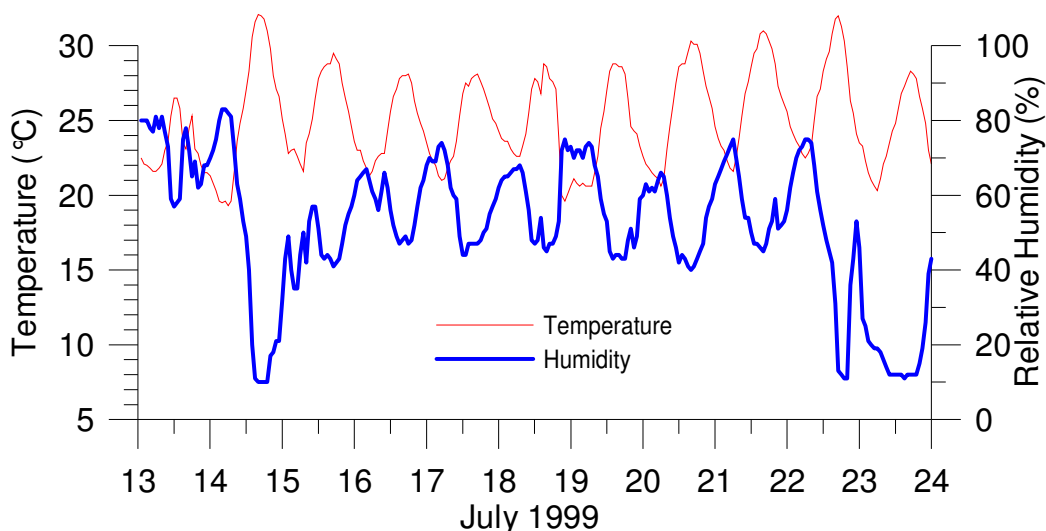


Figure 2.4 Observations from the urban meteorological station of Torino-Consolata.

2.2. Sensitivity to horizontal resolution of NWP and UAQ models

Sensitivity to horizontal resolution of UAQIFS is investigated comparing results of two simulations: the first one with 3 nested grids and final resolution of 1 km, the second one with 2 nested grids and final resolution of 4 km. The different target resolution regarded the whole modelling system: space discretisation of emissions, meteorological and air quality simulations. Resulting forecasts of wind speed, temperature, humidity, NO, NO₂ and O₃ concentrations have been compared to measurements at four stations within Turin Urban Area. The meteorological variables results have been compared with the urban stations of Alenia and CSELT, located inside Torino municipality, and with the rural stations of Druento and Bauducchi, located respectively north-west and south-east of the city centre. Air quality forecasts have been verified using the Torino city urban stations of Consolata and Lingotto, and the suburban stations of Alpignano and Borgaro, located in urban environment at northern and north-western suburbs of Torino. The location of the different monitoring stations is described in Figure 2.5.

Figure 2.6 resumes in graphical form the forecast error statistics for meteorological and air quality parameters. The used statistical indexes (bias, root mean square error and standard deviation error) have been computed over the four considered stations using results of a model simulation covering 72 hours, from July 19th at 00:00 UTC to July 22nd at 00 UTC.

The 1 km run shows a slight improvement of wind speed, mostly evident on the bias values, while no significant difference is detected on temperature and humidity forecasts. The ventilation effect is thus smaller in the 1 km runs, preserving larger concentrations of pollutants. A more significant improvement can be noticed for NO and NO₂ concentrations, with a reduction of bias and a slighter improvement of rmse and stde. For O₃ the observed improvement is much more limited in its statistical significance.

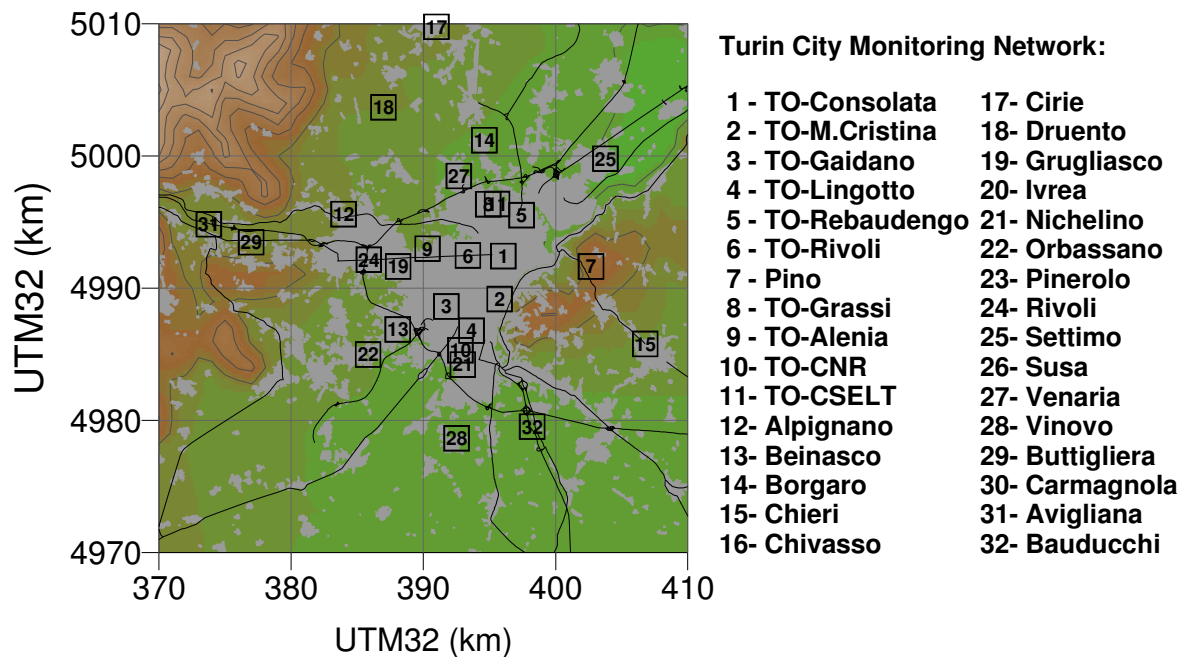


Figure 2.5 Torino urban area air quality monitoring stations location. The urbanised areas are identified by grey colour and terrain heights are depicted coloured field and isopleths (with 200 metres spacing).

The increase of space accuracy, while does not show large improvements in the error statistics of meteorological and air quality variables forecast, strongly enhances the general features of meteorological and concentration fields and shows a better description of emission patterns (Figure 2.7-8). The wind field (Figure 2.7), shows increasing flow channelling in agreement with increased topography details, with significant wind direction changes over Torino urban area. More accurate concentrations patterns for both NO_2 and O_3 are picked out increasing space resolution (Figure 2.8). Urban emission structure and major roads emissions are better recognizable and computed maximum and minimum concentration values show large differences from 4 to 1 km resolution (maximum concentrations are nearly doubled). Moreover, high resolution concentration fields show a closer agreement with the observed space distribution of concentrations depicted by local observations (Figure 2.8), confirming a better description of concentration fields variation from urban to sub-urban locations. As expected, ozone concentration fields show larger scale structure and less evident influence of small scale emission patterns. Nevertheless, the increase of space resolution causes a slight increase of O_3 maximum concentrations and the appearance of details of topographic origin on the western part of the domain (Figure 2.8), where exceedance of legislation threshold ($180 \mu\text{g}/\text{m}^3$) are forecasted at foothills downwind of the Torino urbanised area.

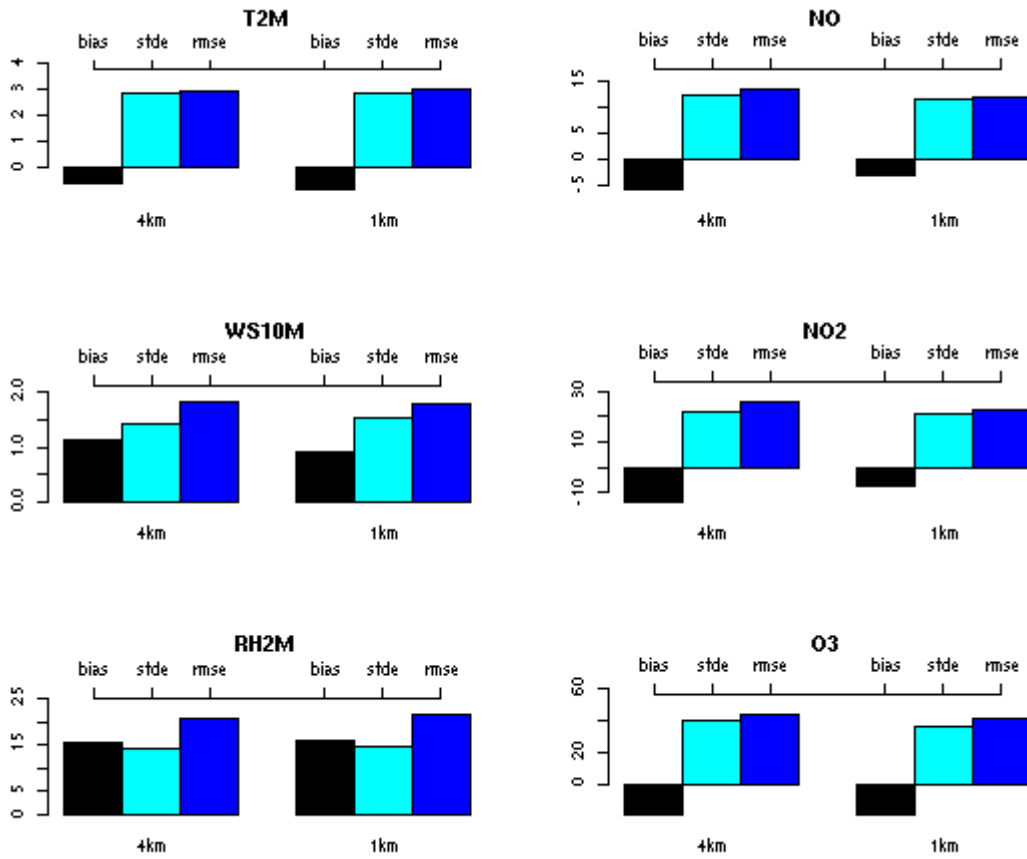


Figure 2.6 Forecast error statistics for the meteorological parameters (left) and the air quality parameters (right), comparing bias (black), standard deviation of error (light blue) and root mean square error (dark blue) in 4 km and 1 km runs.

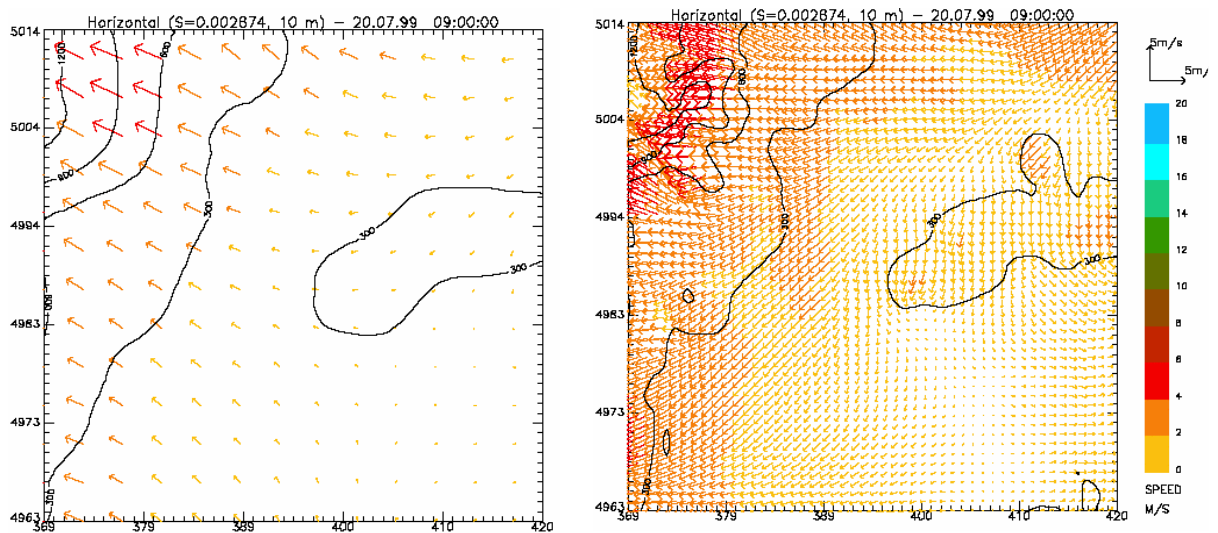


Figure 2.7 Effect of increased resolution on hourly mean wind field, from 1 km (left) to 4 km (right).

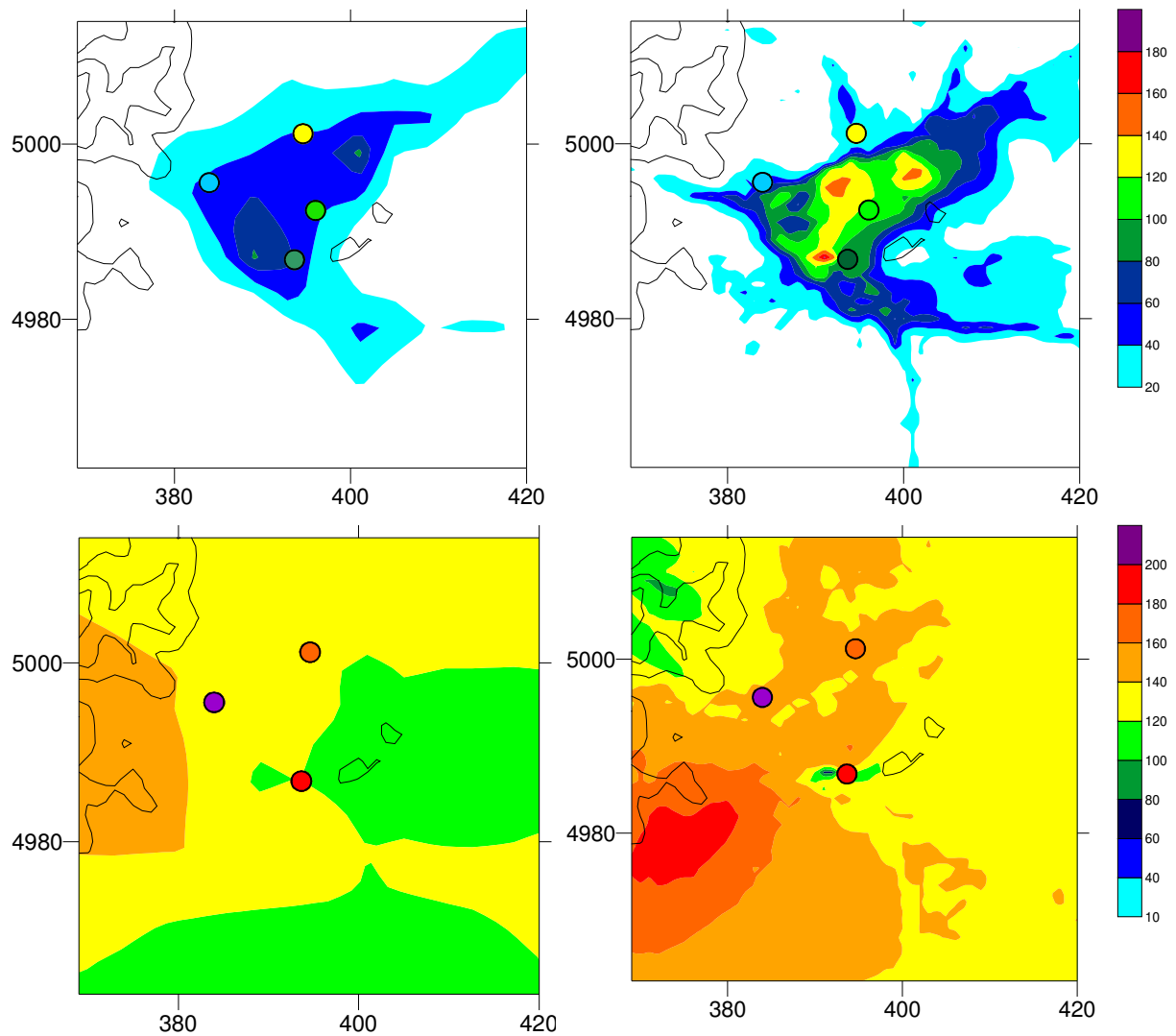


Figure 2.8 Effect of increased resolution on hourly mean concentration of NO₂ on 20/07/1999 at 09:00 (top) and O₃ on 20/07/1999 at 14:00 (bottom). The computed fields at 1 km (left) and 4 km (right) resolution are compared with observations through labels drawn on the maps.

Figure 2.9 shows the direct comparison of computed and measured values for some meteorological variables at the urban station of CSELT and at the rural station of Bauducchi. Wind results are rather satisfactory for the urban station, where wind speed time variations are reasonably well reproduced at both 4 and 1 km resolution. Wind direction forecast is improved at higher resolution especially during night time between July 19th and July 29th. No significant variation is detected on temperature and humidity behaviour enhancing space resolution. In particular we can observe an overestimation of relative humidity and a corresponding underestimation of air temperature. The model performances shows worse results for the rural station of Bauducchi, where the wind speed is overestimated and the wind direction shows larger errors than at the previously presented urban location. For temperature and humidity errors are larger during daytime and smaller during night time, when the experimental data show humidity values near saturation before dawn.

Judging this meteorological model results we have to take into account that the first RAMS computational level is located at 25 m above ground, the rural stations have wind

measurements at 10 m and temperature and humidity measurements at 2 metres, while the urban stations are located over a rooftop, at about 30 m above surface level. In very low wind conditions the position of the urban station probably better exposes it to the mesoscale flow described by model simulation, while the rural station is more influenced by local scale flow.

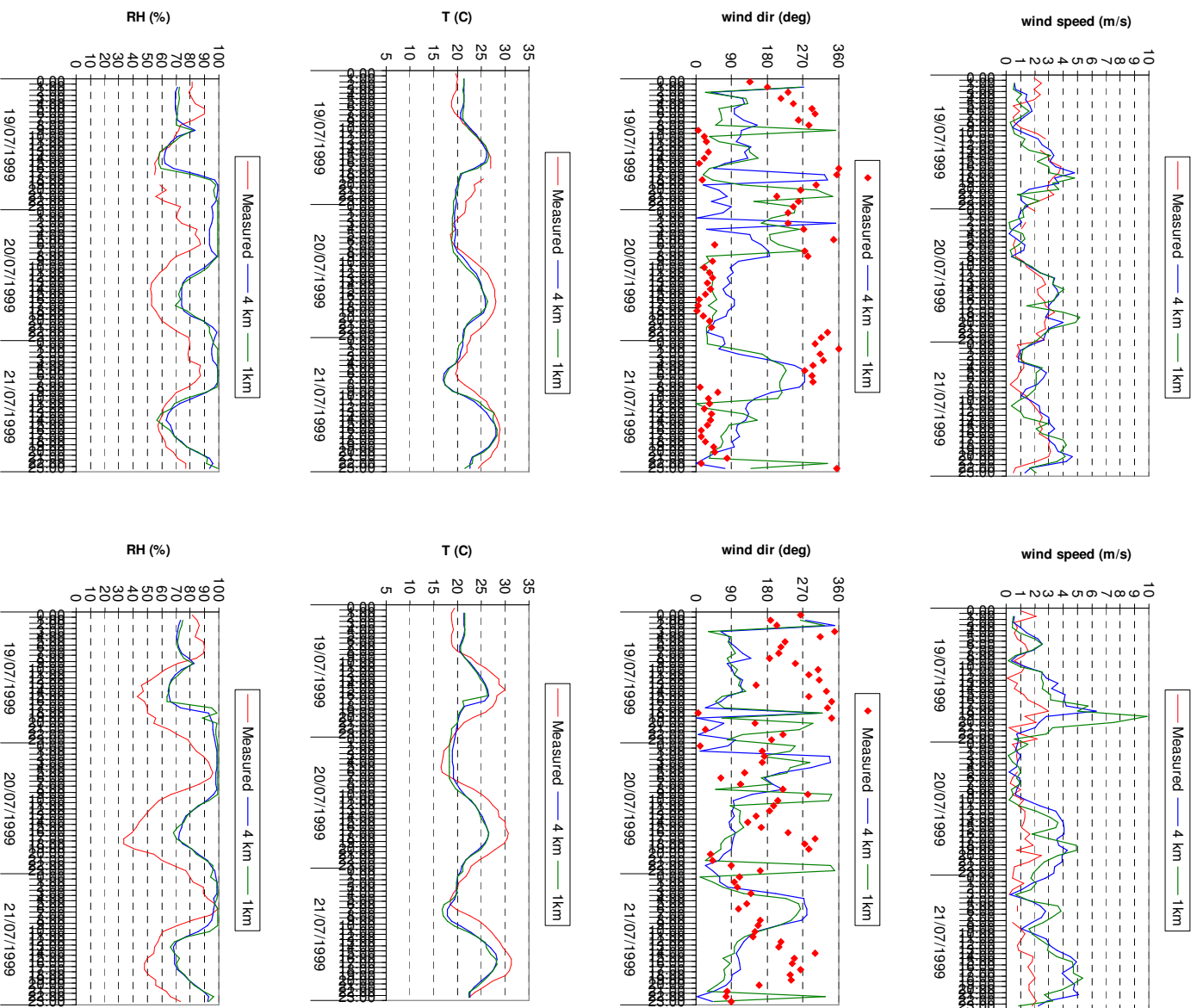


Figure 2.9 Comparison (from top to bottom) among wind speed (m/s), wind direction (deg), temperature (C) and relative humidity (%), at the urban station CSELT (left column) and rural station Bauducchi (right column).

The direct comparison of computed and measured values shows a quite good reproduction of NO_2 concentrations at both urban and sub-urban locations (Figure 2.10). Higher space resolution improves the description of morning maximum values. The larger errors in the simulation of the NO_2 peak value observed at the urban station of Lingotto during the first part of the simulation is due to the spin-up time of the dispersion simulation. Sensitivity analysis showed that initial conditions effects lasts around 12 hours for NO_x , inside model grid 3, while longer influences can be detected on O_3 concentrations under weak synoptic meteorological forcing. The effects of boundary conditions can be neglected due to the use of large scale background computational domain. O_3 concentrations are adequately described at the suburban station of Borgaro, with a slight decrease of the model performance on the third simulation day (Figure 2.10). Larger errors are observed at the urban station on Lingotto. Differently from what expected, the observed concentrations show larger values at the urban station, while the modelling system forecasts slightly larger values at the suburban location. Lingotto station is located near the minimum values of the computed concentration fields (Figure 2.8). Such anomalous concentration behaviour can hardly be described by modelling systems that can access limited resolution physiographic information and that reconstruct hourly emission on the basis of emission inventories, with disaggregation techniques. Higher resolution simulation produced slightly higher O_3 maximum values and enhanced the modelling system performance during night time and morning hours, when minimum observed values are better described.

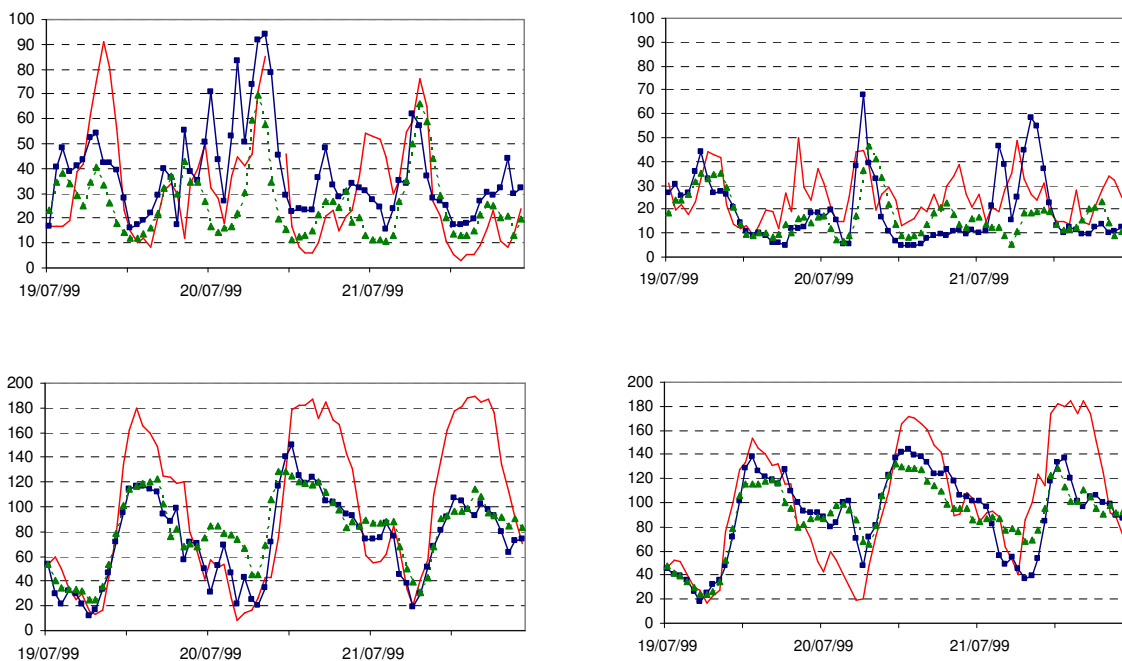


Figure 2.10 Comparison among NO_2 (top) and O_3 (bottom) observed (red solid line) and computed concentrations ($\mu\text{g}/\text{m}^3$) at 4 Km (green triangle line) and 1 Km (blue squares line) resolution, at the urban station Lingotto (left column) and suburban station Borgaro (right column).

2.3. Sensitivity to forecast length

In order to evaluate the spin-up phase of the modelling system and degradation of simulations quality with time, three simulations lasting 72 hours and starting at three consecutive days

have been performed. The focus of the experiment is to define an appropriate forecast time window for the operational application of the UAQIFS. A long lasting simulation, extending the air quality forecast to a few days, would be desirable for air quality management, but it is well known that the meteorological forecast reliability generally decays with forecast length and similar behaviour is expected from air quality forecasts. On the other hand the air pollution forecast quality strongly depends on the geographic location of the target city and on its peculiar topographic, climatologic and emission features, moreover the final choice depends on the specific application purpose (e.g. air quality management, episode forecast, or accidental releases management). A local verification is therefore necessary to define if it is advisable to set up the operational simulation system on a two days time window (from 00 to +48) or extend it to three days.

On the other hand simulations started with the same model parameterisation settings at different date give a first evaluation of the modelling chain results generality or of their dependence on particular meteorological and dispersion condition occurred.

The test simulations lasted three days starting respectively on July 19th, 20th and 21st 1999, at 00 UTC.

The statistical analysis and direct comparison of simulation results have been performed comparing both meteorological and air quality data at differently located measuring stations of the Torino Province and Piemonte Region monitoring networks. The meteorological variables have been compared with measurements taken at the urban stations of Alenia, CSELT, and Consolata, located inside Torino urban area, and at the rural station of Avigliana, located at the entrance of the Susa valley, west of Torino (Figure 2.5). The air quality data have been compared with the sub-urban stations Borgaro and Alpignano and with the urban stations Consolata, which is directly influenced by road traffic emissions, and Lingotto that is an urban background station located inside a park (Figure 2.5).

The direct comparison of computed and measured values for meteorological and chemical variables is plotted in Figures 2.11 and 2.12.

The wind speed value and time variation are better reproduced at the urban station CSELT, while a general overestimation can be observed at Avigliana. A general overestimation of surface humidity can be observed for all simulations. At the urban location humidity is overestimated and temperature underestimated during night time. At the rural station a larger daily cycle variation is observed for both temperature and humidity. At this location the nightly values of humidity and temperature are better captured by model forecasts, while overestimation of humidity minimums and underestimation of temperature maximums are observed during daytime.

From July 22nd afternoon the occurrence of a katabatic flow episode (north-westerly föhn) can be inferred from meteorological measurements, as already described in the meteorological conditions analysis in the section 2.1. The increase in wind speed is correctly forecasted at the urban station in Torino by simulation started on July 20th and 21st, with better results for the former one. The wind speed growth is instead predicted only by the simulation started on July 21st, and underestimated in its strength and duration at the valley station. The drop of relative humidity observed on July 22nd is underestimated by simulations and the only model run available from July 23rd does not describe the persistence of low humidity values. This circulation event doesn't show a clear effect on NO_x concentrations, while causes a decrease in O₃, that is predicted by the forecasting system (Figure 2.12).

The direct comparison of air quality data show rather similar results for the three considered simulations at the suburban stations of Borgaro, while differences are noticeable especially for

NO_x concentrations at the urban station of Lingotto between the simulation started on July 21st and the previous two simulations

If we exclude the spin-up phase, the differences among simulations started at different days seem limited and decay with time of model performances is not clearly detectable from direct comparison of both meteorological and air quality data. Even for the last 24 hours of simulations no significant degradation is picked out and model results are comparable with those obtained for previous time windows (0 - +24 and +24 - +48).

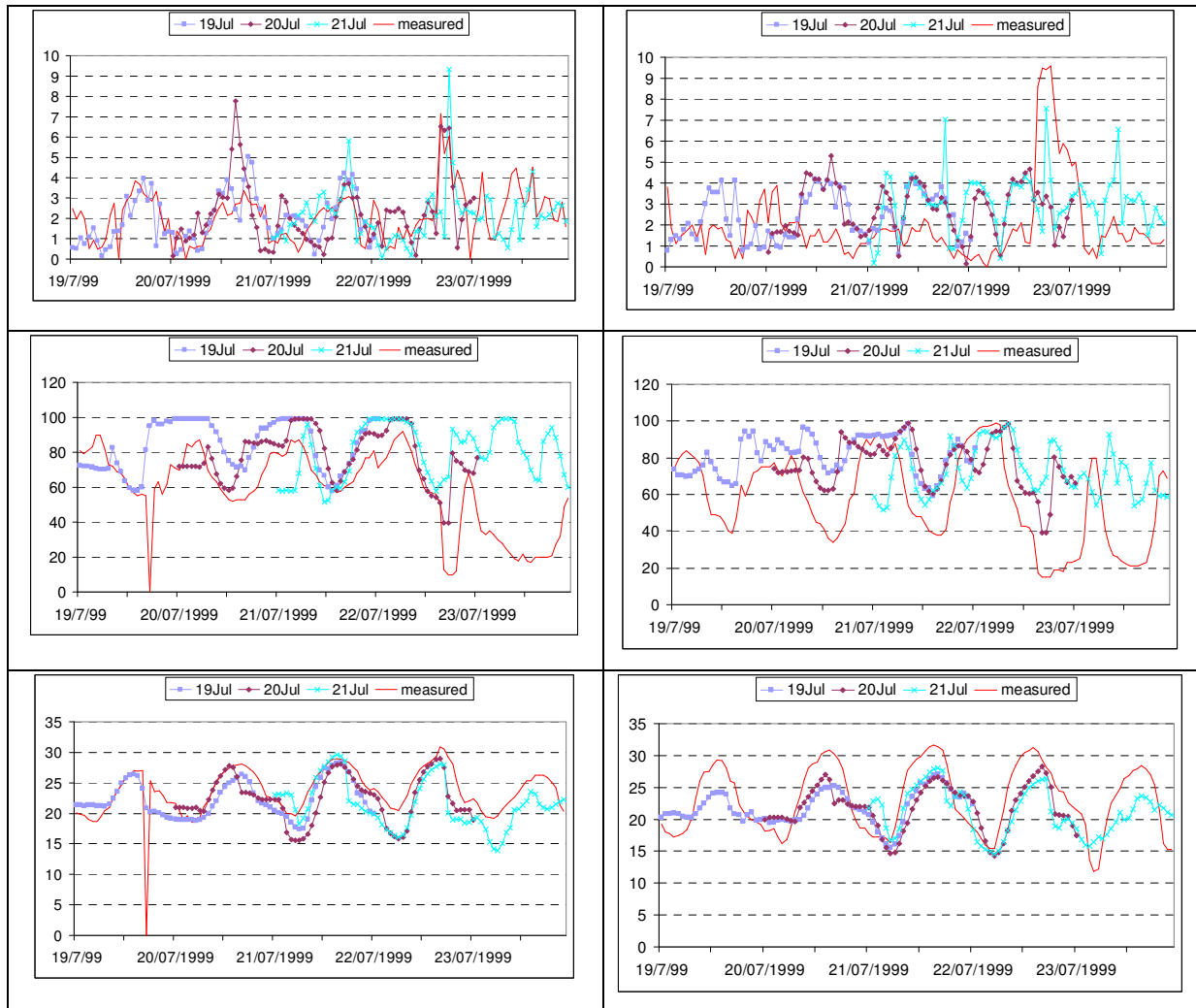


Figure 2.11 Comparison (from top to bottom) among wind speed (m/s), relative humidity (%) and temperature (°C), at the urban station CSELT (left column) and at the rural station of Avigliana (right column).

The analysis of the computed concentrations time sequences shows that a few hours (no more than twelve) are needed to the models (RAMS/FARM) to reach the equilibrium. After this spin-up period the different simulation results usually show similar trends. Concerning chemical species concentrations, the spin-up period is tied to the initialisation process of the chemical transport model (FARM). Initial conditions fields have been built merging local observations and background EMEP 3D fields; this process treats the different pollutant separately and gives rise to 3d fields of species that are not in chemical equilibrium at the beginning of the simulation. Depending on the specific features of the site and of the

simulated episode, atmospheric transport, mixing, chemical reactions and emissions need a few hours to establish local equilibrium conditions.

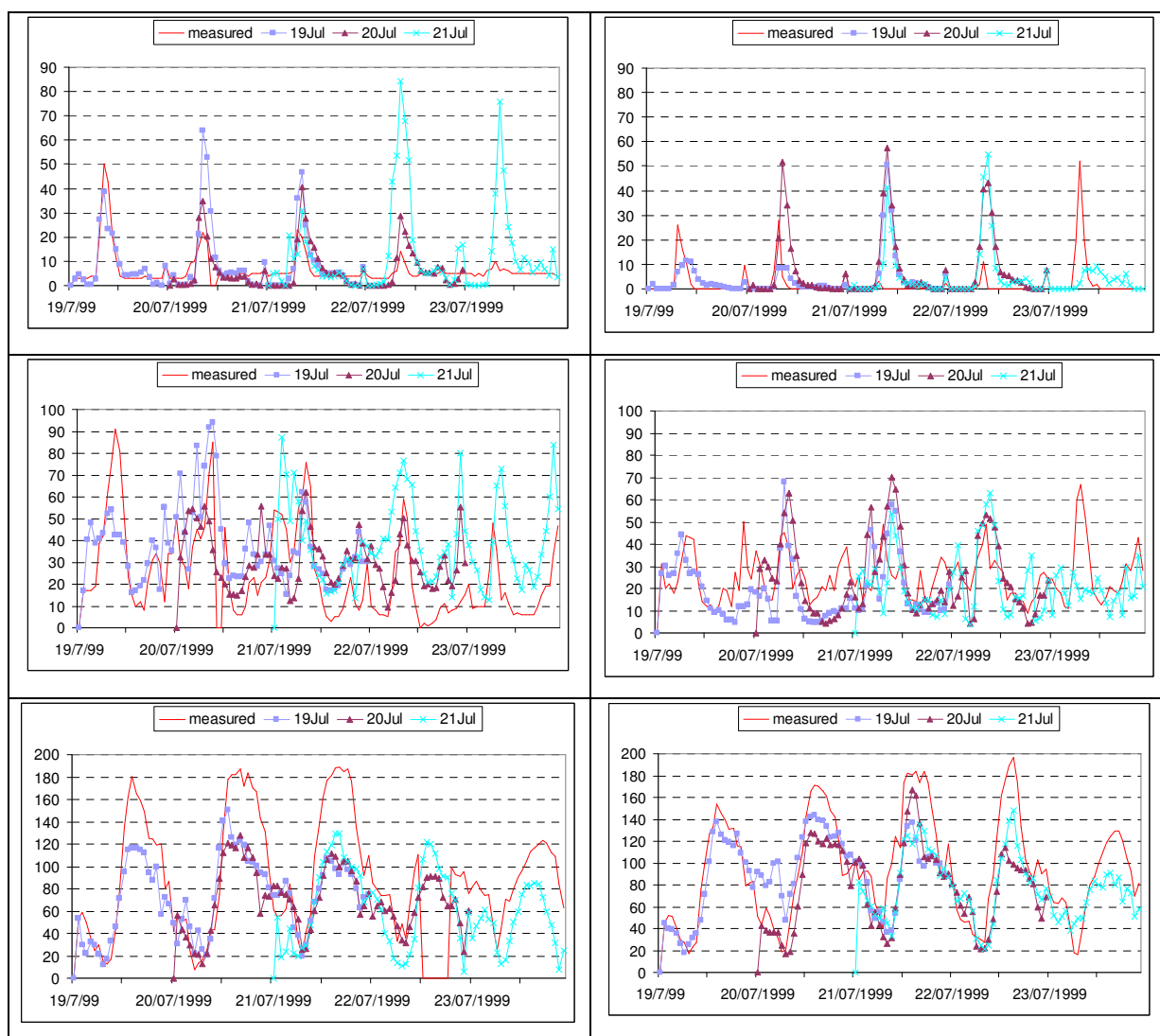


Figure 2.12 Comparison (from top to bottom) among NO, NO₂ and O₃ concentrations at the urban station Lingotto (left column) and suburban station Borgaro (right column).

The analysis of simulations sensitivity to the forecast length has been completed through a statistical evaluation of the UAQIFS performances over the four stations considered for meteorological and air quality evaluation. The root mean square error has been computed for the three simulations considering separately the results obtained during the first (0 - +24), second (+24 - +48) and third (+48 - +72) day of simulation. The results plotted in Figures 2.13 and 2.14 allow verifying the variation with forecast length of the simulation performances both separately and among each other.

For meteorological variables it can be observed that simulations started on July 19th and 20th show similar overall results, while lower score is obtained by the simulation started on July 21st. This behaviour is due to the meteorological event (katabatic flow) occurred on July 22nd and 23rd not well described by this latest simulation and not included in the previous simulations time windows. The variation of results with simulation length can be hardly interpreted: the first and the last forecast tests (started on July 19th and 21st) show best results

during the first day (0 - +24), while the simulation started on July 20th obtained best performance during the second day (+24 -48).

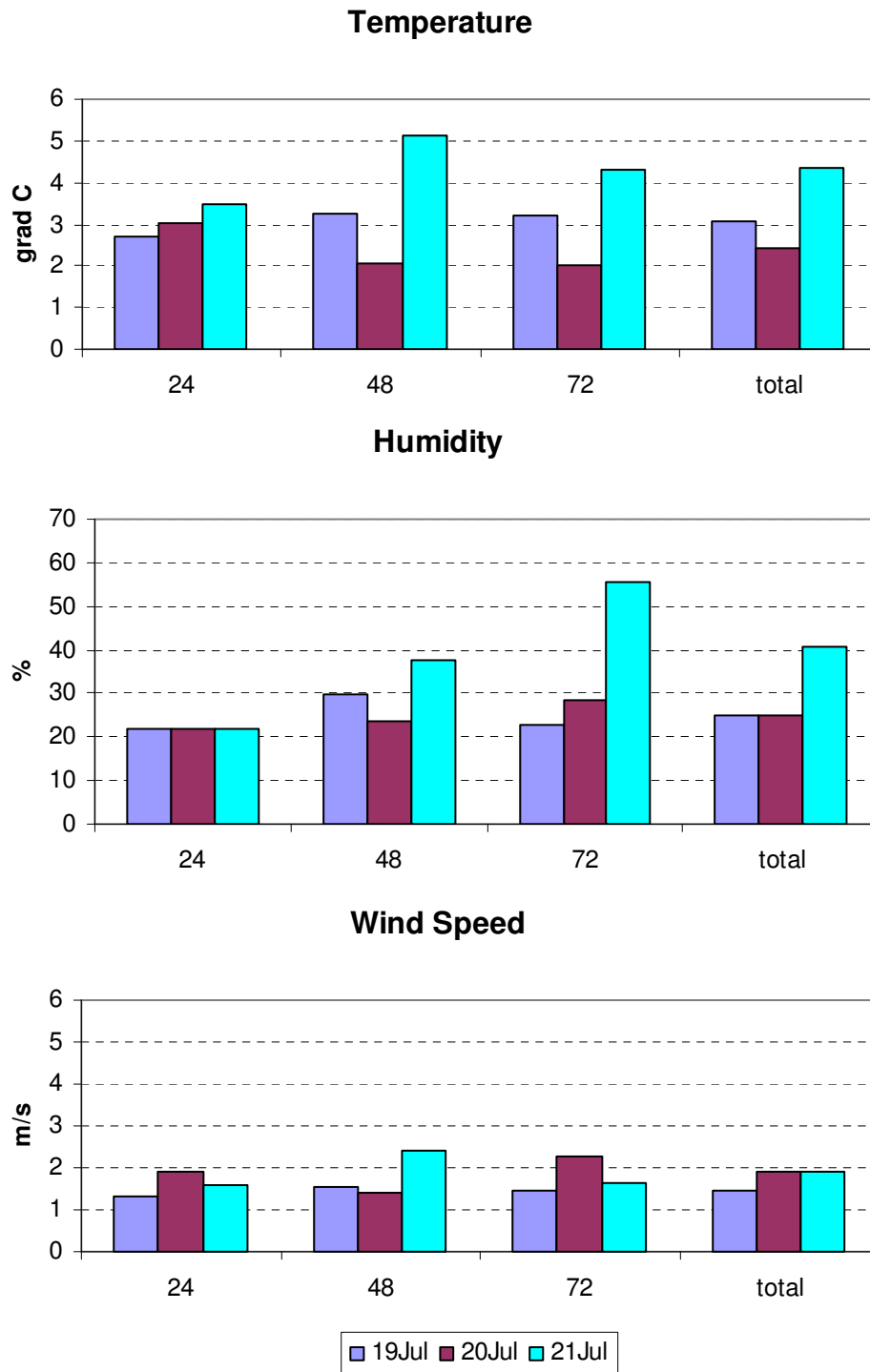


Figure 2.13 Verification scores (root mean square error) for meteorological parameters at forecast lengths +1 - +24, +25 - +48 and +49 - +72 starting at July 19th (blue), July 20th (black) and July 21st (light blue).

The results obtained from the comparison of air quality data are even less straightforward due to the different results obtained for the different pollutants, whose concentrations are correlated by means of atmospheric chemistry. A clear decay of performances with forecast length is shown only for the first simulation for NO₂ and O₃, while NO shows opposite behaviour. The second and third simulations show opposite trend, with NO₂ and O₃ errors decreasing with simulation length. The differences among the three simulation performances are of the same order of magnitude of variation with forecast time, with better results obtained by the simulation started on July 19th.

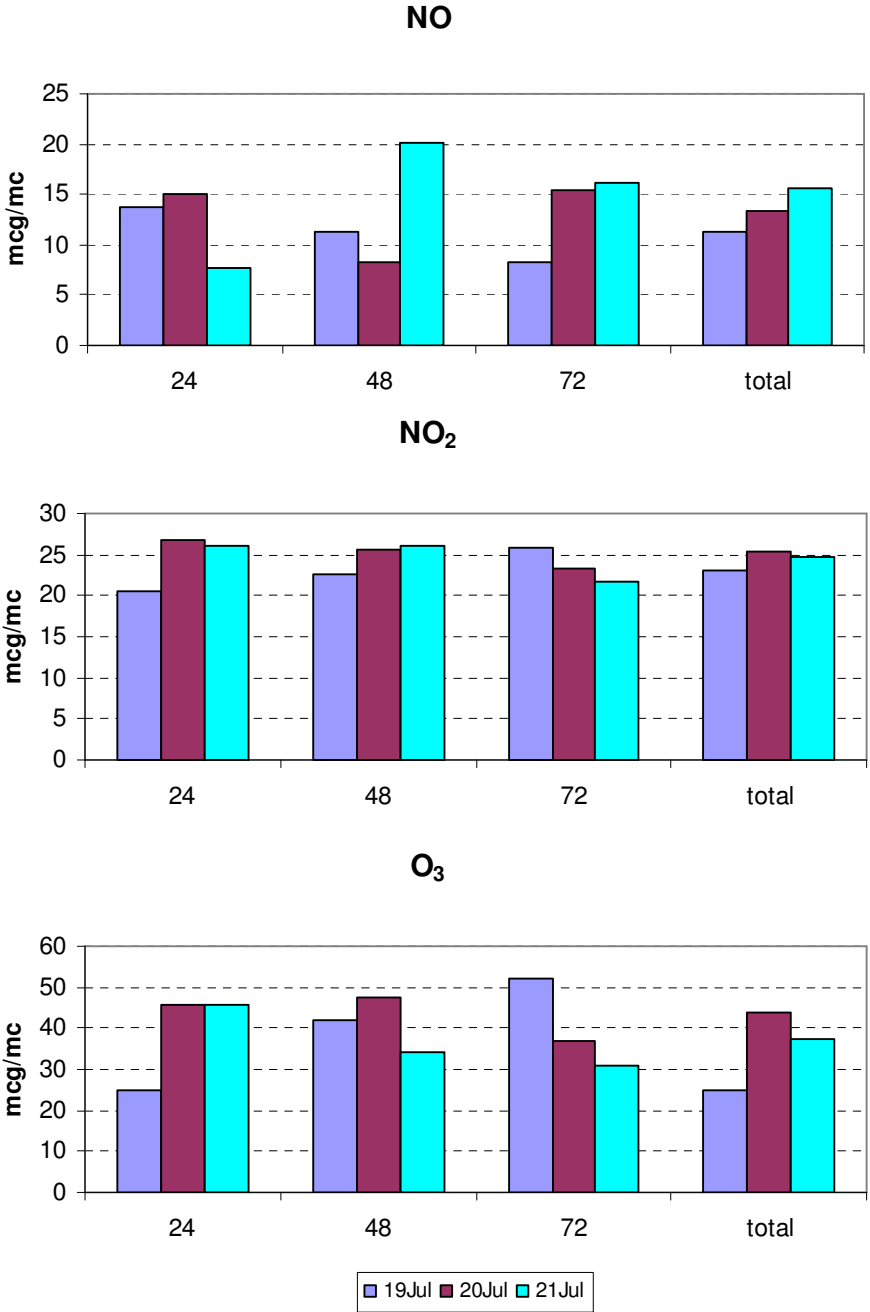


Figure 2.14 Verification scores (root mean square error) for urban air quality parameters at forecast lengths +1 - +24, +25 - +48 and +49 - +72 starting at July 19th (blue), July 20th (black) and July 21st (light blue).

Even though the statistic analysis is computed on three cases only and we cannot consider it enough for a general conclusion, results suggest that different initialisation and synoptic/mesoscale forcing conditions account for larger variations than forecast length. The overall verification results support the option to run with positive results simulations extended over 72 hours for practical applications.

The limited errors found for the first 24 hours confirm the choice of initial conditions and imply a limited influence of the spin-up period, even if experience suggests that it would be better to discard the first six to twelve forecast hours.

3. TARGET AREA CASTELLÓN - UAQ FORECASTS

As said in D6.1 (Guidelines on optimal design of the NWP modelling system for the Castellón target city), at the Mediterranean basin, and in general at whatever area at subtropical latitudes, NWP models used for air quality forecasting must be configured in such a way that they are able to reproduce the mesoscale dynamics. The main atmospheric state variables are insufficient under meteorological conditions marked by non-local dynamical effects, as for example, the compensatory subsidence over the Mediterranean coasts, associated with the orographic injections resulting from the coupling of sea breezes and inland orographic upslope winds (Millán, 2002). When modelling under such conditions, the interaction between different scales must be reproduced; land-use, soil moisture, SST, grid nesting, domain configuration, and horizontal and vertical resolution are key magnitudes/parameters to describe wind flows for air pollution forecasting purposes, and must be set up properly.

For this WP the ozone episode of September 26th-30th 1999 in the Castellón area was simulated with the RAMS meteorological model and CAMx chemical model. Taking into account the above-mentioned issues the next three aspects were chosen to be considered in this study:

- a) Wind recirculation and formation of reservoir layers.
- b) Optimal forecast length.
- c) Impact of RAMS horizontal grid sizes, and nesting grids on ozone concentration patterns modelled by CAMx.
- d) Impact of CAMx horizontal grid sizes on ozone modelled patterns.

Aspects b, c and d are evaluated by means of a standard statistical analysis. Most used metrics in model performance evaluation (Mean Bias, Mean Normalized Bias, Normalized Mean Bias, Mean Normalized Gross Error, Root Mean Square Error, Mean Absolute Gross Error, and Coefficient of determination) are calculated between observations and forecasts of ozone time series. For the optimal forecast length metrics for the first and second 24 hours forecast are calculated and compared. Similarly, to assess the impact of RAMS horizontal grid sizes and nesting grids, metrics are calculated and compared for two grid sizes of the meteorological forecast and a fixed grid size for CAMx forecast (4.5 - 9 km RAMS and 4 km CAMx, respectively). And finally, to assess the impact of CAMx horizontal grid sizes, metrics are also calculated and compared for a fixed grid in meteorological forecast (9 km), and two grid sizes for the photochemical simulation (9 - 12 km). This implies the four cases listed below:

- i) 4.5 km RAMS - 4 km CAMx, first 24 hours (base case).
- ii) 4.5 km RAMS - 4 km CAMx, second 24 hours.
- iii) 9 km RAMS - 4 km CAMx, first 24 hours.
- iv) 9 km RAMS - 12 km CAMx, first 24 hours.

Wind recirculation and formation of reservoir layers must be qualitatively evaluated by means of the analysis of vertical cross sections of concentrations extracted from the photochemical simulations. Section 4 deals with all these aspects. Before that, a description of the photochemical model and a description of the 26th-30th of September 1999 ozone episode are included in sections 2 and 3 respectively.

Description of the photochemical model

The Comprehensive Air quality Model with extensions (CAMx) is a photochemical dispersion model that allows for an integrated “one-atmosphere” assessment of gaseous and particulate air pollution over many scales ranging from urban to super-regional (Environ, 2003). This system constitutes a state-of-the-art tool for regional-scale simulations of photochemical smog, visibility and fine particulates. CAMx is a three-dimensional Eulerian chemical transport model that accounts for horizontal and vertical advection, eddy diffusion, gas-phase chemical transformations, emissions, cloud mixing, aqueous-phase chemical reactions, and aerosol processes. This model solves the pollutant continuity equation for each chemical species on a system of nested three-dimensional grids.

CAMx version 4.03 has been implemented using the area preserving flux-form advection solver of Bott (1989) and K-theory parameterization for vertical diffusion based on the Mellor and Yamada (1982) and Helfand and Labraga (1988) algorithms. The meteorological data used for this simulation have been obtained as output fields from the Regional Atmospheric Modelling System (RAMS) (Pielke, 1992). A detailed description of the equations and algorithms of each component of CAMx are given in Environ (2003). Following is a description of the horizontal and vertical resolution, chemical mechanism, meteorological pre-processor, and emissions that have been implemented to simulate ozone formation in the area of Castellón in the Western Mediterranean basin.

Horizontal and vertical resolution

Two horizontal nests using a Lambert Conformal geographical projection have been defined for the simulation (Figure 3.1). The two-way photochemical nesting capability of CAMx has been used for this simulation. This feature allows CAMx to be run with coarse grid spacing over a wide regional domain in which high spatial resolution is not particularly needed, while within the same run, applying fine grid nests in areas where high resolution is needed. For this application, the first nest covers the entire Iberian Peninsula with a resolution of 12 km and a dimension of 108x92 cells. The second nested domain has a 4-km horizontal resolution, 38x83 cells, and encompasses the Valencian Community (VC). The vertical resolution of both grids is 30 sigma-p layers. These layers directly correspond to the lowest 30 layers of the RAMS simulation.

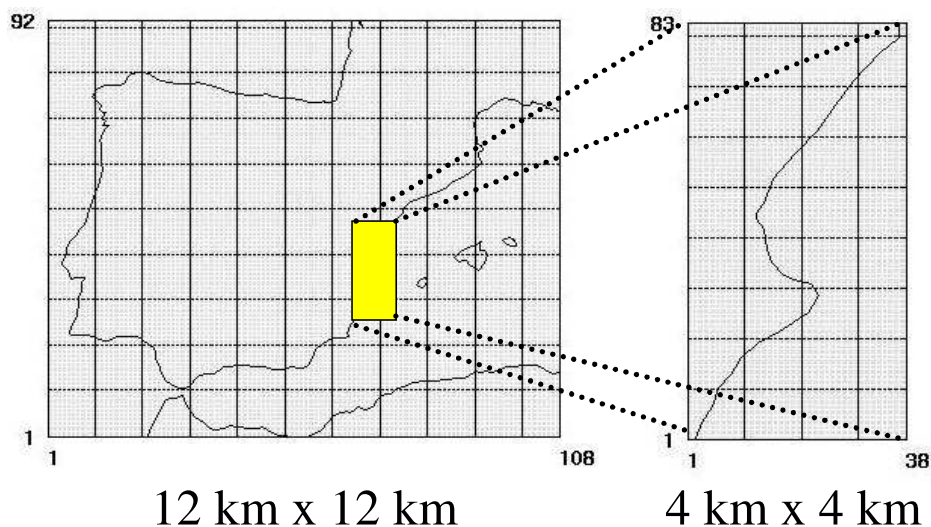


Figure 3.1 Description of photochemical model domains.

Chemical mechanism

The Carbon Bond Mechanism IV (CBM-IV) (Gery et al., 1989) has been used to describe the gas-phase chemical processes that occur within the concentration grids. This chemical scheme utilizes the carbon-bond approach for the lumping of organic species. Under this approach, organic species are disaggregated according to their bond type (for example, as carbon single bonds, carbon double bonds, or carbonyl bonds). The CBM-IV contains over 80 reactions and more than 30 chemical species. The photolysis rate constants needed to calculate the chemical transformations have been computed as a function of the solar zenith angle, cloud cover, ozone column, UV albedo, and optical depth due to absorption plus scattering at 340 nm for each photolyzing chemical species. The Implicit-Explicit Hybrid (IEH) chemical solver (Sun et al, 1994) has been used to integrate the set of stiff ordinary differential equations arising from this chemical system.

Meteorology pre-processor

The RAMS - CAMx interface links the Numerical Weather Prediction (NWP) model, i.e. RAMS, with CAMx to provide a complete set of meteorological data needed for air quality simulations. Because most meteorological models are not build for air quality modelling purposes, this pre-processor deals with issues related to data format translation, conversion of units of parameters, diagnostic estimations of parameters not provided, extraction of data for appropriate window domains, and reconstruction of meteorological data on different grid and layer structures. This pre-processor has also been modified and used to provide land use data as needed by CAMx to calculate dry deposition. The guidelines describing the structure, formulation, and data requirements of the NWP and the photochemical model interface for its application within the FUMAPEX project are described in Finardi (2004).

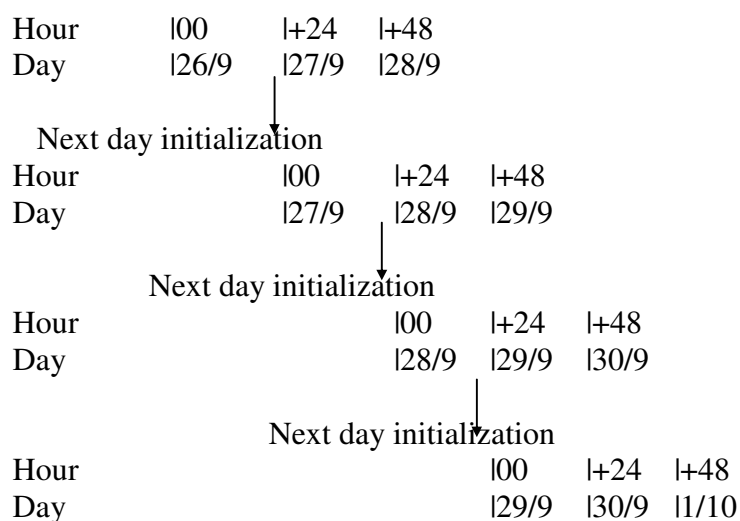
Emissions

Emission calculations have been performed to account for primary pollutants released from sources located in two different domains, the first domain covering the Iberian Peninsula and the second one the VC. These two domains have been defined to be compatible with the photochemical horizontal grids. Sources corresponding to the Iberian Peninsula have been estimated based on EMEP emissions inventory. On the other hand, primary emission of NO_x, VOC and carbon monoxide (CO), corresponding to the CV domain have been calculated based on a local emissions inventory (Martin et al, 1998). This inventory includes mobile, area and industrial sources and encompasses the area of Castellón.

Isoprene and other biogenic species emissions have been estimated using land use, radiation, and biogenic emission factors (Guenther et al, 1993; 1995). Biogenic emissions have been calculated for the Iberian Peninsula as well as for the VC and added to the anthropogenic emissions. Further details on the implementation of the biogenic emissions module for its application within the FUMAPEX project are provided in Finardi (2004).

Simulation description

The period under study includes from September 26th to October 1st 1999. In order to allow the model to build up the chemical species concentrations, thus minimizing the influence of initial conditions, the first simulation day has been run twice and its output treated as the initialization data. The simulations have been performed for 48 hours for each day. Next day simulations have been initialized with the +24 hour output corresponding the previous day. The following scheme depicts the run schedule:



Description of the September 26th-30th 1999 ozone episode

General description of ozone episode events in the Castellón Area

The analysis of the time series of ozone data corresponding to the area of Castellón and its surroundings shows that high concentration levels of this pollutant respond to a characteristic pattern (see D1.2 Identification and classification of air pollution episodes in terms of pollutants, concentration levels and meteorological conditions. Castellón, Spain). Since 1997, the ozone pattern has been repeating itself in 21 of 23 of the registered exceedance in the Valencian Community. The main features of this analysis are described below:

- The exceedance takes place in the spring and summer months under the influence of mesoscale anti-cyclonic circulations and stable atmospheric conditions.
- There is a gradual increase in the maximum ozone concentrations between each consecutive day (recharging period). This occurs when the above-mentioned meteorological conditions are maintained.
- These time periods cover about 30% of the days between the months of April and September, with a maximum in July covering 50% of the days, and they last between 3 to 8 days (4-5-days average)(figures 3.2 and 3.3).
- The ozone recharging periods generally affect all the forecasting area, from the coast to the interior. Not all of these cycles give rise to an ozone exceedance of the 180 µg/m³ threshold; however they usually produce the ozone levels to surpass the objective value for human health protection (120 mg/m³ over an 8-hour average).
- When an exceedance takes place, it rarely surpasses 190 µg/m³ and it don't last more than 2 or 3 hours. These high levels of ozone are generally observed at coastal sites after 2:00 p.m. and at inland stations with a delay of 1 or 2 hours with respect to the coastal locations. The delay is associated to the sea breeze transport of pollutants and their photochemical transformations.

The following figures illustrate some of these aspects.

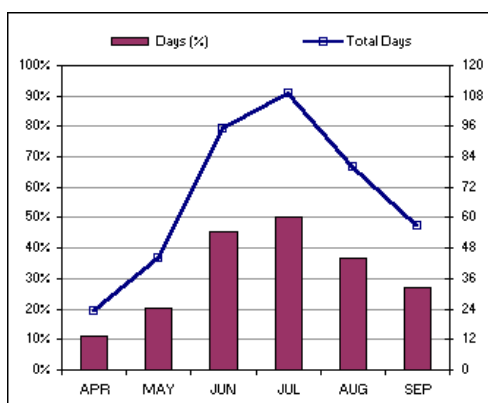


Figure 3.2: Number of days included in the recharging periods between April and September (1997-2003)

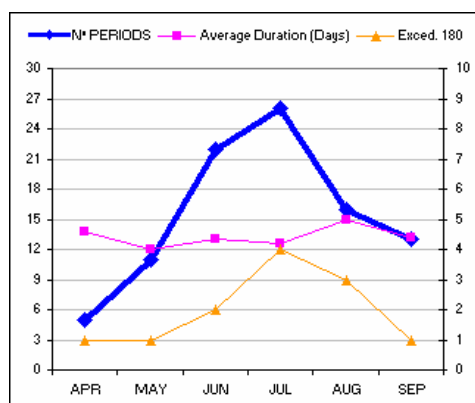


Figure 3.3 Number of recharging periods (left edge), average duration, and number of exceedance of the Information Threshold - 180 $\mu\text{g}/\text{m}^3$ (right edge), by month.

The September 26th-30th 1999 ozone episode

The September 26th-30th 1999 episode was a 4 days recharging period. Two exceedance are registered at Onda site (20 km downwind Castellón), on the 28th (189.75 $\mu\text{g}/\text{m}^3$ at 16h) and 29th (182.25 $\mu\text{g}/\text{m}^3$ at 13h). Mountain stations in the domain (Corachar, Vallibona, Vilafranca, about 80 km inland from the coast), reached values above 170 $\mu\text{g}/\text{m}^3$. The gradual day-to-day increase of the daily maximum concentrations over the entire domain is shown in figure 3.4.

The meteorological synoptic situation during the 26th-29th period shows a zonal flow over the north-eastern Atlantic Ocean forced by two strong perturbations over the northern Atlantic and the Baltic Sea. A high pressure ridge dominates the centre of the Atlantic Ocean and the centre and south of the Iberian Peninsula. There are low isobaric gradients over the Western Mediterranean basin (figure 3.5). The predominant circulations in this period were meso-scale circulations, formed by coupling of sea breezes and inland orographic upslope winds as show wind data in figure 3.4. On 30th the winds became more intense from the NW with the arrival of a cold front which swept the peninsula on that day. As a result the good mix of the air mass produced a general and sharp reduction of the ozone concentrations all over the domain (figure 3.4).

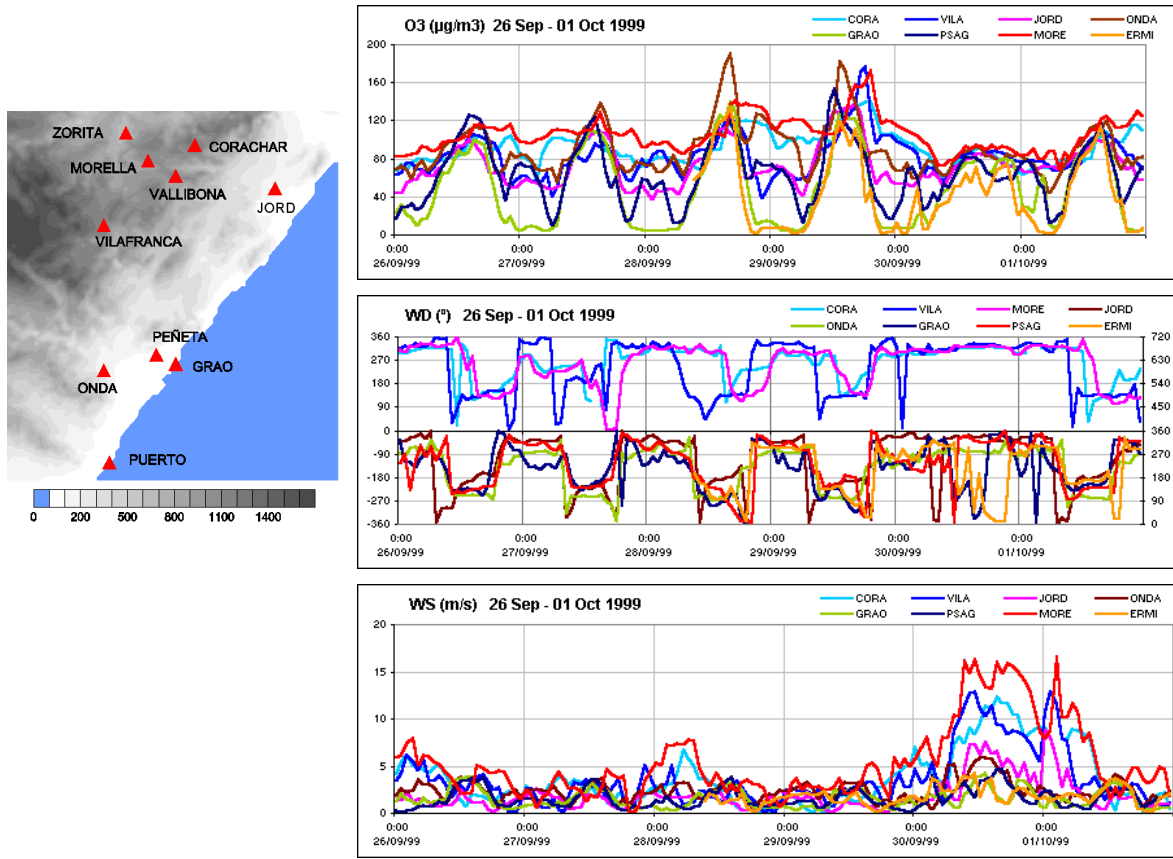


Figure 3.4 Serial data of ozone, wind direction and wind speed registered by the automatic stations in the domain.

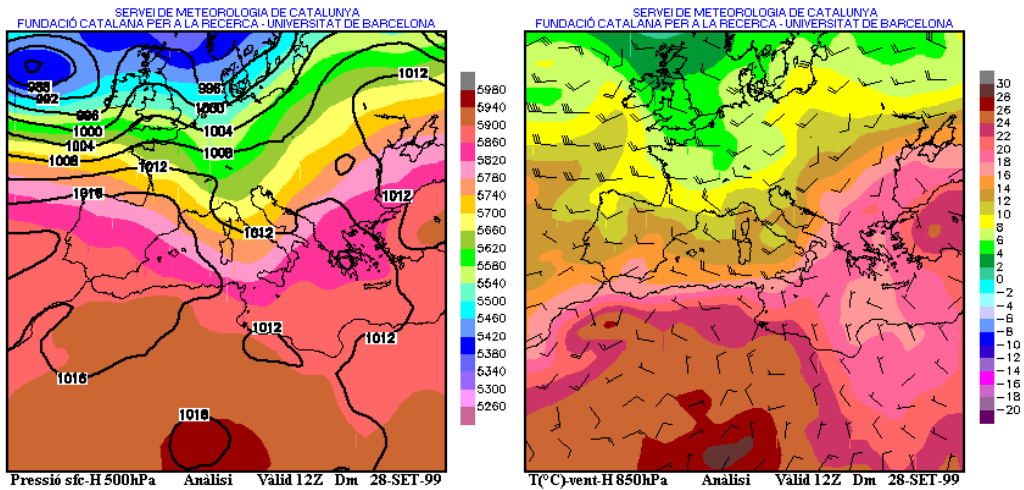


Figure 3.5 Meteorological analysis charts for the 28th (Surface pressure and 500 hPa level, left, and temperature and wind vectors at 850 hPa level, right)

Evaluation of the photochemical simulation performance

Brief interpretation of the photochemical model simulation

The evolution of the simulated ozone geographical distribution at the fine grid corresponding to September 27th 1999 is presented in Figure 3.6 as an illustration of the circulation patterns observed in the area of Castellon. The results show that the nocturnal cooling of inland

ground surface has led to the development of down-slope flow of mountain ranges and valley winds. At this time, domain maximum values of O_3 are simulated nearby mountain-top locations. At this place, flow sinking brings reservoir layer to surface level (see north-western corner of figure 3.6 a, b, c). At coastal sites, the high NO_x emissions and the absence of photolysis have led to low O_3 values. Under these conditions, O_3 is depleted through a reaction with NO emitted mainly from road traffic and industrial areas (Figures 3.6 a, b, c). After sunrise, land surface has warmed up initiating the onset of sea breeze and up-slope flows. At the coast, ozone levels start to raise due to arrival by the sea breeze of ozone from the reservoir layers over the sea and by photochemical production of freshly emitted precursors over the coast (Figure 3.6 d, e). In mid-afternoon, polluted air masses rich in O_3 , while still producing photochemical oxidants, are pushed further inland and topographic injected into reservoir layers late in the afternoon (Figure 3.6 f). Furthermore, Figure 3.7 shows an East-West vertical cross-section around the area of Castellon and illustrates the topographic injection of ozone. Once in those upper layers the pollutants move back toward the sea transported by the return flow where they will create stratified reservoir layers (Figure 3.7 b, c). These processes were documented during the development of EC projects (Millán et al., 1997).

3.1. Sensitivity to horizontal resolution in NWP and UAQ models

Model vs. Measurements: Time series

Annex 1 show the graphics with the superimposed time series of measurements and simulations in the four cases considered:

- i) 4.5 km RAMS - 4 km CAMx, first 24 hours (the base case)
- ii) 4.5 km RAMS - 4 km CAMx, second 24 hours
- iii) 9 km RAMS - 4 km CAMx, first 24 hours
- iv) 9 km RAMS - 12 km CAMx, first 24 hours.

Measurements are hourly averages from raw data (10 minutes registers), and simulations use a four-cell weighted average to determine the predicted concentration at each location.

The main conclusions after a simple observation of these graphics are:

- Model captures daily cycles, although it fits better at coastal (Grao), pre-coastal (San Jordi), and valley sites (Vilafranca), with an almost symmetrical and wide oscillation pattern, than at mountain sites (Corachar), where the delay in the arrival of the coastal air mass, ESE winds, produces an asymmetric pattern which is not as well reproduced at the simulations. On the other hand, at two stations Peñeta and Onda patterns are not well reproduced. The Peñeta station is particularly difficult to reproduce because it is located on elevated ground near the sea. The ozone cycles at this kind of stations depend on the relation between the elevation of the site above the coastal plains and the depths of both the stable surface layer during the night and the marine TBL during the day (Millan et al, 2000)
- Model gets the sharp reduction O_3 concentration on Sep 30th caused by the pass of a cold front that swept the peninsula all through that day.
- Model underestimates Sep 28th levels. The reasons for this seem to be: 1) a PBL height higher than 27th, and, 2) wind at 27th night blows the precursors further over the Mediterranean.

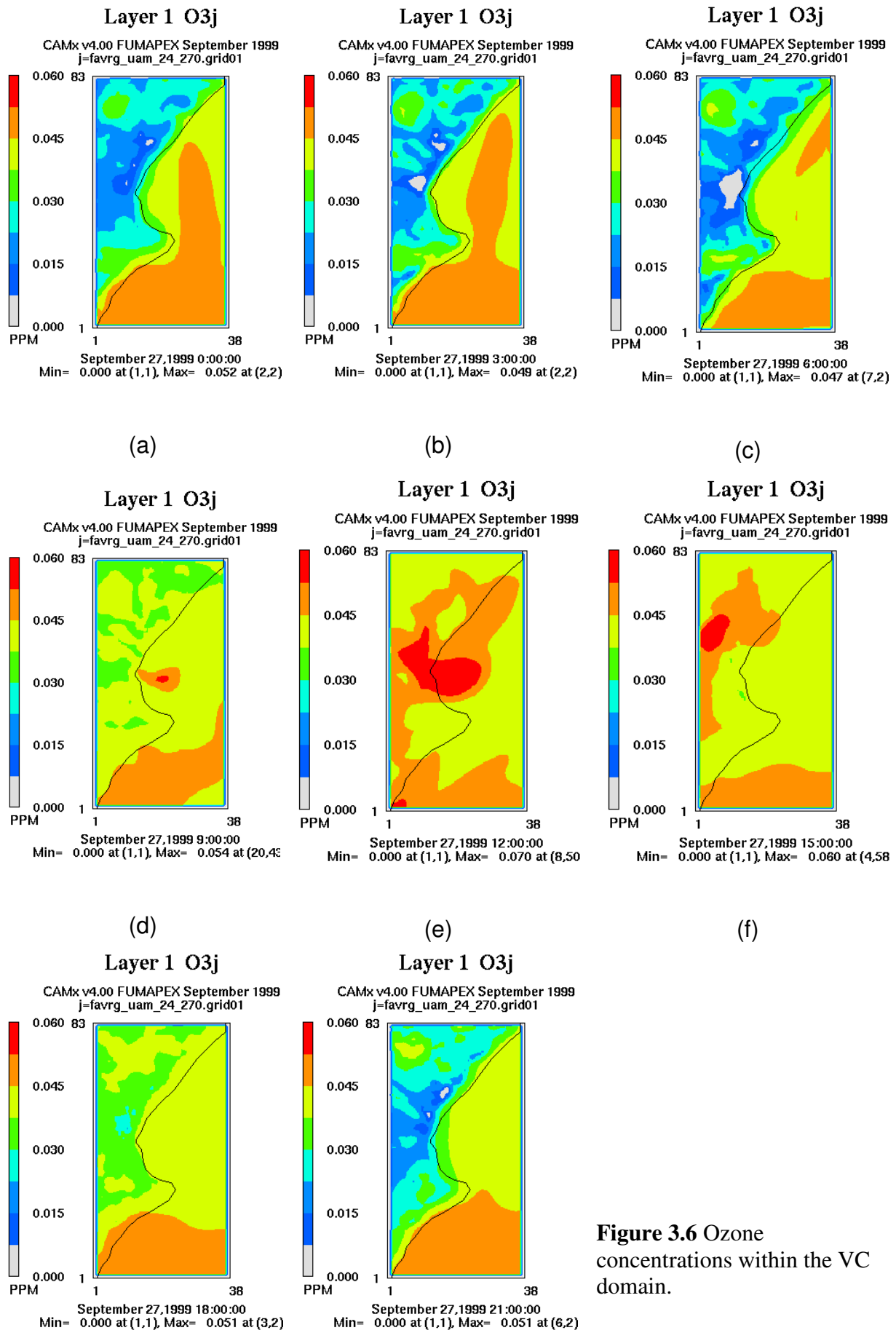
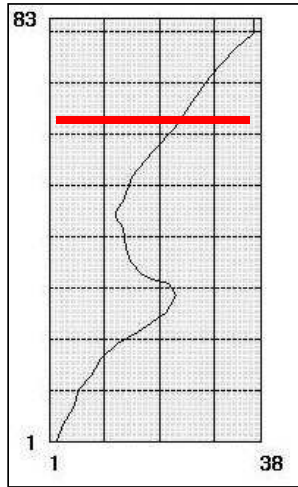


Figure 3.6 Ozone concentrations within the VC domain.

(g)



(h)

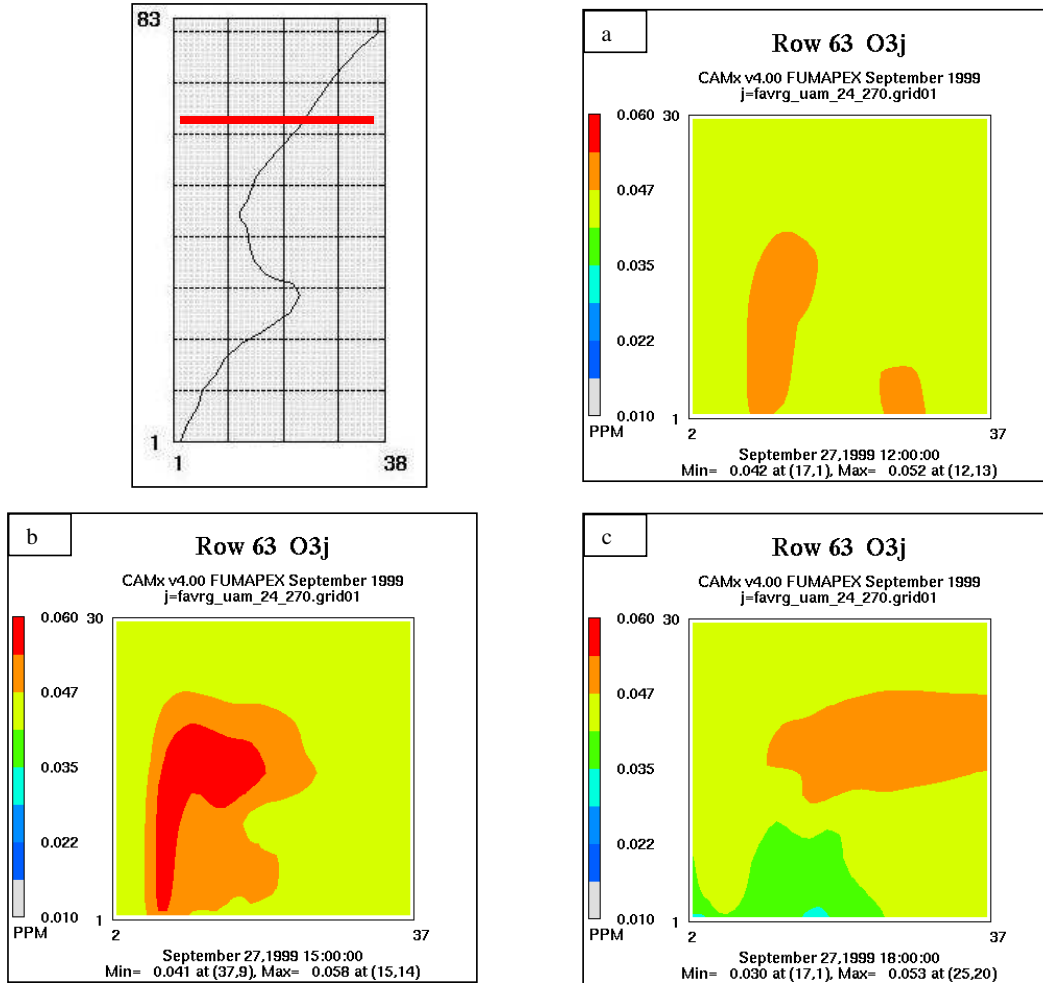


Figure 3.7 East-West vertical cross-section O₃ concentrations (shown in red on the VC domain map). The y-axis denotes the vertical index level. Level 15 corresponds to approximately 1000 m.

Statistics

For each location of the Air Quality Network in the domain, most used metrics in model performance evaluation are calculated between time series of surface ozone observations and simulations matched in space and time. The table below shows the chosen metrics:

Statistical Measure	Mathematical expression
MB: Mean Bias	$\frac{1}{N} \sum_{i=1}^N (P_i - O_i)$

Statistical Measure	Mathematical expression
MNGE: Mean Normalized Gross Error	$\frac{1}{N} \sum_{i=1}^N \frac{ P_i - O_i }{O_i} \quad (\%)$

MNB: Mean Normalized Bias	$\frac{1}{N} \sum_{i=1}^N \frac{(P_i - O_i)}{O_i} \quad (\%)$	RMSE: Root Mean Square Error	$\left[\frac{1}{N} \sum_{i=1}^N (P_i - O_i)^2 \right]^{\frac{1}{2}}$
NMB: Normalized Mean Bias	$\frac{\sum_{i=1}^N (P_i - O_i)}{\sum_{i=1}^N O_i} \quad (\%)$	UPA: Unpaired Peak Accuracy	$\frac{P_{peak}^u - O_{peak}}{O_{peak}} \quad (\%)$
MAGE: Mean Absolute Gross Error	$\frac{1}{N} \sum_{i=1}^N P_i - O_i $	R²: Coefficient of determination	$\frac{\left[\sum_{i=1}^N (P_i - \bar{P})(O_i - \bar{O}) \right]^2}{\sum_{i=1}^N (P_i - \bar{P})^2 \sum_{i=1}^N (O_i - \bar{O})^2}$

The *mean bias* is the degree of agreement between prediction and observation, with lower numbers indicative of better performance. Negative values indicate under-prediction and positive indicate over-prediction. The *Mean Absolute Gross* is the mean of the absolute value of the residuals. Lower numbers indicate better model performance. *Root Mean Square Error* is a good overall measure of model performance. The square of the residuals tends to inflate RMSE for extreme values. Good model should approach zero. *Unpaired Peak Accuracy* inform about the performance for maximum values which are of special interest. These residual-based measures provide quantitative estimates of the deviation of model predictions from observations. On the other hand, *Coefficient of determination* is a measure of statistical association that provide quantitative estimates of the statistical co-variation between observed and predicted values

Usually these metrics are performed for hourly or daily averages and most cases, to avoid the indetermination for zero values in some of the metrics; only data above a fixed value (commonly 60 ppb) are considered. Furthermore, these statistics can be done for each point applied to a time series (then N is the number of hourly values), for each instant applied to a spatial series (then N is the number of sites), or both simultaneously. In this analysis metrics are applied to hourly data. Observed data are actually averages from raw data (10 minutes registers), and corresponding simulations use a four-cell weighted average to determine the predicted concentration at each location. Metrics were calculated for each day of the episode, and only pairs of data in the time window from 8 a.m. to 20 p.m. were considered (similar to consider only data over a fixed value).

Other metrics commonly used to analyse the success of exceedance forecasting are those based on contingency tables, e.g. Probability of Detection, False Alarm Rates, or Critical Success Index. However, these kinds of metrics were not considered in this work for being inadequate in a five-day episode.

The overall results for each day (all instants, all sites in the domain) are shown in figure 3.8. Graphics of figure 3.9 show the same metrics at each one of the nine sites for the base case simulation (4.5 km RAMS- 4 Km CAMx first 24 hours). Appendix 2b comprises data tables with the results of all the statistics calculated.

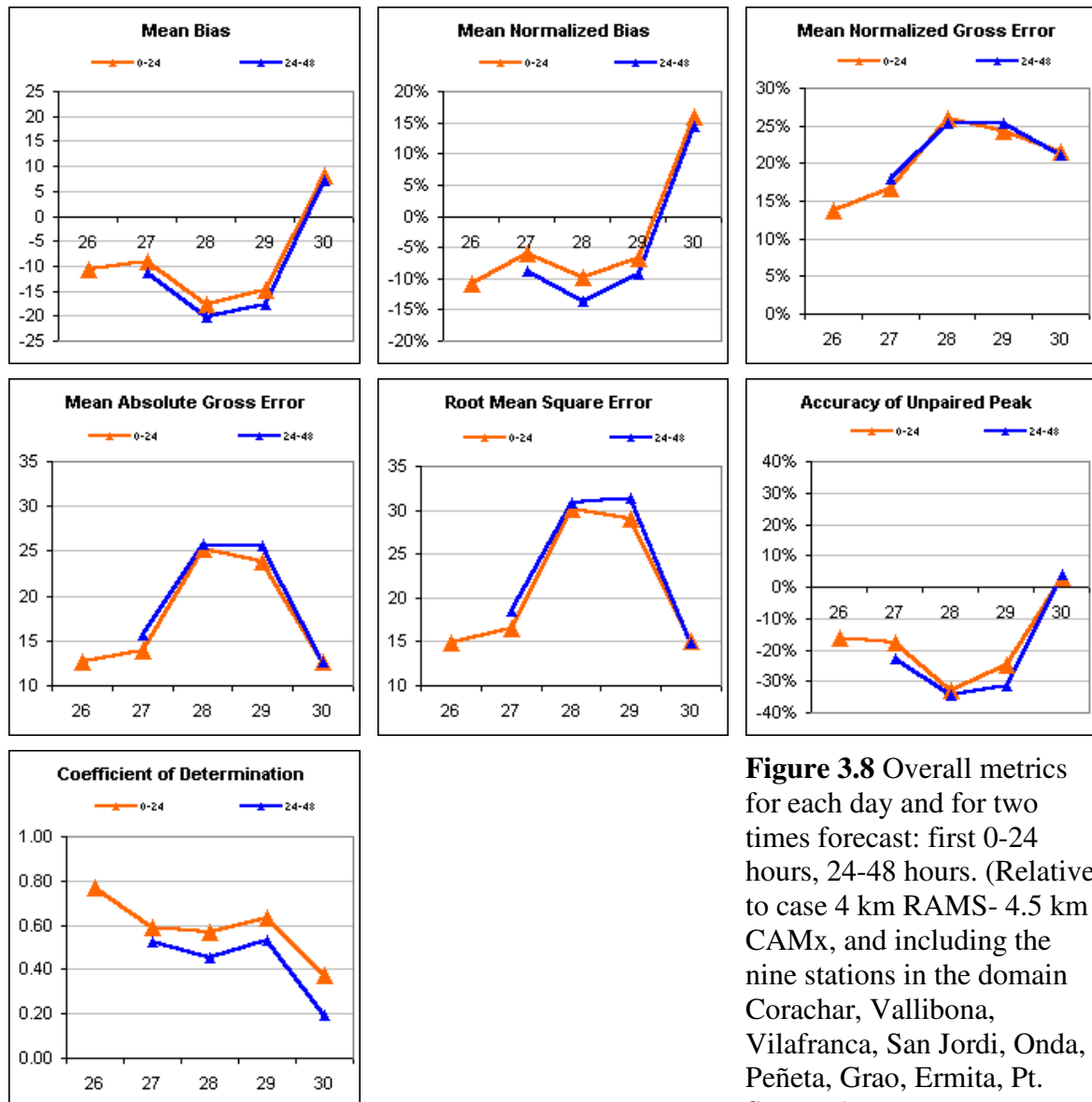


Figure 3.8 Overall metrics for each day and for two times forecast: first 0-24 hours, 24-48 hours. (Relative to case 4 km RAMS- 4.5 km CAMx, and including the nine stations in the domain Corachar, Vallibona, Vilafranca, San Jordi, Onda, Peñeta, Grao, Ermita, Pt. Sagunto)

The following points can be noticed:

- Bias show an under-prediction of ozone levels from 26th to 29th during the recharging period, which is around 5-15% for the mean forecast (MNB), and around 20-30% in the case of maximum values (AUP).
- Metrics get worse day to day from 26th to 29th during the recharging period, with a noticeable step from 27th to 28th, as can be seen for MAGE or RMSE, and then get better on 30th (instead coefficient of determination is clearly lower). The reason for this behaviour is because the days to day increase in ozone concentration is only slightly reproduced by the simulations.
- Results are very similar for the two forecast length, though is better in almost all the cases for the 0-24 forecast.

On the other hand, metrics are in acceptable values which are within the ranges recommended by EPA. (For urban-scale regulatory applications EPA (1994) recommends that the *mean normalized bias* should be less than about 5-15%, the *mean normalized gross error* should be

less than about 30-35%, and *normalized accuracy of maximum* 1-hr concentration unpaired in space and time 15-20 %. No criteria for regional-scale).

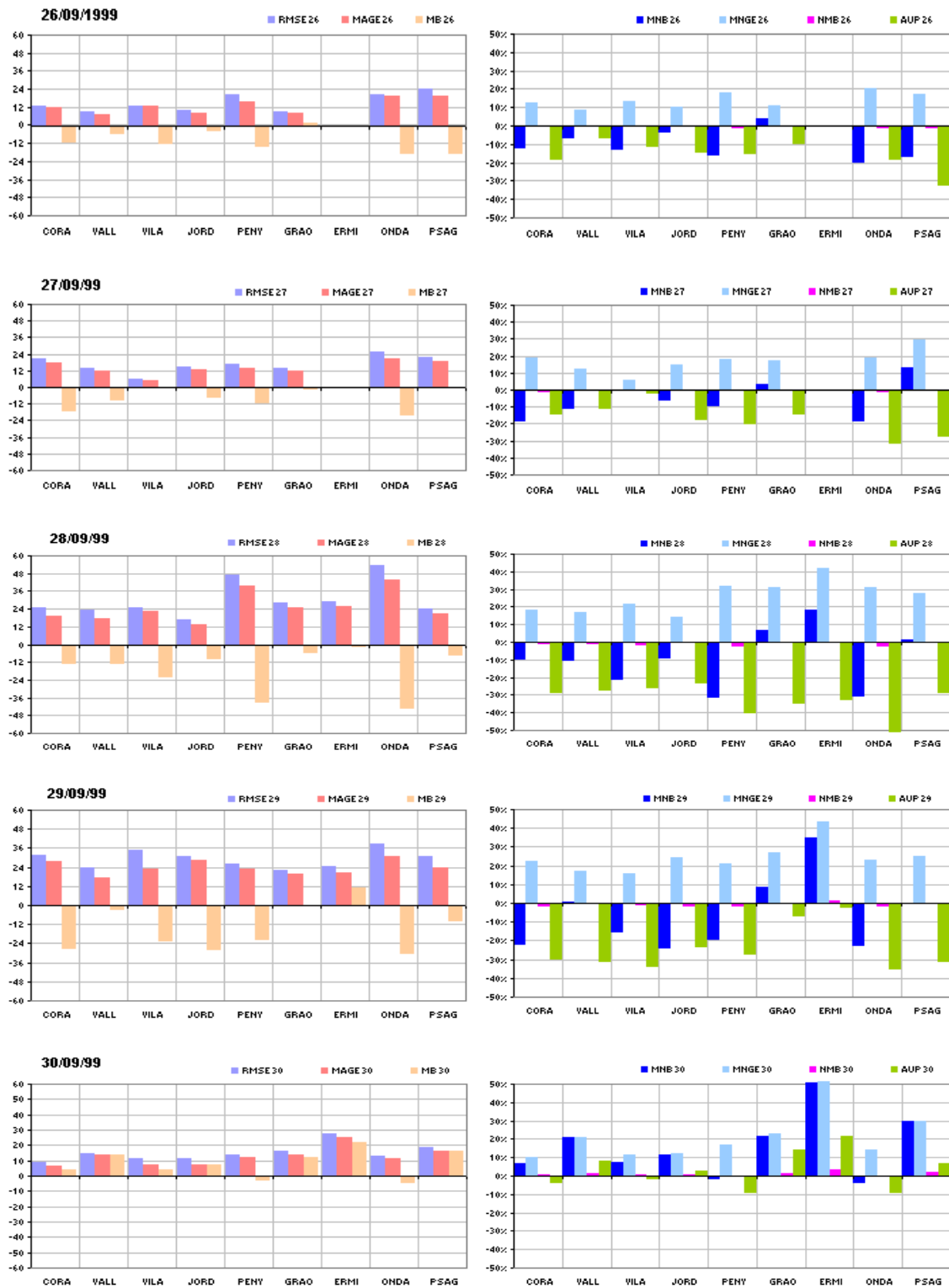


Figure 3.9 Statistics values at the nine automatic stations in the domain for the base case simulation (4.5 km RAMS - 4 Km CAMx first 24 hours)

Particular results for each site in the base case show that under-prediction in the period 26th-29th is generalised in the whole domain. The results are similar for all of the sites except for Onda and Peñeta where are worse.

Effect of RAMS resolution

Comparison between base case (4.5 km RAMS -4 km CAMx) and the 9 km RAMS - 4 km CAMx simulation allows the analysis of the effect of RAMS resolution. Figure 3.11 show the metrics results for the 28th and differences are hardly noted with its equivalent in the base case for the same day (see figure 3.9). Tables AII.1 and AII.2 in annex II contains all the metrics. This result is somewhat expected because the 9 km RAMS run contains information from its inner 4.5 km nest. Therefore, the general meteorological patterns are still captured by the 9 km run without degrading the photochemical result.

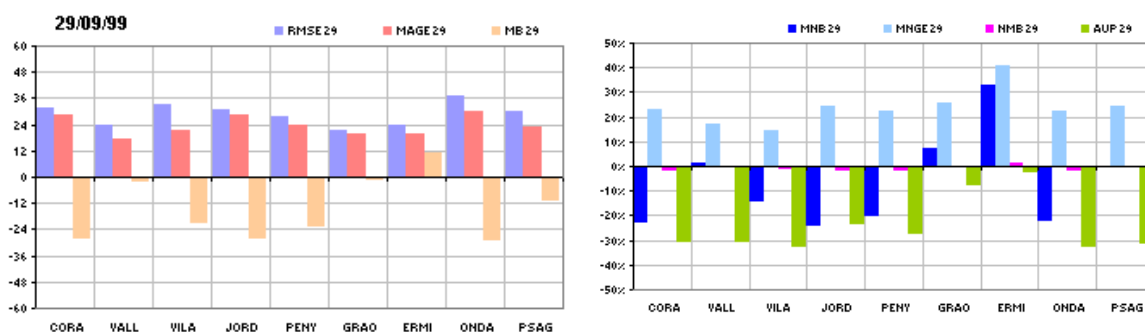


Figure 3.10 Statistical values at the nine automatic stations in the domain for the 9 km RAMS - 4 Km CAMx

Effect of CAMx resolution: 4 vs. 12 km simulation

As a main result, a coarse resolution for CAMx simulation produces an overestimation of night-time surface O₃ in coastal zone (Grao). This is due to underestimation of NO sources at night, which implies less titration and then more ozone. Because only the time window between 8 a.m. and 8 p.m. are considered for metrics calculations the results (figure 3.11) don't show sensible differences respect the 9 km RAMS- 4 Km CAMx case (figure 3.10).

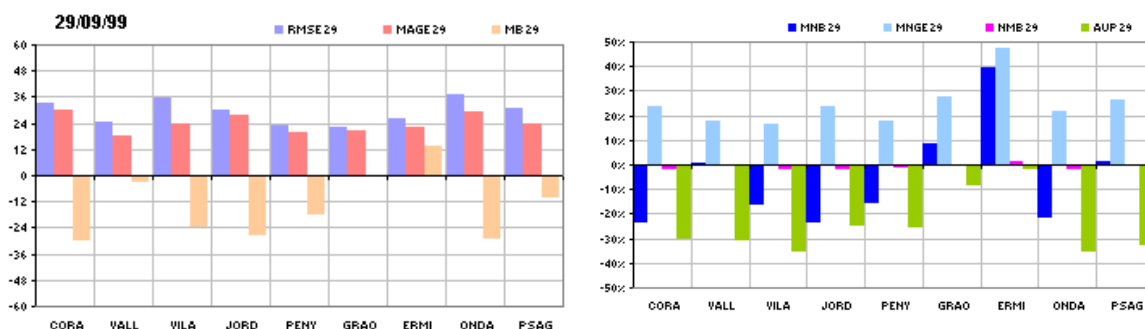


Figure 3.11 Statistical values at the nine automatic stations in the domain for the 9 km RAMS - 12 km CAMx

Wind recirculation and formation of reservoir layers

As commented in 4.1 Figure 3.7 shows an East-West vertical cross-section around the area of Castellon and illustrates the topographic injection of ozone. Once in those upper layers the pollutants move back toward the sea transported by the return flow where they will create stratified reservoir layers (Figure 3.7 b, c). Instead the later drop and accumulation of these strata above the sea isn't forecasted by the model (perhaps it hasn't taken place during this particular episode), it can be said that the simulation reproduces the some of the main processes (topographic injection and formation of stratified reservoir layers) involved in recirculation dynamics. Similar circulation patterns have been modelled for the remaining simulation days. Therefore, the results shown in figure 3.7 are representative of days 26th to 29th of September, 1999.

3.2. Sensitivity to forecast length

As expected, metrics degrade slightly from base case (4 km RAMS - 4.5 km CAMx first 24 hours) to the case 24-48 hours and same spatial resolution forecast. Graphics in figure 3.8 prove it for the overall domain, and it is also true for any particular site. Figure 3.12 contains the 24-48 metrics results for the 28th and shows little, but noticeable differences with its equivalents results in the base case for the same day (see figure 3.9). Tables AII.1 and AII.2 in annex II contains all the metrics. So, shorter forecast length of RAMS simulation produces better results of the CAMx forecasts.

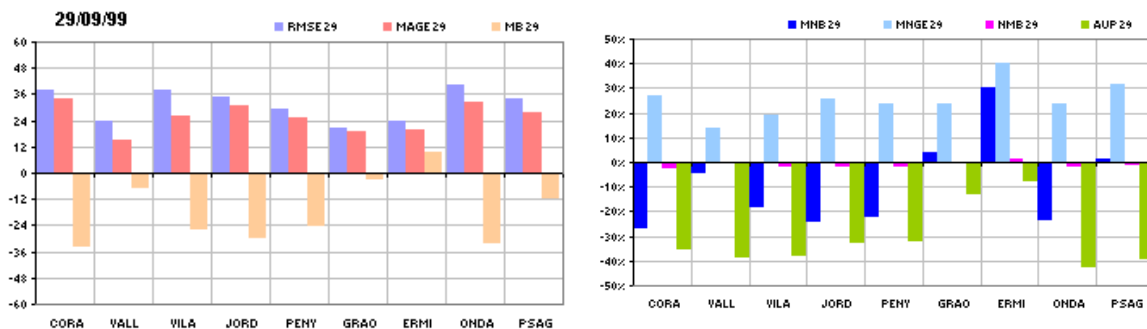


Figure 3.12 Statistics values at the nine automatic stations in the domain for the 4.5 km RAMS- 4 Km CAMx second 24 hours simulation (24-48h)

4. TARGET AREA CASTELLÓN - TRAJECTORY MODEL SIMULATIONS

General information on DWD LM trajectories

The LM trajectory model is an off-line model coupled to the LM with identical resolution, horizontal and vertical grid structure as the corresponding LM model providing the output data. Therefore, no interfaces are needed. The trajectory model is fully three-dimensional, of high numerical order (Euler-Cauchy scheme with iteration of 2nd order accuracy, Kottmeier and Fay, 1998), uses 1-hourly data input from the Lokalmmodell LM, linear interpolation in time and tri-cubic interpolation in space and a very small time step similar to the LM model itself (2 min for the operational LM 7 km trajectories, 60 sec for all FUMAPEX trajectories). This ensures small tangential errors especially in conditions of strongly fluctuating winds and bent streamlines.

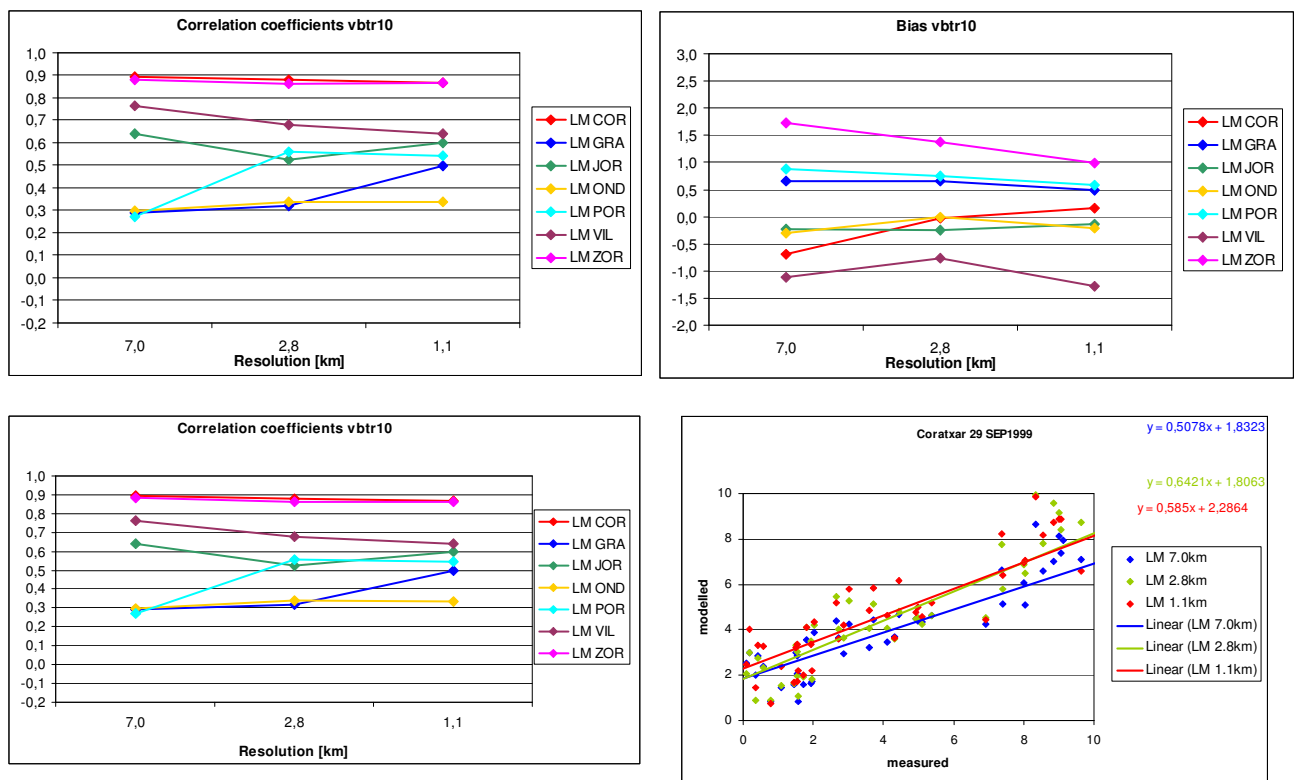


Figure 4.1 48h LM forecast of v10 m for 29 Sep 1999, 00 UTC, for resolutions of 7, 2.8 and 1.1 km. Correlation coefficient, bias and rmse as 48 h average, calculated with MMAS. Scatter plot for Coratxar (near location of trajectories simulated below).

Consequently, the quality of the trajectories will largely depend on the quality of the LM wind fields. The operational 7 km LM results are daily verified using the standard WMO and additional statistics showing a high international standard. Only the target cities Oslo, Bologna and Turin are situated inside the operational LM area, Valencia and Helsinki are outside. These last city domains and, additionally, the higher-resolution LM simulations are experimental and only validated for the FUMAPEX episodes using scatter plots and FMI's statistical package MMAS (described in D3.3 (Fay et al., 2004)). Results for 10 m horizontal wind speed for 7 stations for this one Valencia episode from 26 to 30 Sep 1999 were evaluated. The scatter plots reveal consistent over-prediction of low wind speeds < 2 m/s and

under-prediction of medium and high winds for all LM resolutions, but with slight improvement for increasing resolution. Statistical performance fluctuates between stations and days with an overall downward trend in absolute error and rmse and rise in correlation coefficient with increasing resolution. Examples for the 48h forecasts of 29 Sep 2002, used in the above example, are shown in Fig. 4.1.

Summing up, the quality of the LM wind fields is slightly increasing with resolution. As the performance of 7 km LM trajectories was shown to be very satisfactory on many occasions, the above results for the wind fields point to on average good quality and even slight improvement of trajectories with increased resolution.

In the course of FUMAPEX WP6, the trajectory model was adapted to 2.8 and 1.1 km resolution and tested for the first time for some FUMAPEX episode cases.

All simulations are performed for different trajectory start levels between ~50m above ground and 700 hPa to show the influence of atmospheric wind shear on the trajectories.

Transition episode, Valencia/Castellon 26-30 Sep 1999

Important feature investigated: diurnal land/sea and upslope/downslope circulations and their combination, development of wind field structure (convergence and subsidence areas) because of their relevance to the evolution of the ozone concentration levels throughout the episode.)

4.1. Sensitivity to vertical and horizontal resolution in NWP model

Trajectories with 7 km/35 levels are compared to trajectories with 1.1 km/45 levels for 29 Sep 1999. A fictitious coastal emission site north of Castellon and just south of the Ebro delta is chosen in order to investigate inland/seaward air transport associated with the development of the land/sea breeze.

For the 7 km trajectories, the onset of the sea wind in the morning is earlier and stronger: For the trajectories starting at 8 UTC, the SE-ward drainage trajectories with 7 km resolution starting in the lowest layers up to 925 hPa turn inland soon while the 1.1 km trajectories for the same start levels turn inland only after a longer path (and merge into ESE-ward trajectories in the higher BL and above, Figure 4.2). On the other hand, these 1.1 km trajectories turn sharply E back to the coast after a few hours while the 7 km ones remain lower and thus move into a more northerly direction following the vertical wind shear. This also agrees with the more NE-ward path of all 7 km trajectories. Near-surface pollutants thus move out of the region with the 7 km trajectories while remaining more local in the 1.1 km case even if this may partly be due to different wind directions in the 1.1 and 7 km LM higher up.

For the 11 UTC trajectory start, the differences are very large, with an inland path for the 7 km trajectories starting below 950 hPa while the inland transport is just starting at the coast for 1.1 km resolution (Figure 4.3). For both resolutions, trajectories show clear upward motion around midday very close to the coastline ($w \sim +0.15$ m/s for LM 1.1 km), reach up to ca. 1600 m, but only the 1.1 km trajectories sharply return back to the coast after about 2 hours. At least in the overall synoptic situation on that day (general NW winds) this may coincide with the upper, seabound branch of the sea breeze circulation. This helps to keep the trajectories very local and may reflect the typical local transport situation with pollutants being transported back and forth in the same region and thus accumulating to high concentrations.

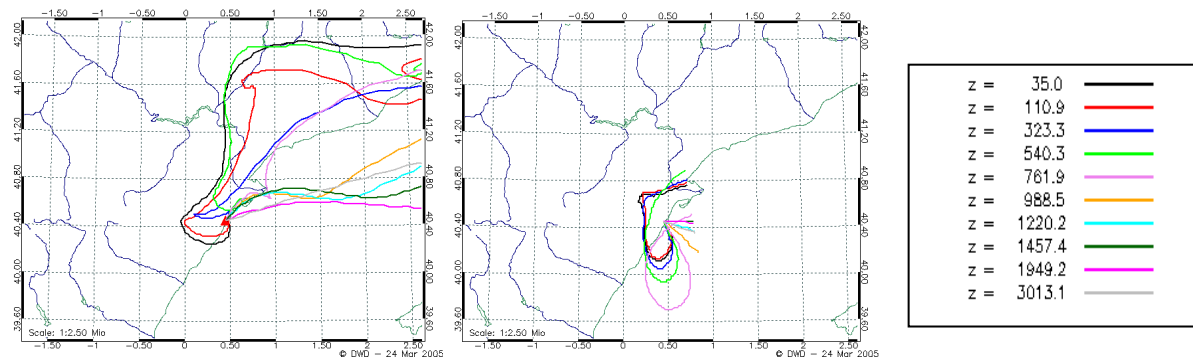


Figure 4.2 LM trajectory forecast for 29 Sep 1999 +8h. Left: 7 km/35 l, right: 1.1 km/45 l levels. Approximated trajectory start levels for 1.1 km run in m (standard atmosphere.)

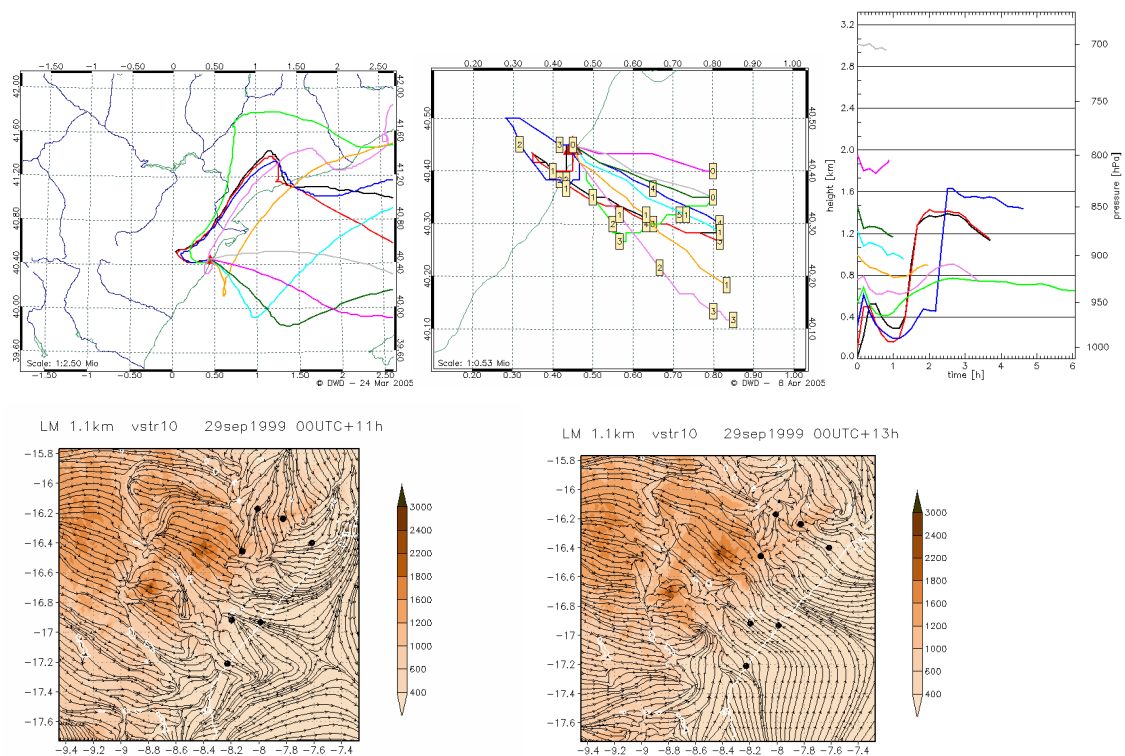


Figure 4.3 LM trajectory forecast for 29 Sep 1999 +11 h. Top: Left: 7 km/35 l, middle and right: 1.1 km/45 l with time markers in hours after start. Approximated trajectory start levels as in Figure 4.2. Bottom: LM 1.1 km forecast, streamlines for 29 Sep 1999, +11 h (left) and +13 h (right), trajectory start near coastal station in the NE.

Investigations of horizontal wind speed in WP3 show that at 11 UTC, the land-sea breeze is generally fully developed in LM 1.1 km and joined to the valley circulation further inland. Near the trajectory start location, convergence lines appear further inland, but also very close to the coast (Figure 4.3 bottom). The low-level trajectories initially move S and rise in some coastal convergence then turn inland and are fully drawn upwards to 1400 to 1600m in the near-coastal convection area after 1 to 2h. They leave the low-level inland airflow and return to the coast in the upper NW-erly airflow and thus retain pollutants closer to the coast. The further trajectory/pollutant pathways cannot be followed here as the trajectories leave the 1.1 km nest already after less than 4 hours.

At 13 UTC, trajectories below 950 hPa start level travel inland for both resolutions, but reach up to twice the height for 1.1 km. Transport is again much more localised back to the coast for 1.1 km (but in a wider circle than for the 11 UTC trajectories) partially due to the more westerly winds higher up compared to SW-erly winds lower down in the 7 km simulations.

Evening and night trajectories (not shown) show the turning of low level trajectories NE-ward at 19 UTC as a transition from the sea to a land breeze with E-ward trajectories at 23 UTC.

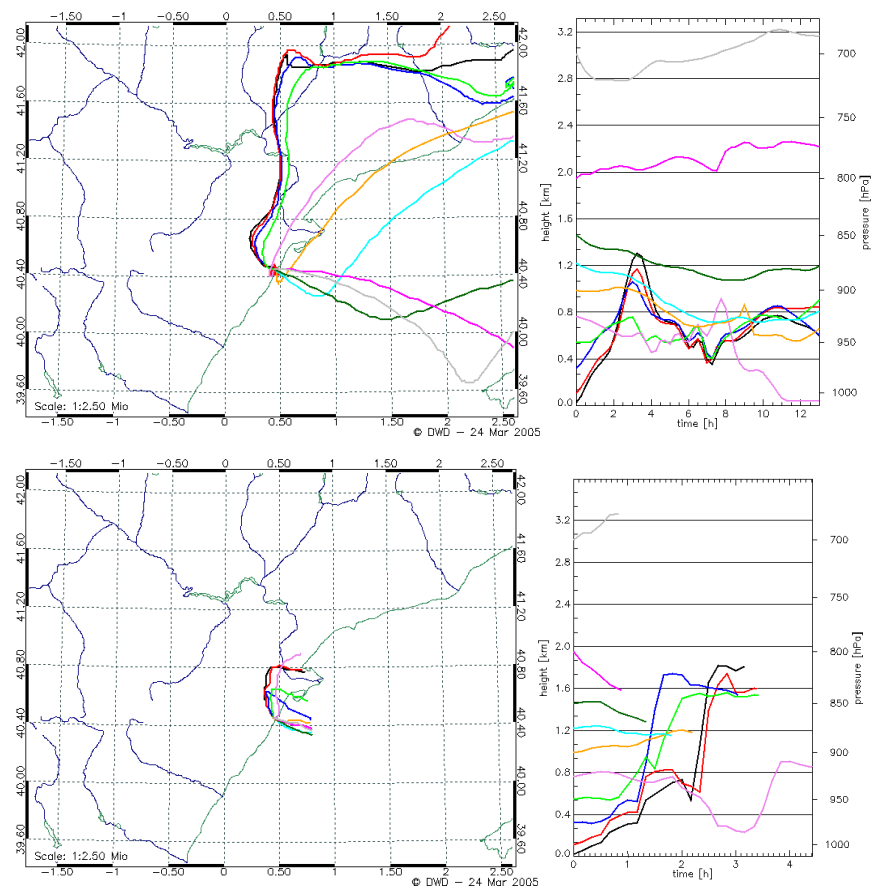


Figure 4.4 LM trajectory forecast for 29 Sep 1999 +13 UTC. Top: 7 km/35 l, bottom: 1.1 km/45 l. Approximated trajectory start levels for 1.1 km as in Fig. 4.1.

Summary

For the cases considered, the 1.1 km trajectories show a much more local behaviour than the 7 km ones and, therefore, probably the better overall performance for the Valencia region. Only the more likely earlier start of the sea breeze (confirmed also with RAMS 1 km simulations in comparison with LM 1.1 km in WP3) is captured better with LM 7 km trajectories (or in the long forecast, see below). For the chosen cross section the 1.1 km trajectories reflect the coastal and near-coastal convergence simulated in LM with strong upward movement and fast return to the sea. This reflects the typical observed pattern of pollutant recirculation leading to high episode concentrations. Further cases will be evaluated to investigate the transport in well developed, combined sea and upslope breezes reaching far inland.

Thus, the LM with high resolution and the corresponding trajectories seem to be able to capture even very small scale local circulations that dominate pollutant transport and concentrations in this complex coastal mountain area.

4.2. Sensitivity to forecast length

Comparison short/long forecast for 29 Sep 1999

In this experiment, trajectory forecasts for identical trajectory start times are calculated using a) a ‘short’ LM forecast starting at 00 UTC on the same morning, b) the ‘longer’ LM forecast starting at 00 UTC on the previous morning.

For the trajectory start on 29 Sep, 8 UTC, the trajectories for 7 and 1.1 km resolutions are much more similar in the long forecast starting at +32h on 28 Sep than in the short one starting at +8h on 29 Sep: For the long forecast, 7 km and 1.1 km trajectories have very similar paths in horizontal and vertical direction and both show the more expected early onset of inland transport (compare Fig. 4.5 to Fig 4.2). The trajectories starting with the +35h forecast on 29 Sep 11 UTC, are again much more similar for both resolution sets than the trajectories from the short +11h forecast from 29 Sep. They both show northward trajectories and thus less sea wind transport due to stronger S wind components at the trajectory heights which are up to 700m lower than for the 29 Sep short forecast trajectories of both resolutions. However, a 90° seaward turn is observed for both sets at night with downward moving trajectories probably reflecting the onset of the drainage flow from the coastal mountains. The 7 and 1.1 trajectories are also much more similar for the long than the short forecasts for starting times of 29 Sep, 13 UTC.

As the trajectory scheme is of high numerical accuracy (see 4.) the quality of the trajectories depends on the quality of the LM wind fields. 7 km trajectories are based on the operation LM model. Initial conditions in the LM are derived with an advanced four-dimensional data assimilation cycle based on a nudging analysis scheme that creates little imbalance. From experience, the operational LM is robust concerning initial imbalances. This leads to small spin-up times (less than 1h for many FUMAPEX-relevant parameters (except precipitation and cloudiness and in high mountains)). Only the lateral boundary data have to be provided from Global Modell (GME) forecasts, with still 60 km in FUMAPEX simulations and now operational 40 km. This nesting creates numerical noise which is effectively avoided by gradually blending the variables of the high-resolution model to those of the driving model within a relaxation zone using the relaxation boundary conditions similar to Davies for one-way nesting (Doms and Schättler, 2002). There is no systematic deterioration with time of the 48h forecast (7 km LM) of wind direction and a slight increase <0.5m/s of rmse for wind speed for the average and/or different subgroups of 16 WMO stations around (potential) European FUMAPEX target cities evaluated for 1 year in D3.4 (Fay et al., 2005)(Fig. 4.5 right). For the experimental 2.8 and the 1.1 km LM nest simulations in FUMAPEX, no data assimilation and initialisation, but boundary relaxation was used. The initial and boundary values were interpolated from the higher LM nest, but with the LM–adapted interpolation tool LM2LM. Additionally, even the innermost LM nest has a relatively large size of 270x200 km². In the many 2.8 and 1.1 km simulations and episode-relevant variables investigated in WP3, spin-up problems were rarely observed and rather small. These arguments lead to the conclusion that spin-up and forecast length errors for wind speed and direction should be small for 48h forecasts for all resolutions and that the deterioration of long compared to short forecasts is on average slow.

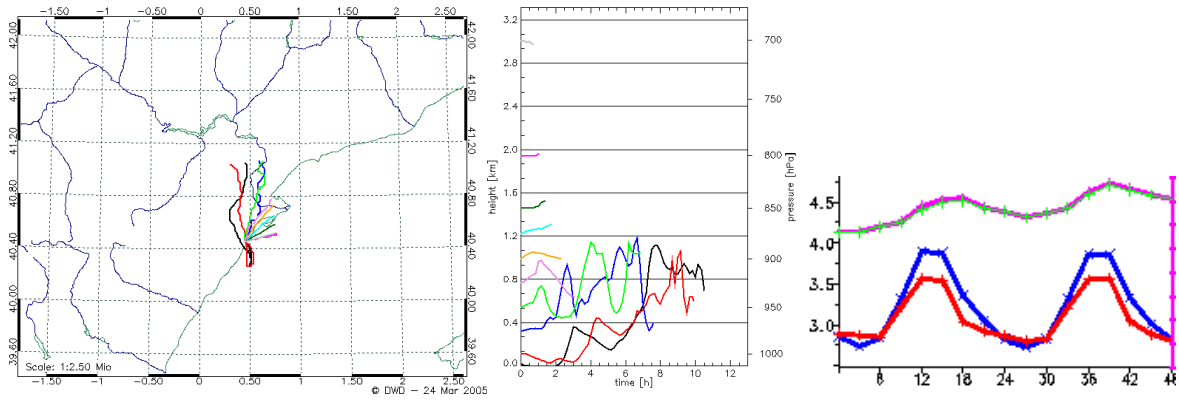


Figure 4.5 Long LM forecast of 28 Sep 1999, 00 UTC +32 hours for trajectory start on 29 Sep 1999, +08 UTC. Left: 7 km/35 l, middle: 1.1 km/45 l. Approximated trajectory start levels for 1.1 km run as in Figure 4.2. Right: statistical scores for 10m wind speed [m/s] for 48h forecast [h] of LM 7 km at 16 WMO stations (see D3.4, Fay et al., 2005) for 3 Sep 2003 to 31 Aug 2004, pink: rmse, blue: observation, red: forecast.

Conclusions

Due to the advanced techniques of 4D continuous nudging data assimilation and relaxation boundary conditions, spin-up time and error and boundary-induced errors are small. 1 year statistical evaluation also shows rmse error rising for the trajectory-relevant wind speed by only $<0.5\text{m/s}$ for the 48h forecast. Thus, the long forecast deteriorates on average only slowly compared to the short forecast.

In the test case, the timely onset of the sea breeze is better captured in the long forecast than the short one for 1.1 km trajectories. In general though, the longer forecast seems to reduce differences between 7 and 1.1 km trajectories and leads to reduced localisation and probably deterioration of the 1.1 km forecast

5. TARGET CITY OSLO - UAQIFS EXPERIMENTS

The episode 5 of the target city Oslo is described in terms of observed meteorological conditions and urban air quality in D1.2 (Valkama and Kukkonen, 2003). The meteorological forecasts for this episode are further illuminated in D3.3 (Fay et al., 2004). The analysis of D3.3 is limited to the days with the highest pollution levels and the strongest surface inversion. For a study of possible model improvement we will take into account the whole period of inversion build up and break down.

The first days of January 2003 start with temperatures down to about -20 °C. During the 6th of January warmer air masses are transported in from north-west at higher altitudes, creating a strong inversion during the 7th, 8th and 9th of January in the central city area. On the 7th hourly NO₂ values up to about 600 µg/m³ are observed, the highest NO₂ values ever observed in Oslo. High PM_{2.5} values observed as well (152 µg/m³ at Kirkeveien). Relatively high concentration levels during night-time at several measurement stations indicate the existence of local recirculation and/or stagnation within the central city area.

The NWP models of the Oslo UAQIFS are two nests (3 and 1 km) with the MM5 model (Grell et al. 1994) nested HIRLAM (Undén (ed.), 2002) in 10 km horizontal resolution.

The vertical temperature gradient is measured and computed at the site Valle Hovin. It represents the near surface conditions. The gradient simulated at Valle Hovin is overestimated from the NWP model during the whole episode. By inspection of the temperature in the different model layers it turns out that the temperature close to the surface (2m) is better forecasted than the temperature in 8 and 25 m (model layers 17 and 16) which are too high.

The vertical temperature gradient presented for Tryvann is an estimated value from the measurements of 2m temperature at Blindern and Tryvann. These observation sites are located with only a few kilometres distance but with a height difference of 400m. The resulting gradient is thus an indication of the stability in a much deeper atmospheric layer. The vertical temperature gradient over the deeper layer is underestimated in the days when deep layers of stability are indicated in the observations. In the interpretation of this result one must have in mind that the Tryvann temperatures are not representative for the free atmosphere at 500m.

The operational setup of the Oslo UAQIFS gives a significant underestimation of the NO₂ levels during the episode. In addition the NWP forecasts slightly overestimate the surface temperature in the city and overestimate the wind speed.

Some important meteorological conditions of the critical hours of this episode are described in figures 5.2 - 5.5. In the evening January 6 at 19 UTC (Figure 5.2 left) it is seen that the northerly flow has reached the elevated areas around Oslo city. Horizontal wind speed at 10m is up to 8 m/s at Tryvann. The wind speed in central town is low (less than 2.5 m/s), and there is an easterly cold air drainage along cross section C. After another 11 hours (January 7, 06 UTC, Figure 5.2 right) the easterly flow is broken up by the stronger northerly winds. The temperature has increased several degrees.

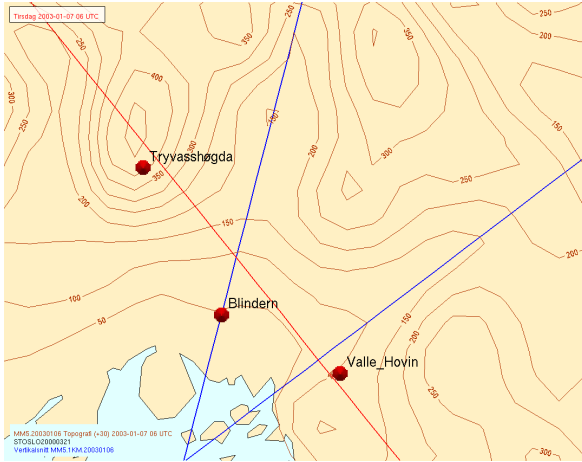


Figure 5.1 Section of MM5 1 km model domain showing the central parts of Oslo. Observations sites are marked red. Topography is shown with 50m isolines. Positions of vertical cross sections (A - NW-SE, B - N-S, C - NE-SW) are also shown with straight lines.

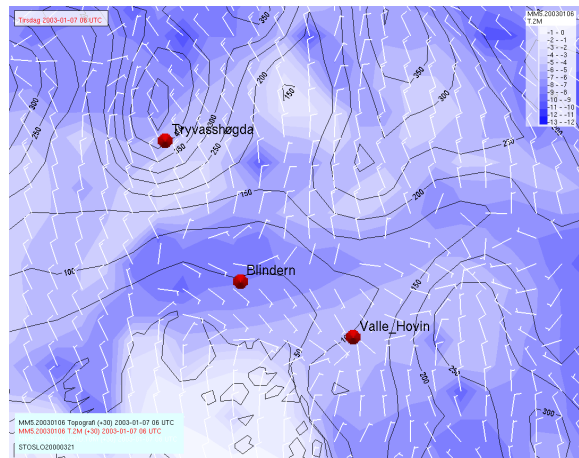
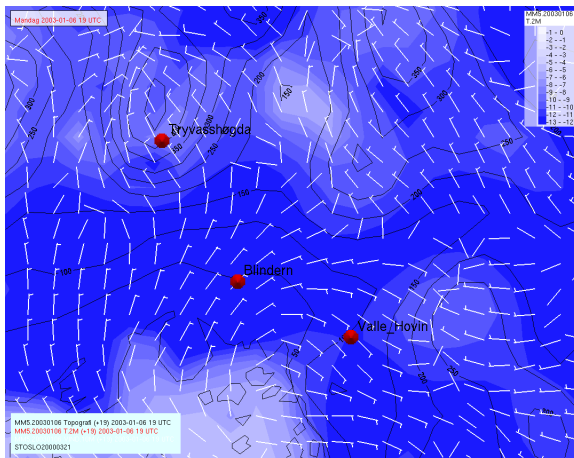


Figure 5.2 Surface wind fields (white arrows), 2m temperature (colour) and topography (black contours) from MM5 1 km initial time 20030106 19h forecast (left), 30h forecast (right).

At 19 UTC the flow along cross section A is following the terrain in the hill down from Tryvann. When reaching the cold pool in the town the flow follows the density surfaces and the warm air floats on the top of the cold pool (Figure 5.3 left). During the next hours the wind speed increases significantly and penetrates down to the cold pool (Figure 5.3 right).

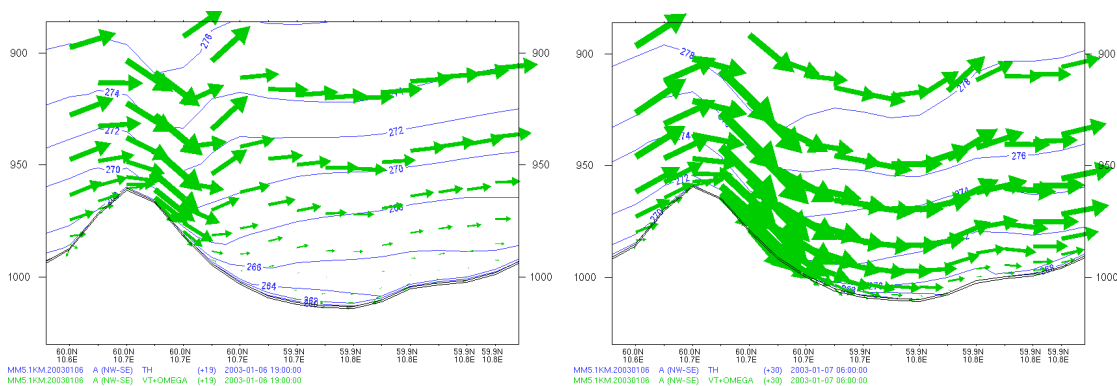


Figure 5.3 Vertical cross section (A) showing velocity vertical and tangential to the cross section (green) and potential temperature (blue), time as in Figure 5.2

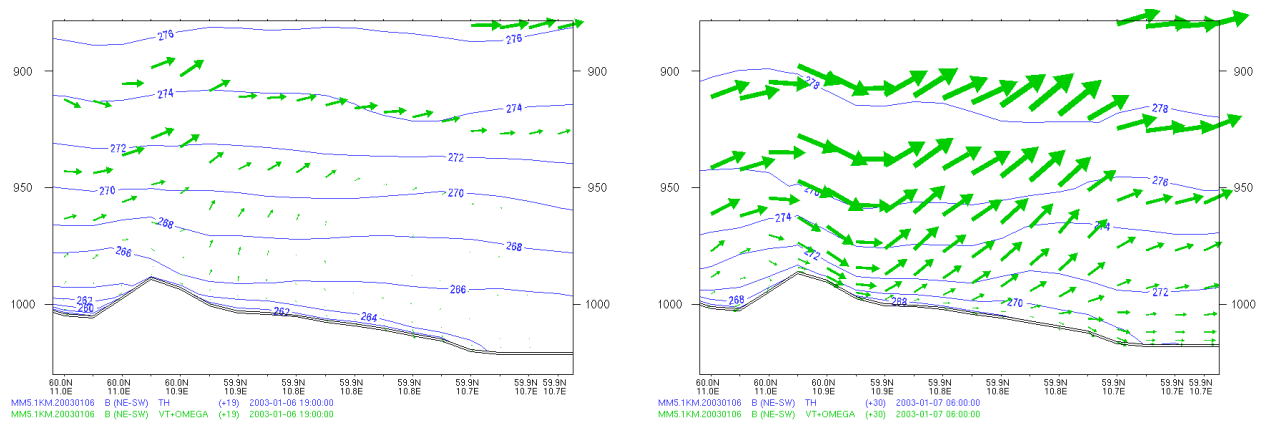


Figure 5.4 Vertical cross section (C) showing velocity vertical and tangential to the cross section (green) and potential temperature (blue), time as in Figure 5.2

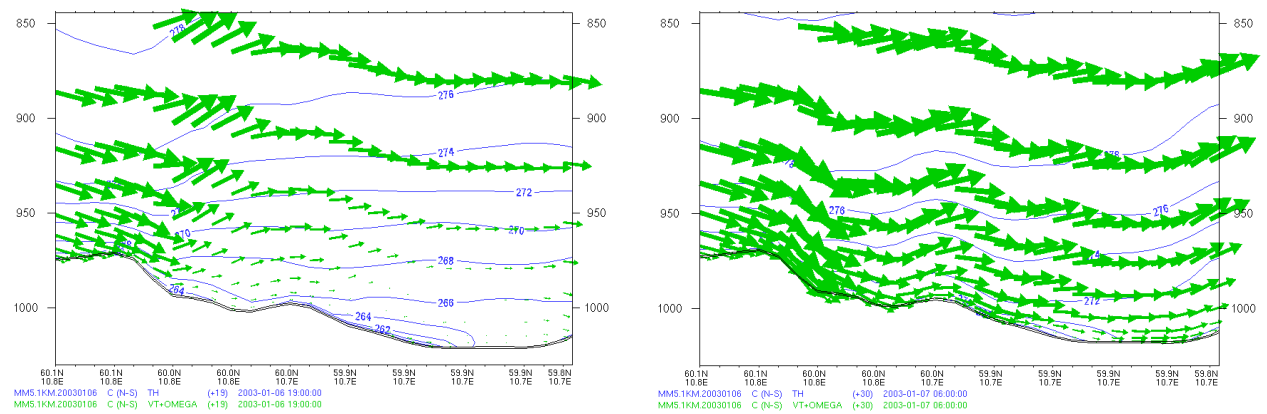


Figure 5.5 Vertical cross section (B) showing velocity vertical and tangential to the cross section (green) and potential temperature (blue), time as in Figure 5.2

The flow along cross sections C and B for the same time can be followed in Figure 5.4 and 5.5 respectively.

According to the observations at Tryvann, Blindern and Valle Hovin the timing of increase in wind speed and temperature in the elevated areas is quite good, while the break up of the inversion layer is too fast and too effective in the model. The evolution of temperature, the vertical temperature gradient and the wind speed at Tryvann, Blindern and Valle Hovin are shown in Figure 5.6. A large temperature difference between level 0m and 2m in MM5 at Valle Hovin reveals a stable situation in the model. Also temperature is increasing continuously with height. Corresponding observations show that the coldest level is in 8m thus the strongest inversion layer between 2 and 8m from January 7th. Observations at Blindern and Tryvann show a deep inversion layer developing from the same time. Wind speed is significantly higher in MM5 than observed, in particular at Blindern where calm conditions dominate from the beginning of the inversion period.

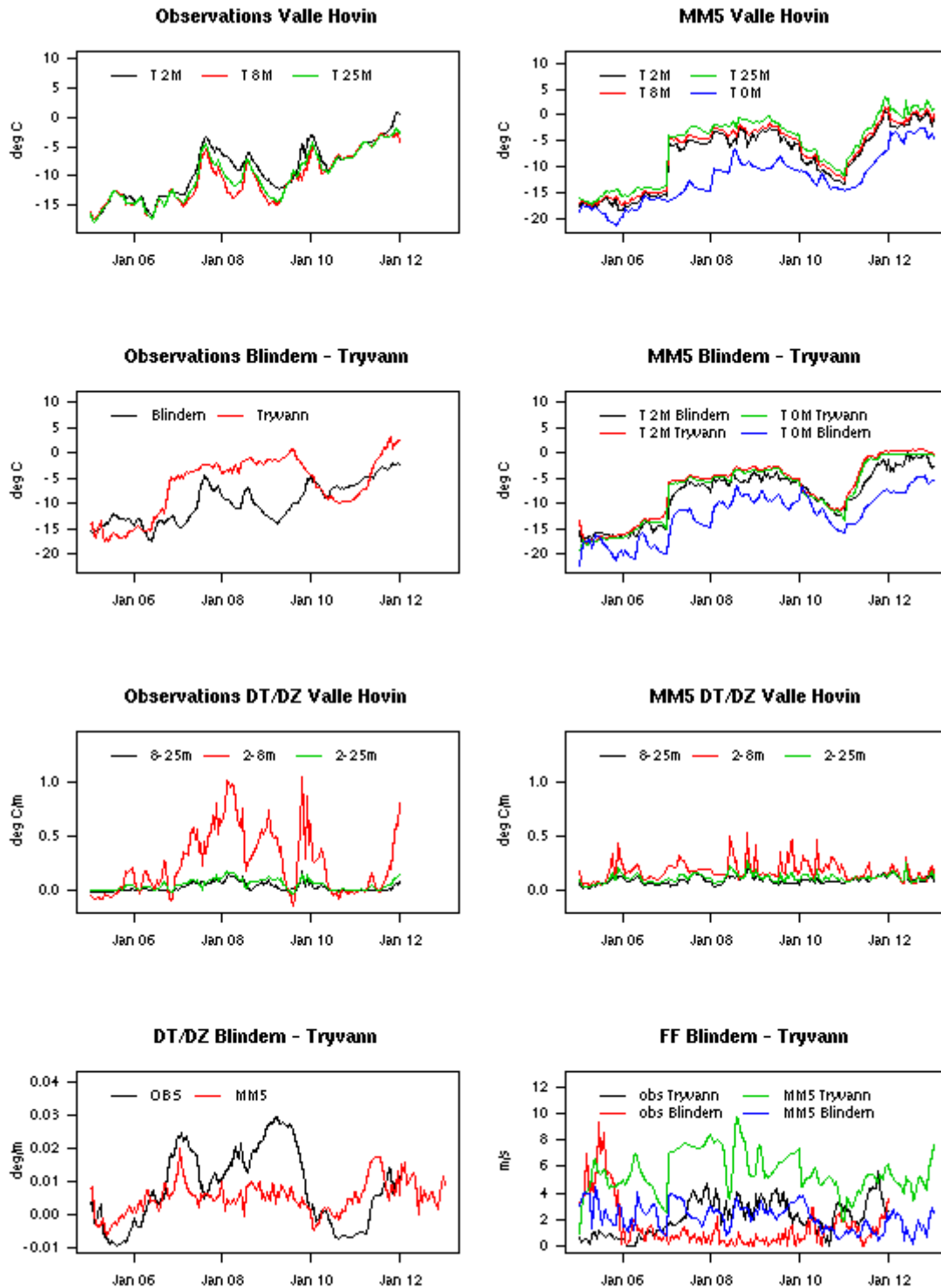


Figure 5.6 Time series of observed (left) and modelled (right) temperature at Valle Hovin (top), Blindern and Tryvann (second row), vertical temperature gradient at Valle Hovin (third row) and vertical temperature gradient Blindern-Tryvann (bottom left) and wind speed observed and modelled at Blindern and Tryvann (bottom right).

5.1. Vertical resolution

At *met.no* the MM5 model is run in operational configuration with 17 vertical layers. 9 of these layers are below approximately 1500m, as shown in Figure 5.7.

The sensitivity to vertical resolution has been investigated by additional simulations with 26 vertical model layers. The 26 layers (Figure 5.8) have been chosen so that the three lowermost layers are identical to the 17 layer version. This is to avoid impact on the forecasts related to the effect of pollution sources being located in another layer of the UAQ model.

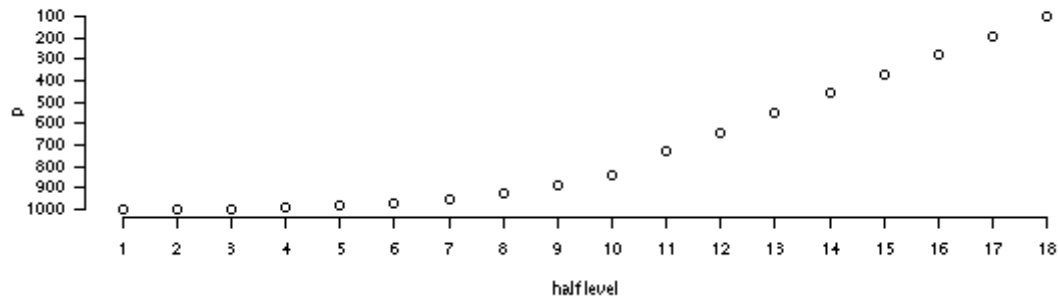


Figure 5.7 Pressure of the 17 model levels in the operational configuration of MM5 at met.no

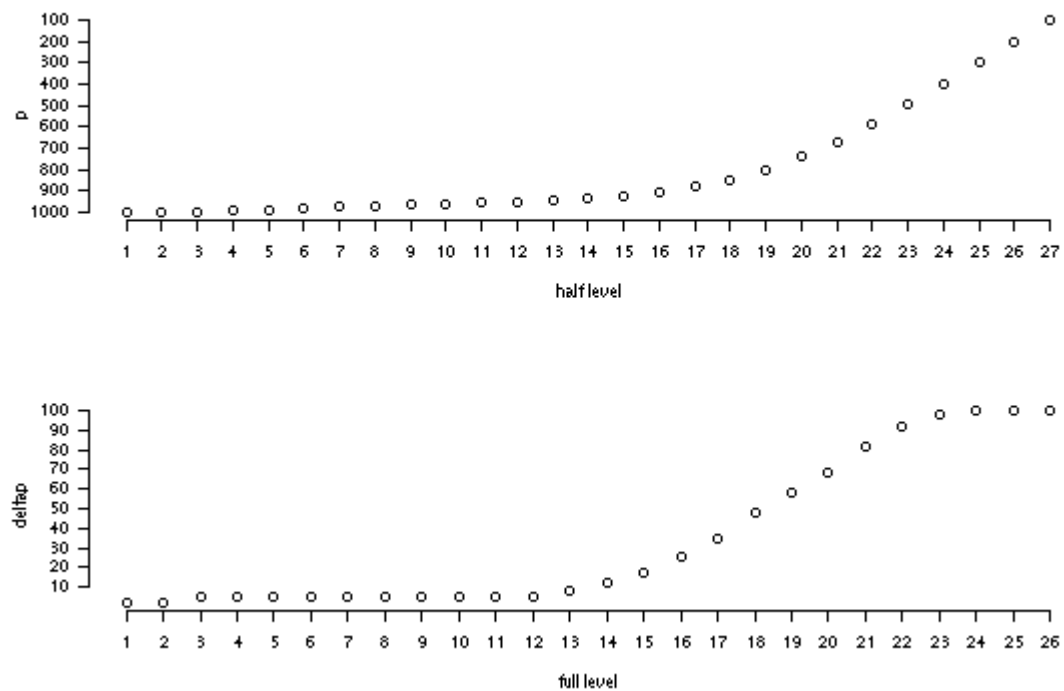


Figure 5.8 Pressure of the 26 model levels in the experimental configuration of MM5 (top) and layer thickness in hPa (bottom)

The effect on the forecasts of near surface temperature and wind speed by increasing vertical resolution in MM5 is limited, at least when the lowermost three layers are kept unchanged. The forecasts for the station Valle Hovin are shown in Figure 5.9.

The wind forecasts seem to be slightly more sensitive to vertical resolution than are the temperature forecasts.

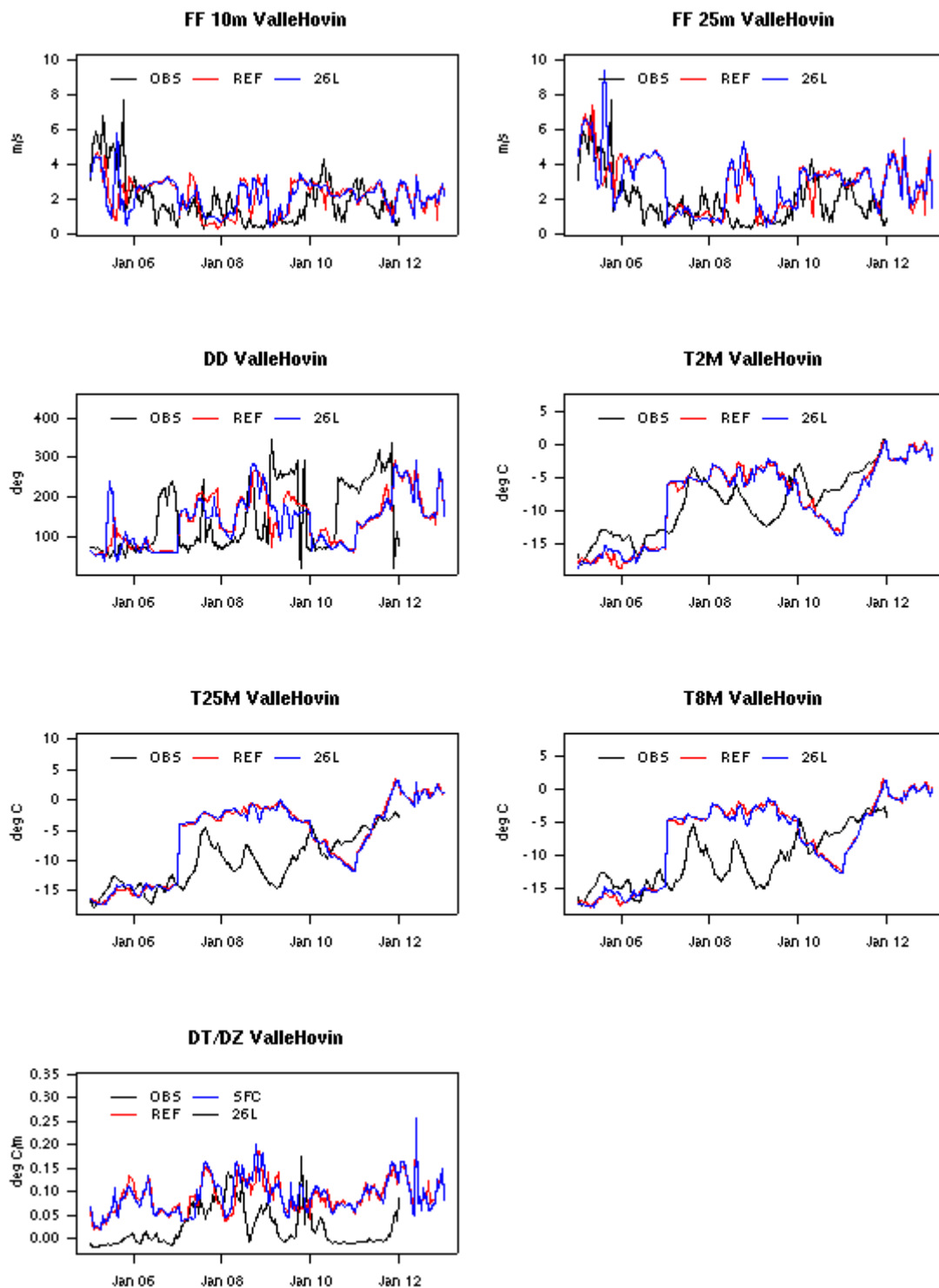


Figure 5.9 Observed and modelled meteorological parameters at the cite Valle Hovin.

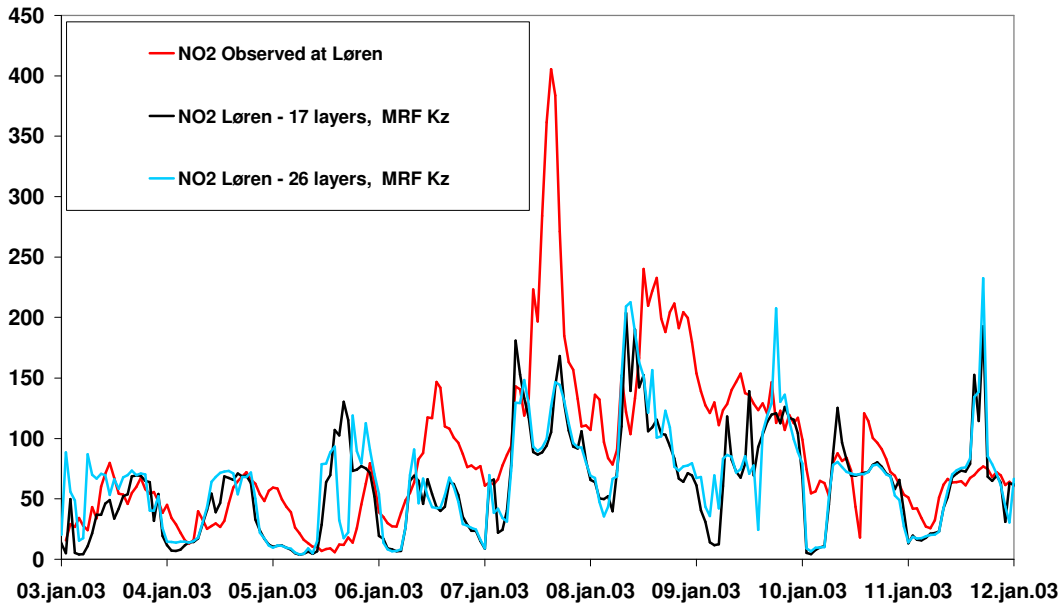


Figure 5.10 Observed and modelled NO₂ at Løren, an air quality monitoring site approximately 1 km away from Valle Hovin.

Test with increased vertical resolution does not lead to significant improvements. Still the temperature and the wind spread increases too early compared to observations, and the forecasted air quality is only marginally altered by the increased resolution, as seen in Figure 5.10. One explanation could be that in the experiment the three lowermost model layers, i.e. the layers within which the emission of pollutants are distributed, are kept unchanged in the NWP model. By changing the definition of the layers receiving the emissions it would have been difficult to address the observed changes to the model's response to vertical resolution. The change in distribution of emission sources on the vertical levels would contribute as well, as illustrated in Figure 5.11

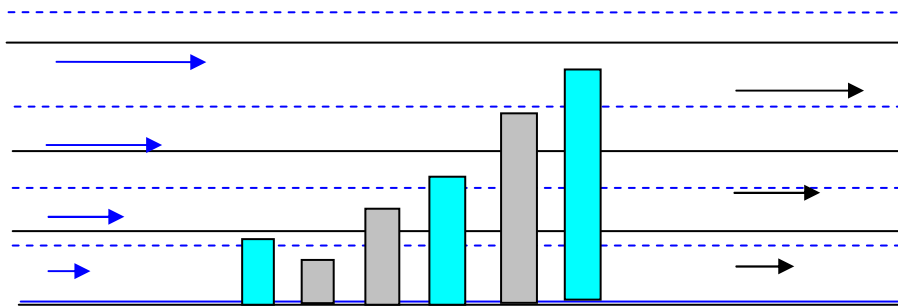


Figure 5.11 Schematic illustration of the distribution of emissions on vertical layers. By a hypothetical increase in vertical resolution from three layers (black solid lines) to two layers (blue dashed lines) three out of six (blue boxes) emissions are displaced to a higher numbered layer. The horizontal velocity will represent an average over a layer which is differently defined in the higher resolution. Four out of six (grey boxes) are exposed to a different horizontal velocity due to the new

definition of the corresponding layer. Lengths of arrows indicate horizontal wind speed in the middle of the higher and lower vertical resolution layers, blue and black respectively.

These results indicate that in situations with little vertical exchange (i.e. during stable conditions) the increased resolution in the higher levels of the NWP model will not have a strong impact on the low level forecasts. This interpretation is confirmed when looking at two times when the forecasts show differences: In the late hours of January the 5th the vertical stability is less in the 26 levels run. This leads to increased wind speed and higher temperature in 2m which again leads to a reduced NO₂ level. The experiment is thus not designed to investigate the impact of increased vertical resolution in the planetary boundary layer during neutral and unstable situations. There is however an indication that there would be more impact on cases with more "dynamics" as in e.g. a "spring-dust" episode.

5.2. Forecast length

The UAQIFS for Oslo is designed for providing UAQ forecasts for +24 to +48 hours. A longer forecast length is not possible at present due to the operational routines of the HIRLAM models which provide input data to MM5. The sensitivity to forecast length is studied by comparing the original forecast by the one obtained by using the +1 to +24 hours forecasts instead.

Figure 5.13 shows the results for meteorological parameters at Valle Hovin. There is no obvious sign that the shortest forecasts are closer to the observations than the longer forecasts. On the contrary the short forecasts are showing clear signs of unbalances in the initial temperature fields. The 2m temperature is 2-3 deg. lower in the first hour of the forecasts than the balanced level which is reached after 2-3 hours. Comparing the time series for surface temperature (T 0m) and temperature in 8m it seems clear that it is not the surface field that is out of balance, rather the atmospheric temperature. The shorter prognosis period do not lead to any detectable improvement in the forecasted air quality either, as shown in Figure 5.14.

The initial surface fields of the model suffer from at least two weaknesses. First the initial field is result of an analysis performed on a grid that is much coarser than the MM5 grids. The analysis is interpolated from 20*20 km to 10*10 km and further to 3*3 km and 1*1 km. In addition the analysis is performed on pressure surfaces. Thus the initial state in MM5 results from just a few values interpolated to a high resolution grid, the temperature and geopotential is adjusted to high resolution orography and the winds are in balance with the geopotential and the temperature fields. Small scale variability in the fields results from orography alone. In addition the land surface fields including temperature and soil moisture suffer from insufficient information on land surface property and insufficient resolution in the observed state, as surface temperature and snow cover.

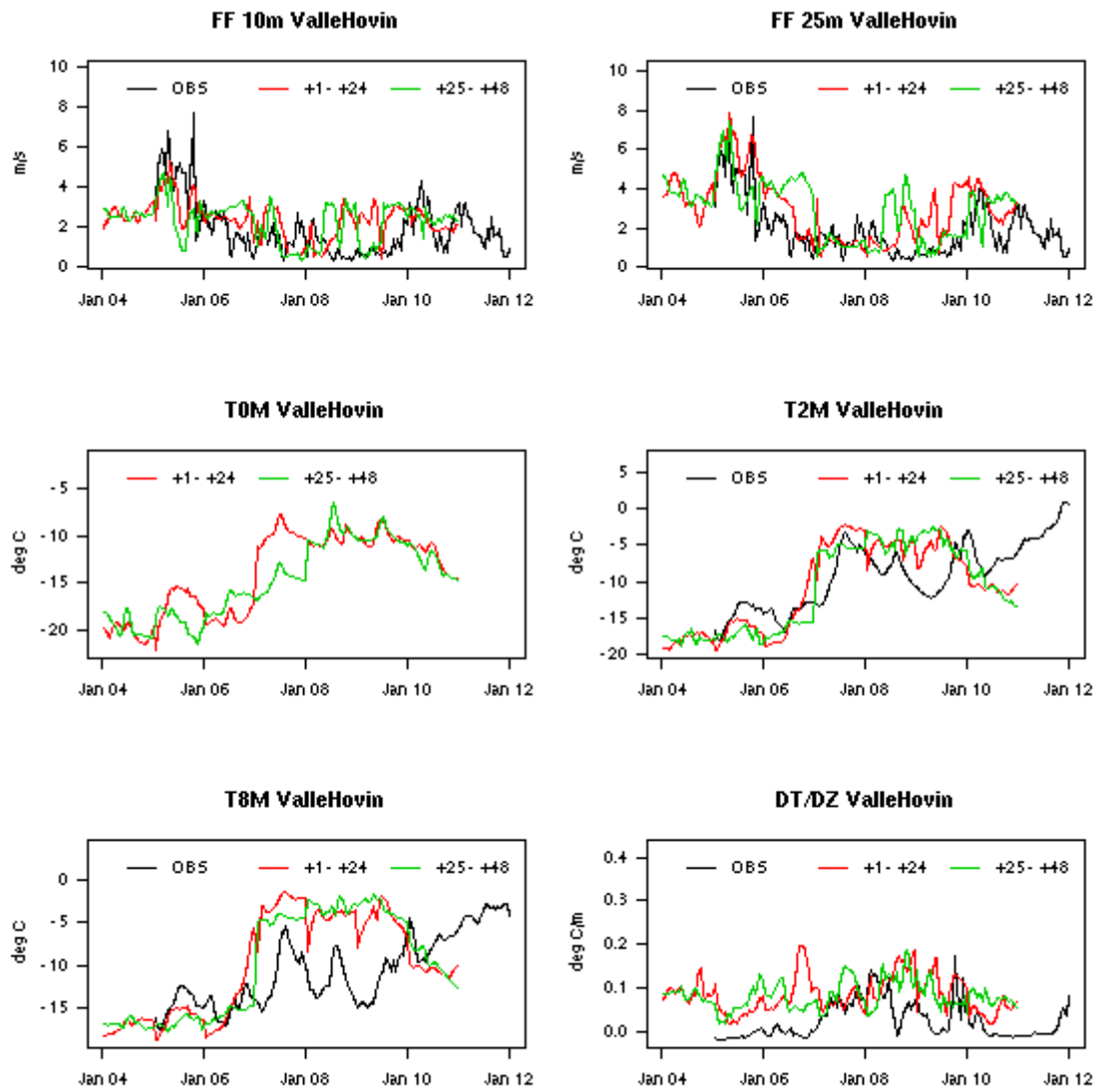


Figure 5.13 Observed and modelled meteorological parameters at the cite Valle Hovin.

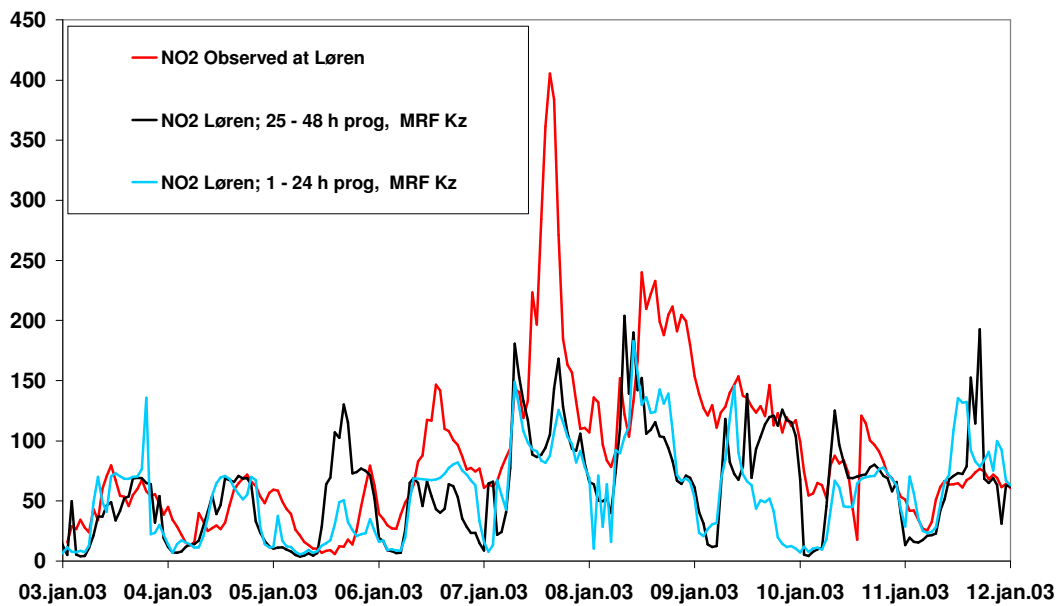


Figure 5.14 Observed and modelled NO₂ at the air quality monitoring station Løren, close to Valle Hovin.

On the basis of this finding we have also run MM5 with only initialization at the beginning of a 170 hours simulation. The idea is that the model would need a physically realistic time of several days to build up a pool of cold air near the surface cold. The relative coarse vertical resolution of the input data from HIRLAM was assumed to disrupt the fields when forced into MM5 each 24 hours.

As seen from Figure 5.15 the continuous forecast running from January 3rd is smoother, in particular in the temperature time series. The jump in the temperature is eliminated, but still the near-surface warming comes too early compared to the observations. The wind speed is still increasing though slightly less and the evolution is somewhat delayed. The observed wind speed during the most heavily polluted period is still observed to be very much lower than simulated.

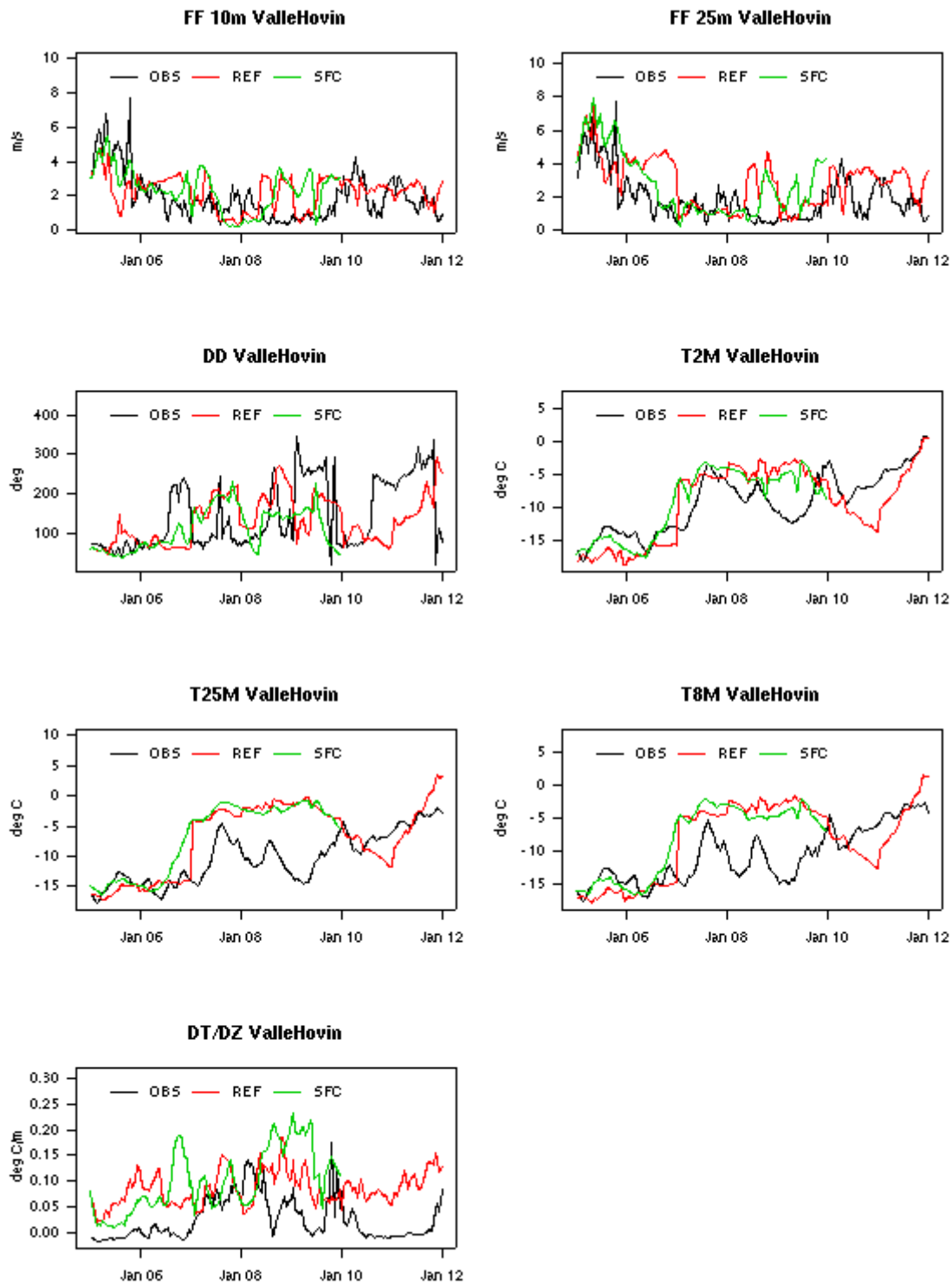


Figure 5.15 Observed and modelled meteorological parameters at the cite Valle Hovin.

5.3. Planetary boundary layer parameterizations

The operational configuration of MM5 in Oslo UAQIFS (Grell et al., 1994) uses the so-called MRF turbulence scheme (Hong and Pan, 1996). The MM5 model has 7 different options for PBL parameterization of which the following have been tested: (1) The Gayno-Seaman scheme, hereafter GSE (Shafran et al., 2000) which is a TKE-predictive 1.5-order closure scheme, where the eddy diffusivities are functions of TKE and mixing length scales, (2) the Blackadar scheme, hereafter BLD (Blackadar, 1976, 1979, Zang and Anthes, 1982) which is a K-theory scheme with eddy diffusivities calculated from the Richardson number and the Blackadar length scale and (3) a modified MRF scheme, hereafter MRFE (Sorteberg,) where the MRF stability functions have been redefined for stable conditions according to the Richardson number formulations of Louis et al. (1982) and applying parameter values proposed by Beljaars and Viterbo (1998). These are all compared to the default v3.4 MRF named REF in the figures.

The operational MM5 configuration produces too strong near surface inversions compared to the temperature measurements at 2, 8 and 25m at Valle Hovin. The suspicion is therefore that the vertical temperature exchange is too low. However the wind speed in low levels is usually too high in stable low wind situations. The modified version of the MRF scheme is developed in particular to solve this problem while the reason for testing the other schemes is more general.

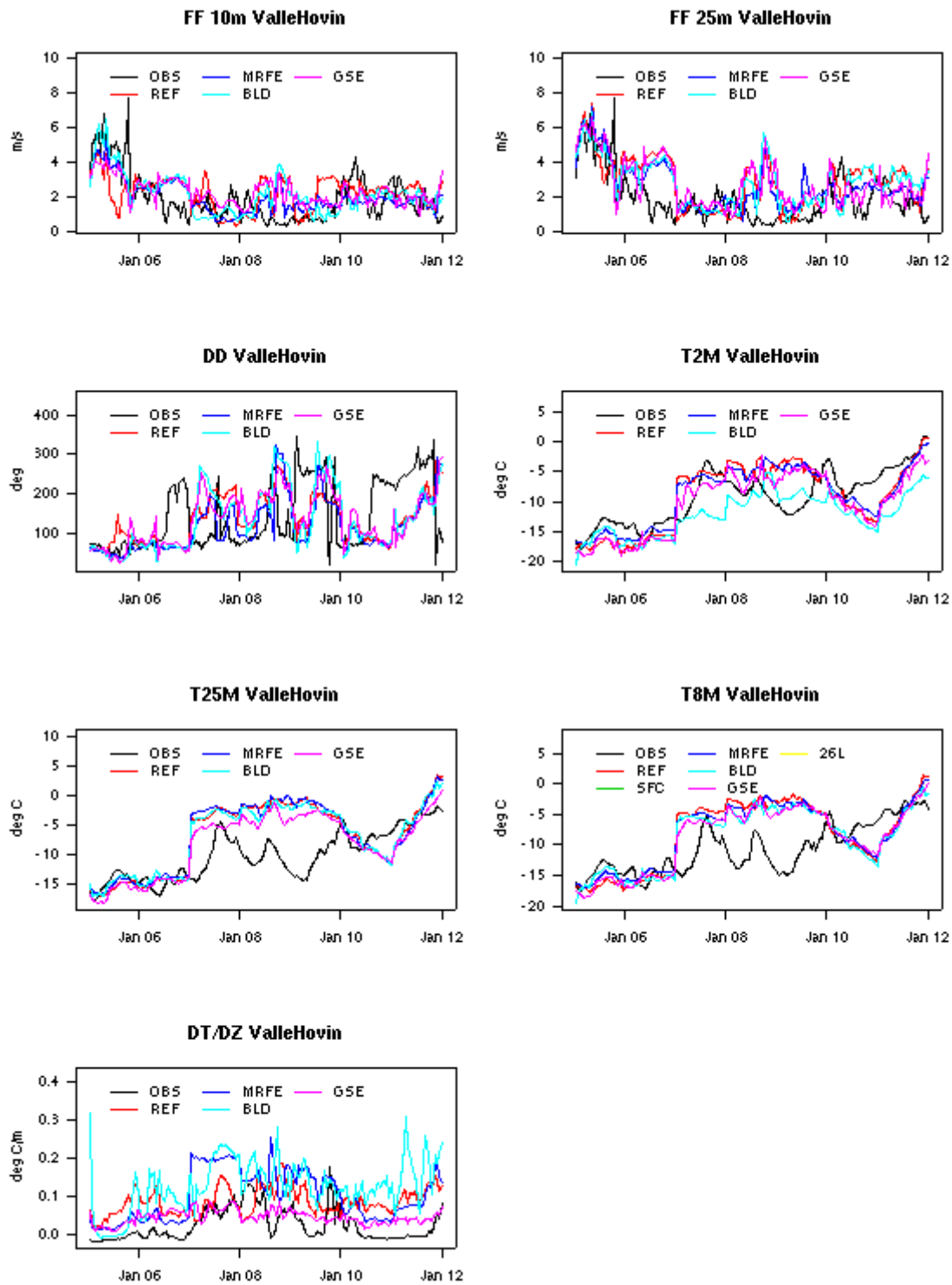


Figure 5.16 Meteorological parameters from MM5 compared to observations at Valle Hovin.

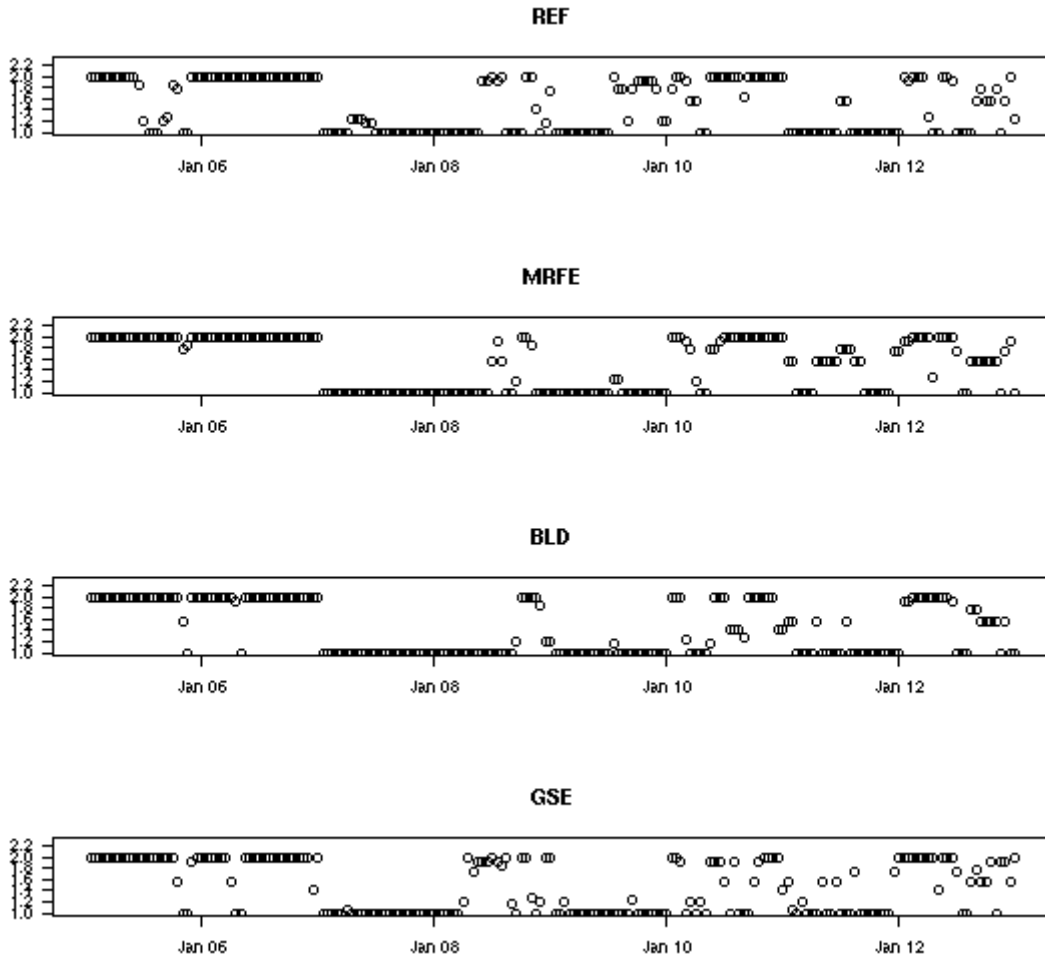


Figure 5.17 Stability regime defined by four different parameterization schemes for the boundary layer. Regime is defined from Richardson number (RN) as night-time stable conditions (regime=1) when RN is greater than 0.2, damped mechanical turbulent conditions (regime=2) when RN is between 0 and 0.2, forced convection conditions (regime=3) when RN is equal to 0 and free convection conditions (regime=4) when RN is less than 0. Values between the integers result from interpolation between gridpoints with different regimes to station location.

From the stability regime plots in Figure 5.17 it can be seen that all parameterization schemes more or less agree on the stability conditions in this particular situation. A period with damped mechanical turbulence (regime 2) is replaced by stable conditions (regime 1) from the January 6th late afternoon. The timing is identical, only the amount of turbulence around January 10th is differing somewhat. The reference version returns to regime 2 12 hours earlier than the other schemes, which can also be seen as an earlier increase in wind speed (red line upper left in Figure 5.16). The vertical temperature gradient is however more varying (Figure 5.15), which only means that the Richardson number and the stability regime are more robust parameters than the vertical temperature gradient between level 17 and 16 in the model.

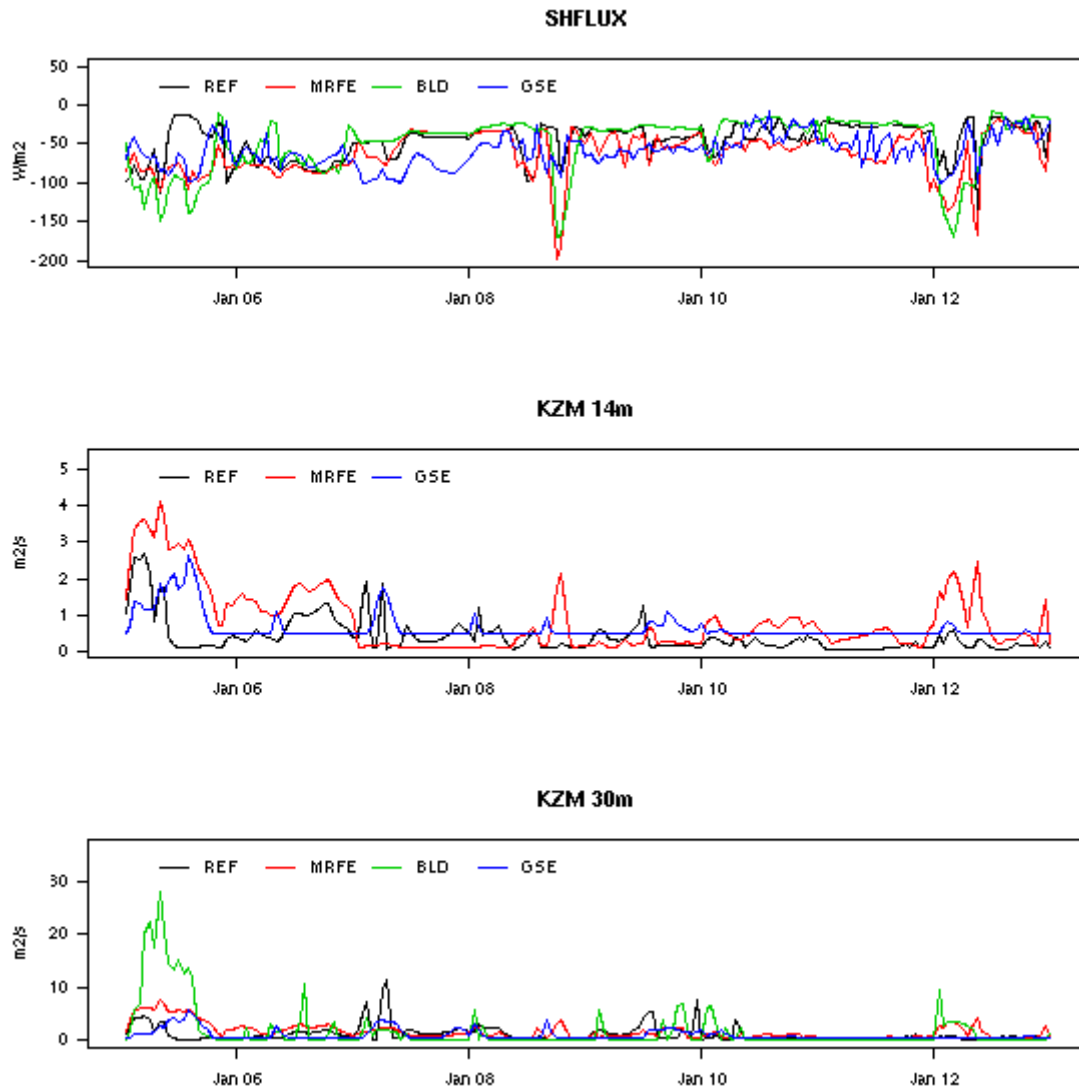


Figure 5.18 Fluxes calculated for the site Valle Hovín. Surface sensible heat flux (top), momentum diffusion coefficient between the two lowermost model layers (middle), momentum diffusion coefficient between layer 16 and 15 (bottom).

Surface sensible heat fluxes are directed upwards during the entire period from January 5th to 12th, thus surface cooling is dominating. Diffusion coefficients for momentum are small in all parametrization schemes, indicating that all the schemes are "doing their job", that is to inhibit vertical exchange of momentum during stable conditions (Figure 5.18).

The resulting UAQ forecasts based on the different schemes are shown in Figure 5.19. From the curves in this figure it is seen that none of the schemes are able to capture either the extreme observed pollution levels or the observed night time concentration build-up, during the three day period from the evening of the 7th to the evening of the 10th.

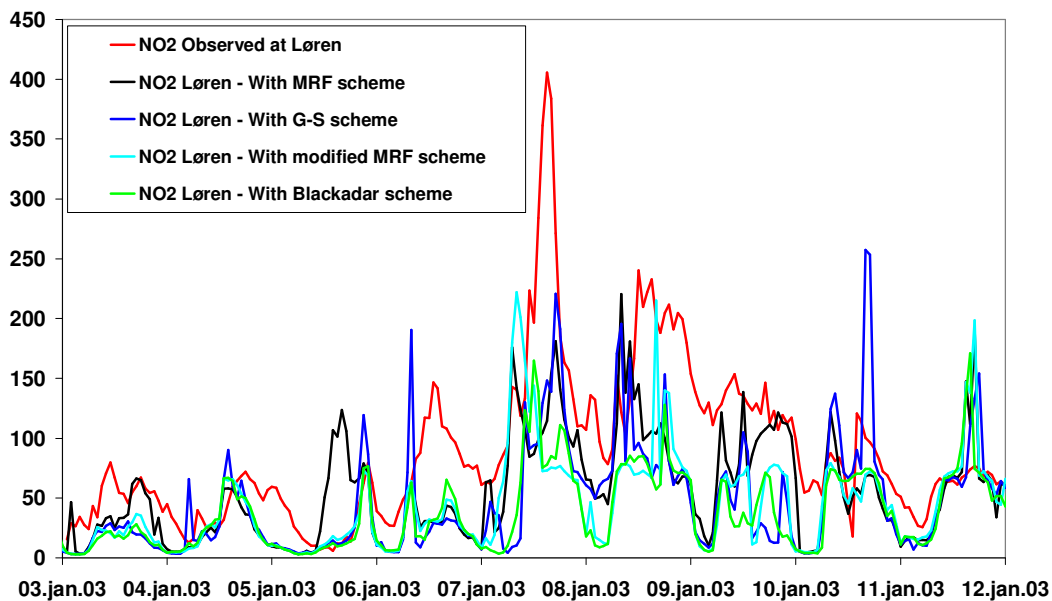


Figure 5.19 Observed and modelled NO₂ at the air quality monitoring station Løren, close to Valle Hovin.

The following general conclusions can be drawn from the above results:

- All of the schemes predict almost zero surface layer turbulence during the pollution episode.
- Surface layer wind speeds are generally too high during the three day pollution episode.
- MM5 generally produce a too strong temperature inversion between the two lowermost model layers.
- The above findings are valid for all of the turbulence schemes that have been tested.
- Application of different turbulence schemes in MM5 leads to clear differences in the AQ forecast, but the general underestimation and lack of concentration build-up during night time during the three-day pollution episode persists.
- All of the turbulence schemes predict more or less zero turbulence between the lowermost model layers during the episode, thus inclusion of enhanced dispersion by urban effects will not improve the AQ-forecast.

5.4. Conclusion

The challenging problem of the stable boundary layer and the winter time inversions combined with complex orography is illuminated by sensitivity studies of the MM5 model. What comes out is that the model's failure to describe the meteorology is not related to forecast length or to the choice of the available planetary boundary layer parameterizations. The break up of the inversion is not caused by vertical turbulent exchange of heat and momentum, but by horizontal flow. As long as the surface wind is overestimated the NO₂ levels will inevitably be underestimated from the air quality model as well. The role of vertical resolution is more difficult to establish. Additional sensitivity tests on the meteorological model alone, without having to cope with the emission level problem, could help to understand how the vertical resolution close to the surface influences the flow.

6. TARGET CITY OSLO - TRAJECTORY MODEL SIMULATIONS

General information on DWD LM trajectories

The trajectory model is an off-line model coupled to the LM with identical resolution, horizontal and vertical grid structure as the corresponding LM model providing the output data. Therefore, no interfaces are needed. The trajectory model is fully three-dimensional, of high numerical order (Euler-Cauchy scheme with iteration of 2nd order accuracy, Kottmeier and Fay, 1998), uses 1 hourly data input from the Lokalmmodell LM, linear interpolation in time and tri-cubic interpolation in space and a very small time step similar to the LM model itself (2 min for the operational LM 7 km trajectories, 60 sec for all FUMAPEX trajectories). This ensures small tangential errors especially in conditions of strongly fluctuating winds and bent streamlines.

For trajectory evaluation see chapters 4 and 7.

The Lagrangian Particle Dispersion Model (LPDM) forecasts the concentration and deposition of radionuclides released from one or several point sources. The emitted material is represented by a large number of particles (10^5 - 10^6), which are advected along trajectories. Diffusion is calculated with the "Monte Carlo" technique. Radioactive decay, dry and wet depositions are considered.

The LPDM uses the output of the DWD numerical weather prediction (NWP) models GME and LM as meteorological database (esp. 3D winds, turbulent kinetic energy). Like the trajectory model TM of the DWD it is an off-line model, coupled to the GME or LM with identical resolution, horizontal and vertical grid structure. For more detailed information on the LPDM, refer to Glaab et al. (1998) or D2.2 (Sokhi et al., 2003).

In the course of FUMAPEX WP6, the trajectory model and Lagrangian particle dispersion model LPDM were adapted to 2.8 and 1.1 km resolution and tested for the first time for some FUMAPEX episode cases.

6.1. Sensitivity of LM trajectories to horizontal and vertical resolution in LM

Trajectory experiment, important feature investigated: channelling of transport/ trajectories in mountain valley NW of Oslo.

All simulations are performed for different trajectory start levels between ~50m above ground and 700 hPa to show the height-differentiated differences between trajectories.

A fictitious (radioactive/chemical) accident in Hallingdal in the morning at 6 UTC and in the evening at 18 UTC is studied by comparison of trajectories with 7 km/35 levels, and 2.8 and 1.1 km/45 levels for 6 and 7 Jan 2003.

The lowest trajectory level is about 50m above model topography which varies between ca. 250m (1.1 km), 400m (2.8 km) and 700m (7 km) due to differences in topography with resolution (deeper valleys and higher mountains with increasing resolution).

Comparison of trajectories with 7 km/35 levels, and 2.8 and 1.1 km/45 levels for 6 and 7 Jan 2003

Location height of accident between ca. 250m (1.1 km), 400m (2.8 km) and 700m (7 km) due to differences in topography with resolution (deeper valleys and higher mountains with increasing resolution). Trajectories are simulated with start levels up to 1500m to show the influence of effective source height and atmospheric wind shear.

a) Evening start, night time trajectories

With increasing resolution, the overall channelling of trajectories increases. The most intensive and longest channelling of trajectories with start levels up to 920 hPa is visible for 1.1

km resolution due to the largest mountain-valley height differences in topography. Nevertheless, some channelling is also found for 7 km resolution possibly due to the relatively low and broad valleys for the coarser resolution. On both 6 and 7 Jan, the lower trajectories for 1.1 and 2.8 km resolution may rise in the first 1-5 hours of transport apparently climbing the valley walls and temporarily or finally leaving Hallingdalen and not getting permanently channelled there. They even (for 2.8 km) shortly channel NW into a neighbouring valley against the main mesoscale wind direction before turning SE again. A similar, less distinct effect is found for the 7 km trajectories possibly pointing to a weak local circulation.

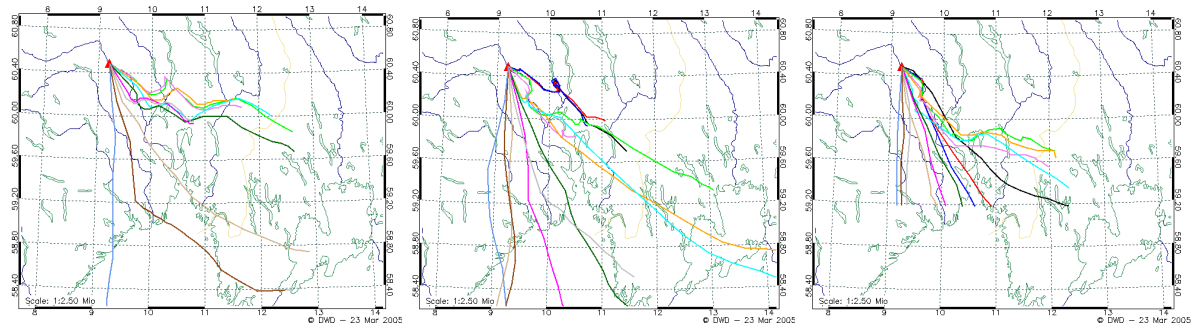


Figure 6.1a LM trajectory forecast for 7 Jan 2003, +18 UTC, left: 7 km/35 levels, middle: 2.8 km/45 levels, right: 1.1 km/45 levels

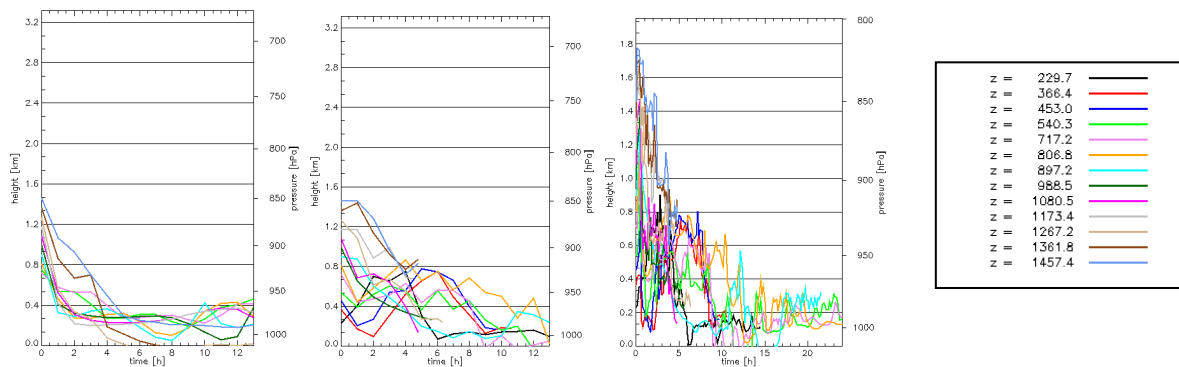


Figure 6.1b LM trajectory forecast for 7 Jan 2003, +18 UTC. Vertical cross sections: left: 7 km/35 levels, middle: 1.1 km/45 levels, hourly output, right: 1.1 km/45 levels, 10-min output. Approximated trajectory start levels for 1.1 km run in m (standard atmosphere)

With higher resolution especially in mountainous terrain, LM vertical motions (see WP3) and accordingly trajectory vertical motions increase in frequency and amplitude. It proved crucial for these simulations to increase the frequency of trajectory position output for the graphs from the operational 1 hour to 10 to 15 minutes in order to show the very variable vertical paths (Figure 6.1b, middle and right). This may increase the probability of trajectories leaving the valleys instead of channelling there. It needs mentioning that the time step of these trajectory simulations was already reduced from the operational 120 to 60 sec for all resolutions and should be small enough for the trajectories to follow even fast vertical wind fluctuations.

b) Morning start, daytime trajectories

The overall trajectory behaviour is very similar to the evening cases. The short-lived circulation along a neighbouring valley axis is again found, this time also for a 1.1 km trajectory. It is apparently dependent on the specific time-space position of the trajectory in relation to topography and wind direction.

Summary

For all start times the trajectories following the main mesoscale NW-erly wind direction independent of time of day, i.e. there is only a small but distinct influence of local circulations (when existing at all during the winter episode) on transport.

Trajectories with 7, 2.8 and 1.1 km show increasing channelling. The channelling is less pronounced than expected possibly because the induced stronger vertical motions at 1.1 km resolution combine with vertical wind shear to move the trajectories out of the narrower and steeper valleys of the high-resolution topography.

6.2. Sensitivity of Lagrangian Particle Dispersion Model (LPDM) to horizontal and vertical resolution in LM

In WP3 it was shown that horizontal grid refinement may lead to some improvement of NWP model results, and that this is mainly due to an improved land/sea and soil type distribution and, for more mountainous terrain like e.g. Oslo, to an improved topography with higher mountains and deeper valleys (exemplarily Figure 6.2, for more details Fay et al., 2004, Neunhäuserer et al., 2004, Fay and Neunhäuserer, 2004a, Fay and Neunhäuserer, 2004b, Neunhäuserer and Fay, 2005a, Fay et al., 2005). For the Oslo case study, the impact of the refined topography and LM meteorological data on the LPDM results is investigated.

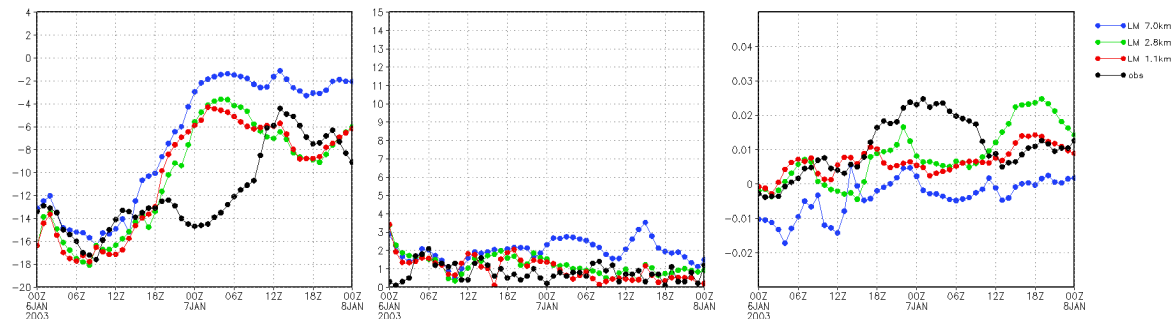


Figure 6.2 LM time series starting 06 Jan 2003, 00 UTC +00, and observations (obs). Left: Blindern, 2m temperature. Middle: Blindern, 10m horizontal wind speed. Right: temperature gradient $(T_{2m}(\text{Tryvann}) - T_{2m}(\text{Blindern})) / \Delta z$.

Model set-up

Episode meteorological simulation runs (48h forecasts) were performed with the mesoscale non-hydrostatic LM in the operational set-up (7 km horizontal resolution, 35 layers, lowest layer height about 68m) and in two one-way nested versions (2.8 km / 45 layers and 1.1 km / 45 layers, lowest layer height in both cases about 41m). Figure 6.3 shows the area of the innermost nest with 1.1 km horizontal grid resolution, the locations of three meteorological stations in the Oslo area from where meteorological observations are available, the location of the city of Asker west to the Oslo fjord, which will be used for discussion of the LPDM results, and a red line indicating a vertical cross section along which LPDM results will be presented.

LPDM simulations were carried out for a fictitious radioactive accident at 60°N, 10°E, and west of Oslo and south of the Tyrifjord (Figure 6.3). Cs-137 was emitted with a constant rate of $4.629 \cdot 10^{10}$ Bq/s over 12 hours, amounting to $2 \cdot 10^{15}$ Bq in total, at a height of 30m. Three 12h LPDM forecasts were calculated, starting on 6 Jan 2003, 00 UTC +18 h, 7 Jan 2003, 00 UTC +6 h and 7 Jan 2003, 00 UTC +18 h, using the corresponding LM model results of 7 km / 35 layers, 2.8 km / 45 layers and 1.1 km / 45 layers as meteorological input.

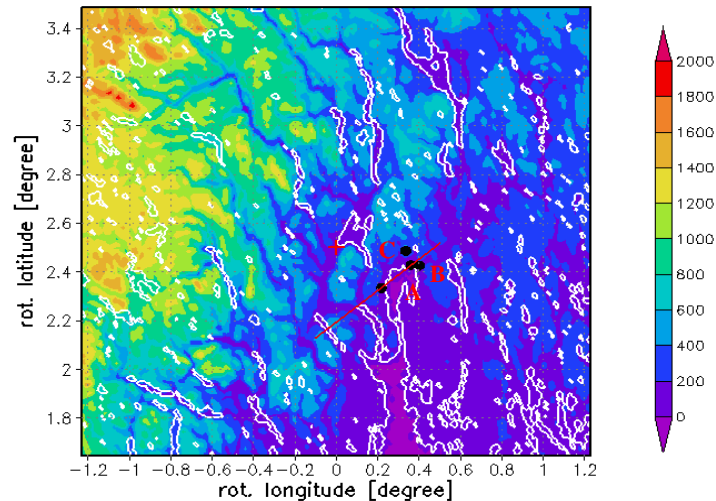


Figure 6.3 Oslo high resolution modelling area (approx. 150km x 150km) with topography for DWD LM / LPDM. Black dots are locations of meteorological stations (A: Blindern, B: Valle Hovin, C: Tryvann) and of the city of Asker (D: Asker). Red cross: Location of fictitious radioactive accident. Red line: Location of vertical cross section.

Results and discussion

For the first Oslo LPDM run, release of Cs-137 was started on 6 Jan 2003, 00 UTC +18 h and continued during the night time hours until 6 Jan 2003, 00 UTC +30 h. Figure 6.4 shows the horizontal distribution of Cs-137 together with the corresponding streamlines of horizontal velocity at 06 Jan 2003, 00 UTC +24 h, after 6h of constant release. Horizontal grid resolution from left to right is 7 km, 2.8 km and 1.1 km. The concentration values are averages in space over the grid box size and the thickness of the lowest model layer (67.7m for 7 km and 40.6m for 2.8 km/1.1 km horizontal grid resolution) and in time over three hours of LPDM forecast. The streamlines are derived from the spontaneous velocities valid at the given forecast hour. Obviously, the grid refinement with its improved orography leads to a much more structured wind field and a channelling of the Cs-137 plume within the valleys, with the plume axis moving slightly in more westerly direction. The secondary maxima of the 2.8 km and 1.1 km plume may possibly be numerical artefacts which may appear for very stable situations.

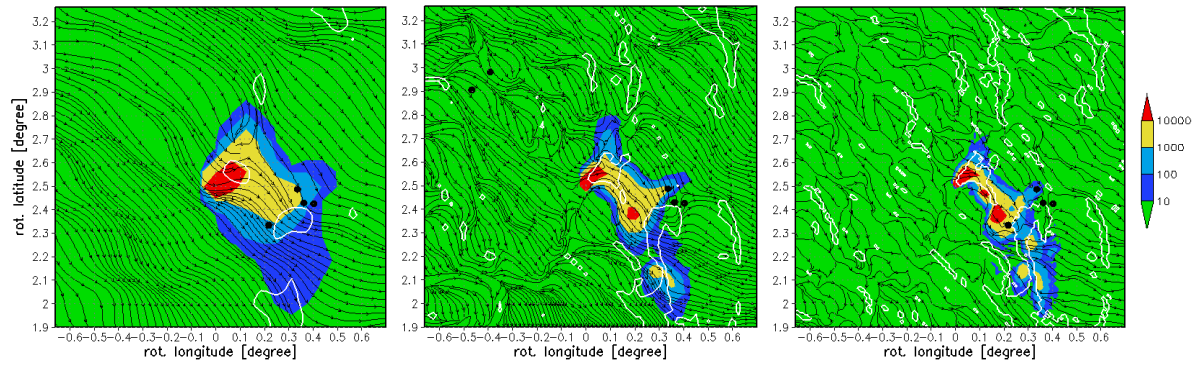


Figure 6.4 Horizontal distribution of Cs-137 concentration and streamlines of horizontal velocity at 06 Jan 2003, 00UTC+24h (after 6h of Cs-137 release), average values over lowest model layer thickness and 3h forecast (00UTC+21h - 00UTC+24h). Left: LPDM 7.0km, lowest model layer thickness 67.7m. Middle: LPDM 2.8km, lowest model layer thickness 40.6m. Right: LPDM 1.1km, lowest model layer thickness 40.6m.

The same can be observed in the corresponding vertical cross section in Figure 6.5. The 7 km resolution has a very smooth orography and provides a rather flat and wide concentration plume which completely fills the valley of the Oslo fjord (Figure 6.5, left). Orography and plume sharpen with increasing grid resolution, the maximum values of the plume move towards the western edge of the Oslo fjord, and the plume reaches higher up into the atmosphere (Figure 6.5, middle and left). This behaviour is supported by the increasing vertical winds (Figure 6.6) which are induced by the higher mountains and lower valleys of the improved topography.

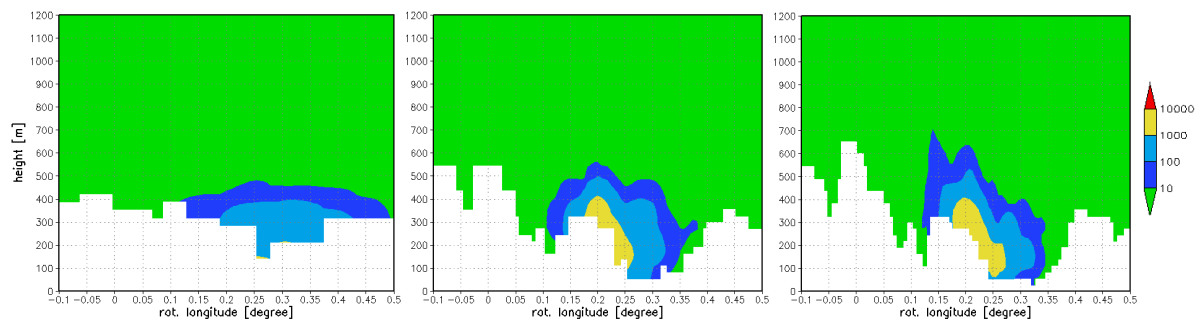


Figure 6.5 Vertical distribution of Cs-137 concentration at 06 Jan 2003, 00UTC+24h (after 6h of Cs-137 release) along cross section, average values over 3h forecast (00UTC+21h - 00UTC+24h). Left: LPDM 7.0km. Middle: LPDM 2.8km. Right: LPDM 1.1km.

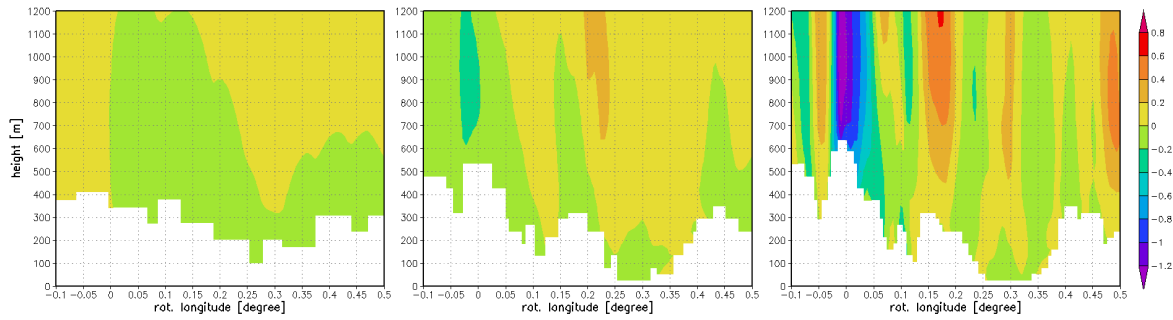


Figure 6.6 Vertical distribution of vertical velocity [m/s] at 06 Jan 2003, 00UTC+24h along cross section. Left: LM 7.0km. Middle: LM 2.8km. Right: LM 1.1km.

The time series of the Cs-137 concentrations in Figure 6.7 demonstrate the influence of the grid resolution on the model results at given locations. The city of Asker shows the lowest values for the 7 km results (Figure 6.7, left), because the plume axis with the maximum concentration values runs east of Asker. In this case, Blindern is affected by the plume as well, while with the two finer resolutions it is not (Figure 6.7, right). The 2.8 km grid resolution brings the highest concentration values to Asker, with the plume axis being very close to the city. For 1.1 km grid resolution, the plume axis is located even slightly more westerly, providing lower concentration values for Asker compared to the 2.8 km results.

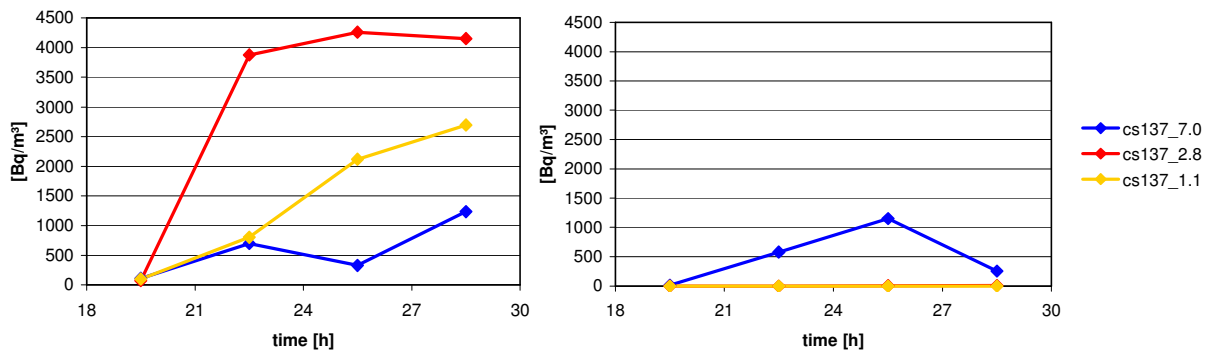


Figure 6.7 Time series of Cs-137 concentration, starting at 06 Jan 2003, 00UTC+18h. Values are averaged over lowest model layer thickness and 3h forecast each. Blue: LPDM 7.0km. Red: LPDM 2.8km. Yellow: LPDM 1.1km. Left: Asker. Right: Blindern.

The second Oslo LPDM run is a daytime run, starting the Cs-137 release on 7 Jan 2003, 00 UTC +06 h. Generally, it shows some effects similar to the first run, i.e., channelling of the plume and larger vertical extend of the plume due not only to the improved topography itself but to the increase of vertical winds as well. But now, simulation with the three grid resolutions results in concentration plumes whose general form is much more similar to each other than for the first run, as exemplarily shown in Figure 6.8. A possible reason is that during night time stable conditions in wintertime Oslo, orographic effects may have a larger impact on the concentration distribution than during the less stable daytime. While the 2.8 km results produce increased maximum values at Asker (Figure 6.8, middle, and Figure 6.9) due to channelling effects, the 1.1 km simulation provides a wider, meandering plume with lower concentration values at Asker (Figure 6.8, right, and Figure 6.9), which may be attributed to the less stable situation during daytime as well.

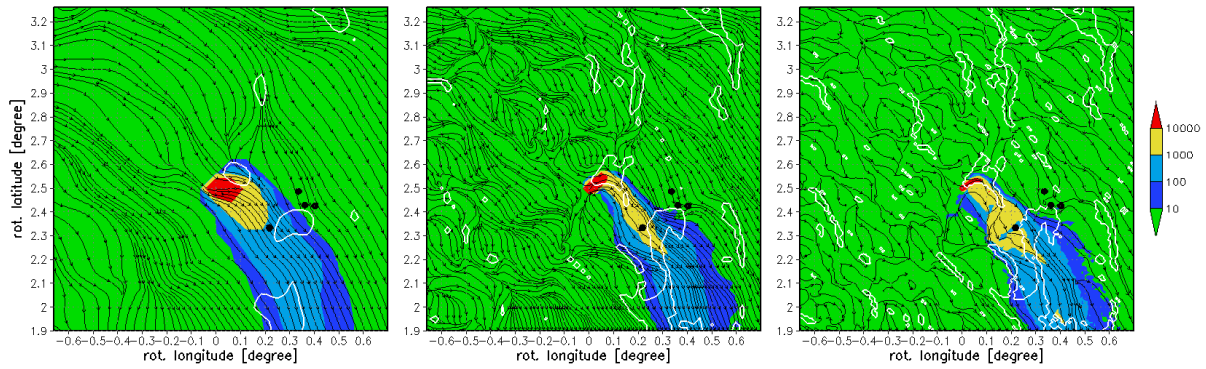


Figure 6.8 Horizontal distribution of Cs-137 concentration and streamlines of horizontal velocity at 07 Jan 2003, 00UTC+12h (after 6h of Cs-137 release), average values over lowest model layer thickness and 3h forecast (00UTC+09h - 00UTC+12h). Left: LPDM 7.0km, lowest model layer thickness 67.7m. Middle: LPDM 2.8km, lowest model layer thickness 40.6m. Right: LPDM 1.1km, lowest model layer thickness 40.6m.

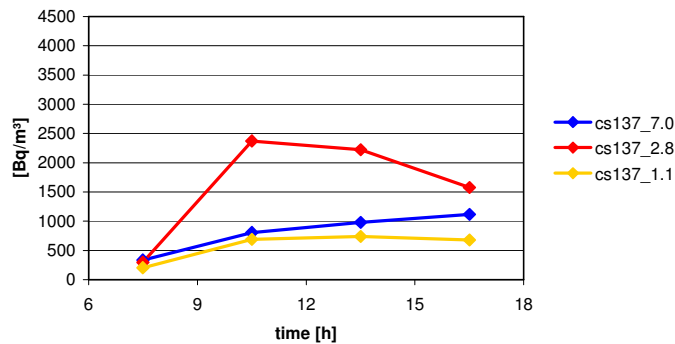


Figure 6.9 Time series of Cs-137 concentration for Asker, starting at 07 Jan 2003, 00UTC+06h. Values are averaged over lowest model layer thickness and 3h forecast each. Blue: LPDM 7.0km. Red: LPDM 2.8km. Yellow: LPDM 1.1km.

The third Oslo LPDM run is a night time run again, starting at 07 Jan 2003, 00 UTC +18 h. As for the first run, the results show a distinct impact of the orography (Figure 6.10 - Figure 6.12). Most remarkable in this case is the development of two plume axes, to the east and to the south of the release location, with a hilly region of about 600m-700m height in between. This can be observed after 6h of Cs-137 emission for the 1.1 km resolution results (Figure 6.10) and after 12h of Cs-137 emission for both the 2.8 km and the 1.1 km results (Figure 6.11). As mainly north-westerly winds prevail during this episode, a stagnation point builds up windward of the hilly region, and the location of this stagnation point determines the direction of the concentration plume at a given moment. The precise location of the stagnation point again depends on the orography. The 7 km resolution topography seems to be too smooth to create this type of channelling effect.

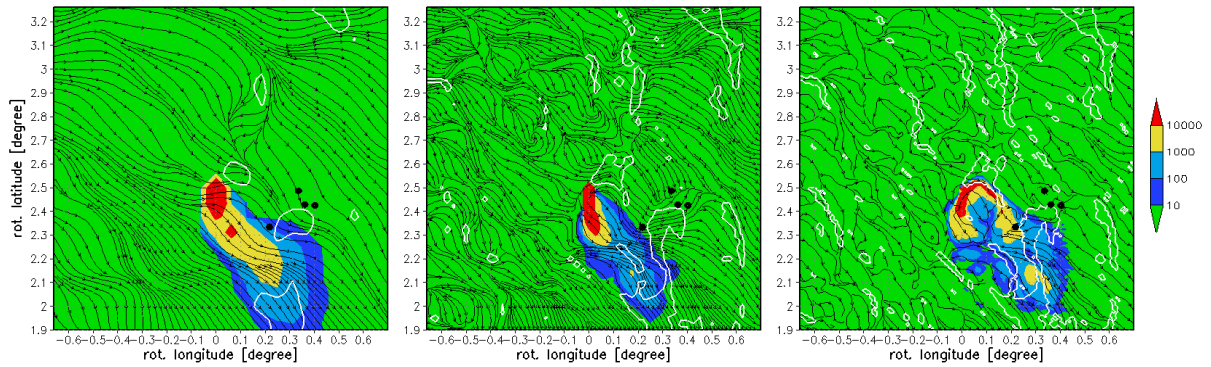


Figure 6.10 Horizontal distribution of Cs-137 concentration and streamlines of horizontal velocity at 07 Jan 2003, 00UTC+24h (after 6h of Cs-137 release), average values over lowest model layer thickness and 3h forecast (00UTC+21h - 00UTC+24h). Left: LPDM 7.0km, lowest model layer thickness 67.7m. Middle: LPDM 2.8km, lowest model layer thickness 40.6m. Right: LPDM 1.1km, lowest model layer thickness 40.6m.

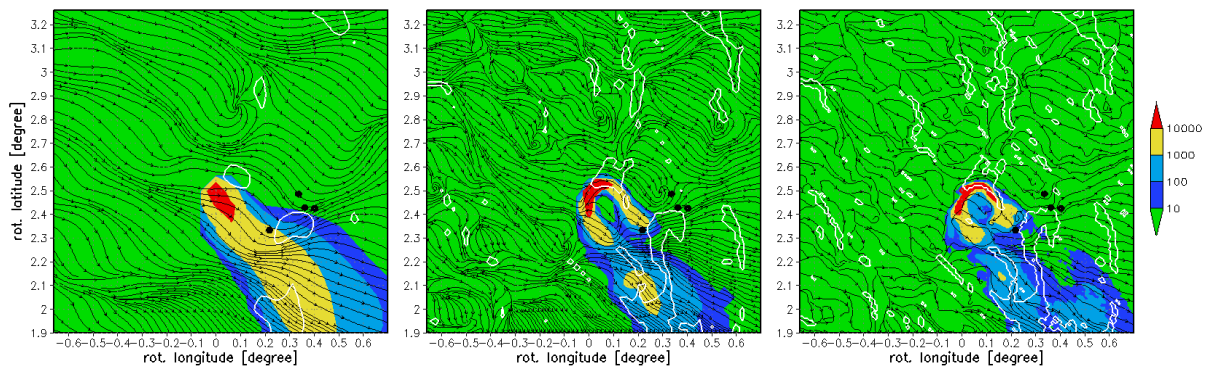


Figure 6.11 Horizontal distribution of Cs-137 concentration and streamlines of horizontal velocity at 07 Jan 2003, 00UTC+30h (after 12h of Cs-137 release), average values over lowest model layer thickness and 3h forecast (00UTC+27h - 00UTC+30h). Left: LPDM 7.0km, lowest model layer thickness 67.7m. Middle: LPDM 2.8km, lowest model layer thickness 40.6m. Right: LPDM 1.1km, lowest model layer thickness 40.6m.

The concentration distribution along the vertical cross section after 12h of Cs-137 emission shows two maxima for the 2.8 km and 1.1 km resolution as well, indicating two main plume axes, one close to the western edge of the Oslo fjord and the other one more westerly, while there is only one plume axis for the 7 km resolution (Figure 6.12).

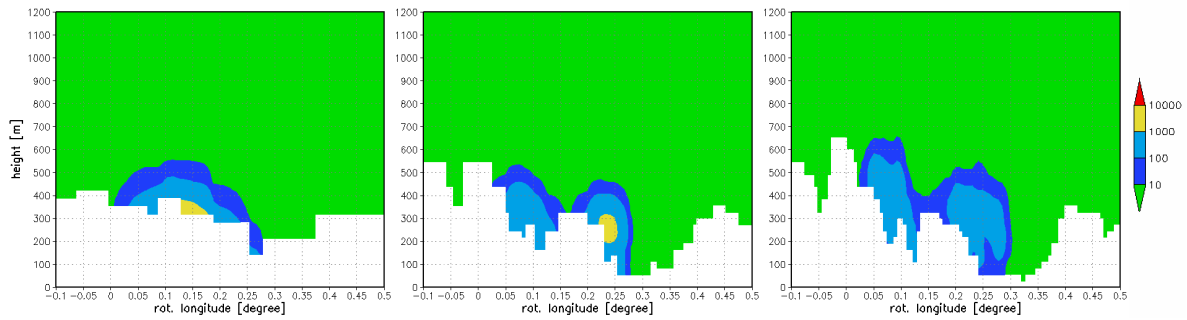


Figure 6.12 Vertical distribution of Cs-137 concentration at 07 Jan 2033, 00UTC+30h (after 12h of Cs-137 release), average values over 3h forecast (00UTC+27h - 00UTC+30h). Left: LPDM 7.0km. Middle: LPDM 2.8km. Right: LPDM 1.1km.

The impact of grid resolution on the results for a given location is again shown for the city of Asker in Figure 6.13. The 7 km simulation provides concentration values which increase steadily with the plume becoming wider and coming closer with time. The 2.8 km results are close to zero for the first nine hours because the plume prefers the more southern way during this time. Concentration at Asker rises only for the last three hours of simulation, when the eastern arm of the plume reaches the city. Finally, the 1.1 km grid resolution produces high concentration values for the second three hours, when the eastern arm of the plume reaches the city for the first time. After that, the values recede to close to zero while the plume chooses the southern axis, and increase again with the eastern arm becoming stronger again.

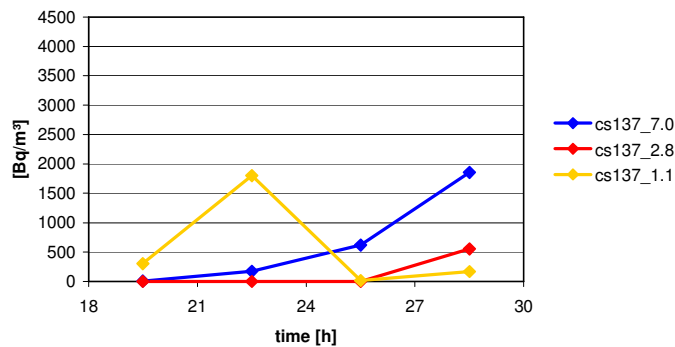


Figure 6.13 Time series of Cs-137 concentration for Asker, starting at 07 Jan 2033, 00UTC+18h. Values are averaged over lowest model layer thickness and 3h forecast each. Blue: LPDM 7.0km. Red: LPDM 2.8km. Yellow: LPDM 1.1km.

Conclusions

The investigation in this chapter shows that the concentration distribution simulated with the LPDM on the basis of LM meteorological data is extremely sensible to the horizontal grid resolution. Differences occur due to the size of the grid cell over which the number of particles is averaged (spread of the plume), due to the orography (channelling effect) and due to the refined meteorological input data which itself depend on the orography (location of stagnation points, vertical velocity).

7. TARGET CITY HELSINKI - TRAJECTORY MODEL SIMULATIONS

General: information on DWD LM trajectories:

The trajectory model is an off-line model coupled to the LM with identical resolution, horizontal and vertical grid structure as the corresponding LM model providing the output data. Therefore, no interfaces are needed. The trajectory model is fully three-dimensional, of high numerical order (Euler-Cauchy scheme with iteration of 2nd order accuracy, Kottmeier and Fay, 1998), uses 1 hourly data input from the Lokalmmodell LM, linear interpolation in time and tri-cubic interpolation in space and a very small time step similar to the LM model itself (2 min for the operational LM 7 km trajectories, 60 sec for all FUMAPEX trajectories). This ensures small tangential errors especially in conditions of strongly fluctuating winds and bent streamlines.

Consequently, the quality of the trajectories will largely depend on the quality of the LM wind fields. The operational 7 km LM results are daily verified using the standard WMO and additional statistics showing a high international standard. Only the target cities Oslo, Bologna and Turin are situated inside the operational LM area, Valencia and Helsinki are outside. These last city domains and, additionally, the higher-resolution LM simulations are experimental and only validated for the FUMAPEX episodes using FMI's statistical package MMAS (described in D3.3 (Fay et al, 2004)). Results for 10m horizontal wind speed and 2m temperature (relevant for LPDM simulations) for 4 stations for the Helsinki episodes were evaluated. Statistical performance fluctuates between episodes, stations and days with less improvement for increased resolution than in the Valencia episode (chapter 4). This is also due to the extreme and hard-to-model inversion episode of Dec 1995. The overall statistical scores of the Helsinki LM wind fields are similar for all LM resolutions. As the performance of 7 km LM trajectories was shown to be very satisfactory on many occasions, the overall performance of higher-resolution trajectories is also expected to be good.

The statistical scores for T2m show more improvement with increasing resolution which would affect LPDM simulations positively. No statistical evaluation was performed for the introduction of urbanised external parameters and an anthropogenic heat source in LM, but the results especially for LM, LPDM and mixing heights (WP5) show a clear improvement in urbanised features.

The Lagrangian Particle Dispersion Model (LPDM) forecasts the concentration and deposition of radionuclides released from one or several point sources. The emitted material is represented by a large number of particles (10^5 - 10^6), which are advected along trajectories. Diffusion is calculated with the "Monte Carlo" technique. Radioactive decay, dry and wet depositions are considered.

The LPDM uses the output of the DWD numerical weather prediction (NWP) models GME and LM as meteorological database (esp. 3D winds, turbulent kinetic energy). Like the trajectory model TM of the DWD it is an off-line model, coupled to the GME or LM with identical resolution, horizontal and vertical grid structure. For more detailed information on the LPDM, refer to Glaab et al. (1998) or D2.2 (Sokhi et al., 2003).

In the course of FUMAPEX WP6, the Lagrangian particle dispersion model was adapted to 2.8 and 1.1 km resolution and tested for the first time for some FUMAPEX episode cases, also including LM results with urbanised external parameters and an additional urban heat source.

7.1. Sensitivity of trajectories to horizontal and vertical resolution in LM

Comparison of trajectories with 7 km/35 levels, 2.8 and 1.1 km /35 and 2.8 and 1.1 km/ 45 levels for extreme winter inversion episode on 28 Dec 1995. Trajectories were simulated for start levels up to 3000m to account for the influence of effective source height and atmospheric wind shear.

Fictitious accident about 100 km windward of city is simulated. Start times +6 h (daytime trajectories), +18 h (night time trajectories), +40 h (trajectory start at approximate time of warm front passage).

The trajectories for 7, 2.8 and 1.1 km resolution for each start time show the same direction and area covered for all start levels between 50m above ground to 700 hPa. The trajectories in 2.8 and 1.1 km were simulated with 35 levels (as with 7 km resolution) and with 45 levels leading only to small effects in the horizontal and vertical spread of the trajectories (Figure 7.1). This is explained with the very small changes of topography with resolution for the flat Finnish coast. Additionally, the episode day is extremely cold and stably stratified above land even during the day for that extreme inversion episode, thus reducing any potential differences.

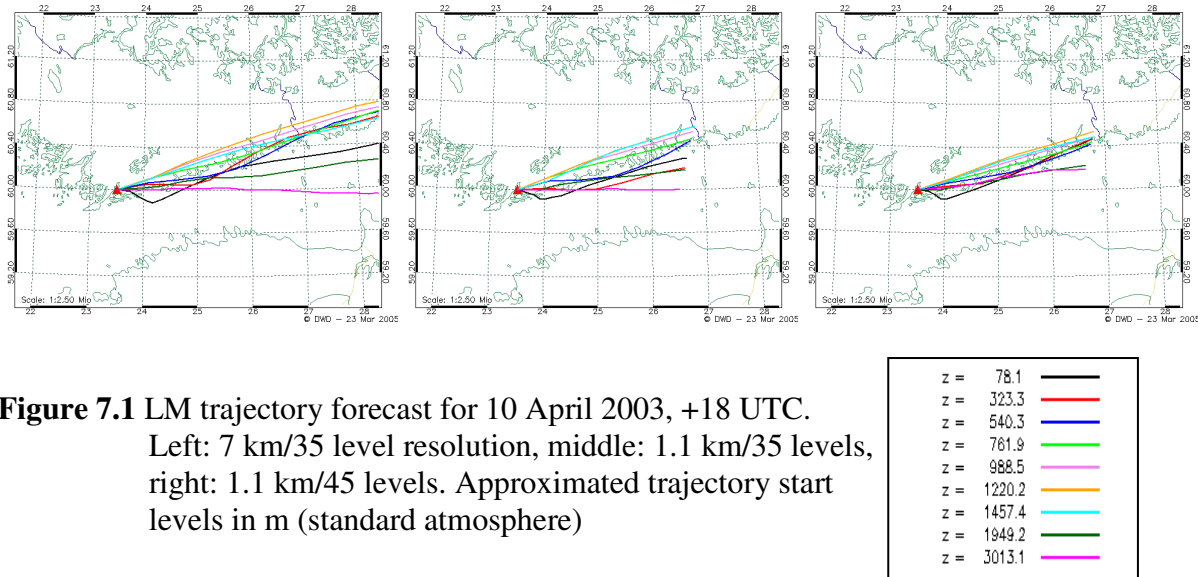


Figure 7.1 LM trajectory forecast for 10 April 2003, +18 UTC. Left: 7 km/35 level resolution, middle: 1.1 km/35 levels, right: 1.1 km/45 levels. Approximated trajectory start levels in m (standard atmosphere)

7.2. Sensitivity of trajectories surface data and land surface parameterizations

Case 2: Fictitious accident in Kaisaniemi for spring episode on 10 April 2002

Start times at different times of day: +6 h (daytime trajectory), +12 h, +18 h and (night time trajectory) and +40 h. All trajectories in 1.1 km resolution, 45 levels, based on the corresponding LM version, but

- trajectories with operational LM version,
- with urbanised external parameters,
- with urbanised external parameters and constant anthropogenic heat source of 60W/m² at the surface

Only the near-surface trajectories starting between 50m above ground up to 950 hPa may show differences due to the urbanised parameters for Helsinki but the differences in arrival points and times are negligible (except for the 50 m-trajectory starting at +6 h, >120 km

difference after 24 h forecast time). The reasons for this small effect on the trajectories are as follows: A direct influence of the above urbanisation measures in LM is found on many parameters (energy balance (radiation, sensible and latent heat fluxes), turbulence, T2m etc., also streamlines). Trajectories depend directly only on the grid-scale wind speeds (streamlines) and thus show a reduced effect compared to more complex models. Additionally, the trajectories start in the middle of town and experience the modified influence only for a very short time span of minutes/1h before leaving the city area. Also there are too few trajectories to capture all wind changes due to urbanisation above the city.

Case 3 and 4:

Locations close to, but windward of Helsinki in order to increase influence through longer length of stay of trajectories above the urbanised city area.

Case 3:

Setup as in case 2, but source/trajectory starts at +6 h about 30 km NNE windward of Helsinki. Trajectory paths are affected for start levels up to 900 hPa. The resultant changes in horizontal trajectory position are below 50 km after 20h forecast time. However, there are differences in single trajectories reaching/missing the Helsinki urban area in the first 6 to 12h after the emission/start which would influence transport and contamination in the city in a real emergency event. The main differences are visible in the vertical motion of the trajectories both in the upward and downward direction (shown only smoothed in 1-hourly intervals, probably more distinct in higher time resolution as described in Oslo section).

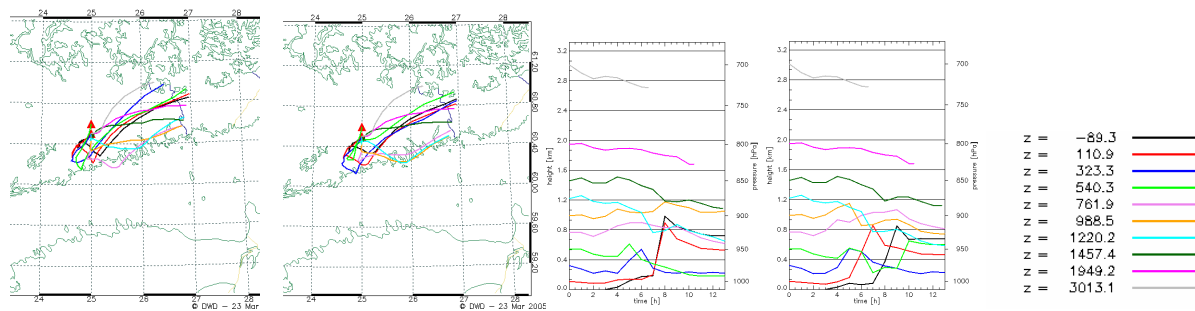


Figure 7.2 LM trajectory forecast with 1.1 km/45 levels, for 10 April 2002, +6 UTC. Left: Horizontal paths: original LM and urbanised version (ext. parameters + heat source), middle: as left, but vertical paths. Right: approx. trajectory start levels in m (standard atmosphere).

Case 4:

Setup as case 3, but source/trajectory starts at +12h about 20 km windward in SE of Helsinki on the Baltic Sea. Trajectory paths are only affected for start levels up to 925 hPa, and the differences are smaller than in case 3. This is explained by the shorter length of stay of these trajectories above the urbanised Helsinki area and its hinterland where the main influence of urbanisation is located (see sensibility study of meteorological parameters incl. mixing heights in WP4, WP5) while in case 3 the trajectories circle and remain longer above the city area due to the change from nocturnal land to diurnal sea breeze circulation.

Summary

Influences of urbanisation of external parameters and addition of an anthropogenic heat source **are visible** in the near-surface trajectory paths. As trajectories are determined from

grid-scale winds they are not a very sensitive instrument to show influences that are manifested on many parameters (temperatures, various terms of the surface energy heat balance, turbulence, streamlines). Therefore, the described urbanisation will show larger effects on dispersion models that explicit depend on temperature and sub-grid scale parameters (turbulent kinetic energy etc.) like the DWD's Lagrangian particle dispersion model and the LM mixing height scheme (WP5).

7.3. Sensitivity of LPDM to surface data and land surface parameterizations

In WP4, urbanised external parameters and an anthropogenic heat source were implemented into the LM, as the operational LM version like many other NWP models does not provide descriptions or functionalities for urban areas. It was shown that these first steps towards urbanisation lead to some improvements of the model results compared to measurements, namely to an increase of daytime 2m temperature and a decrease of daytime 2m relative humidity (Figure 7.3), and generally to a more "urbanised character" of the results, i.e., a warming of the atmosphere over the city area and an increase of the importance of the storage heat flux (Neunhäuserer and Fay, 2005b). In this chapter, the influence of the LM meteorological output (urbanised by varying the external parameters and the anthropogenic heat flux) on the LPDM results is discussed for the Helsinki April 2002 episode.

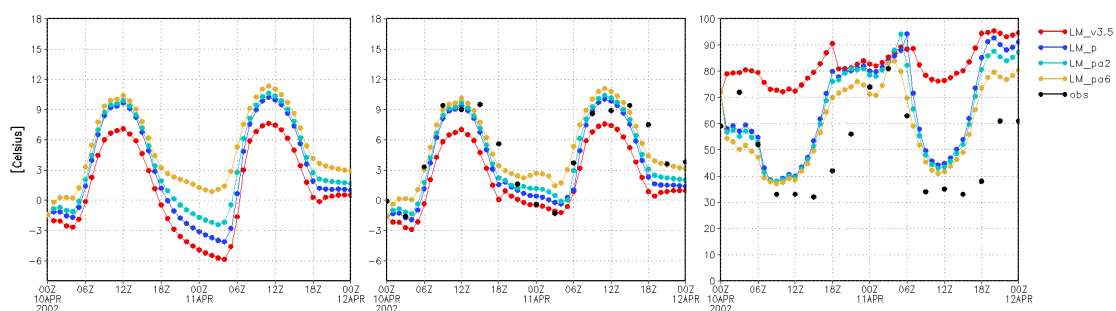


Figure 7.3 LM time series at Kaisaniemi for cases A-D starting 10 Apr 2002, 00 UTC +0, and observations (obs) when available. Cases A, B and D in the figure correspond to cases A, B and C in table 7.1 and the text. Left: Surface temperature. Middle: 2m temperature. Right: 2m relative humidity.

Model set-up

Just as for the Oslo study described in chapter 6.2, meteorological simulation runs of 48h forecasts were performed with the LM in its operational version (7 km / 35 layers) and in two one-way nested versions (2.8 km / 45 layers and 1.1 km / 45 layers). Three test cases are investigated here, namely case A using the operational LM without urbanised parameterisation, case B with the newly implemented soil type for urban areas ("city") and case C with "city" soil type and an additional anthropogenic heat source within the city area. The corresponding parameter values are listed in Table 7.1, with the city parameters chosen according to Kinouchi and Yoshitani (2001). The soil type distribution without (case A) and with (case B, C) "city" soil type is depicted in Figure 7.4 for the innermost modelling area with 1.1 km horizontal grid resolution. In addition to the parameters given in Table 7.1, for cases B and C the city soil type area was enlarged compared to the real world Helsinki area, the surface roughness length was increased in the urban area, the leaf area index and the plant cover fraction were set to zero, and very small values were assigned to pore volume and field capacity in order to enforce the urban effects. The anthropogenic heat source was included as

an additional term to the surface energy balance equation and may represent a heat source from e.g. buildings. Its value is chosen from a range of about 10-100 Wm⁻² considered in literature (Kinouchi and Yoshitani, 2001, Best and Betts, 2004) and for this study was held constant in time.

case	name	soil type in city area	albedo [%]	thermal conduc. [W m ⁻¹ K ⁻¹]	thermal capac. [J m ⁻³ K ⁻¹]	anthrop. heat source [W m ⁻²]
A	LM_v3.5	3-6	25-30	1.15-1.55	1.3E6-1.5E6	0
B	LM_p	11	12	1.7	2.1E6	0
C	LM_pa6	11	12	1.7	2.1E6	60

Table 7.1 Test cases for LM meteorological simulation runs and their external parameters. Soil types: 3: sand, 4: sandy loam, 5: loam, 6: clayey loam, 11: city.

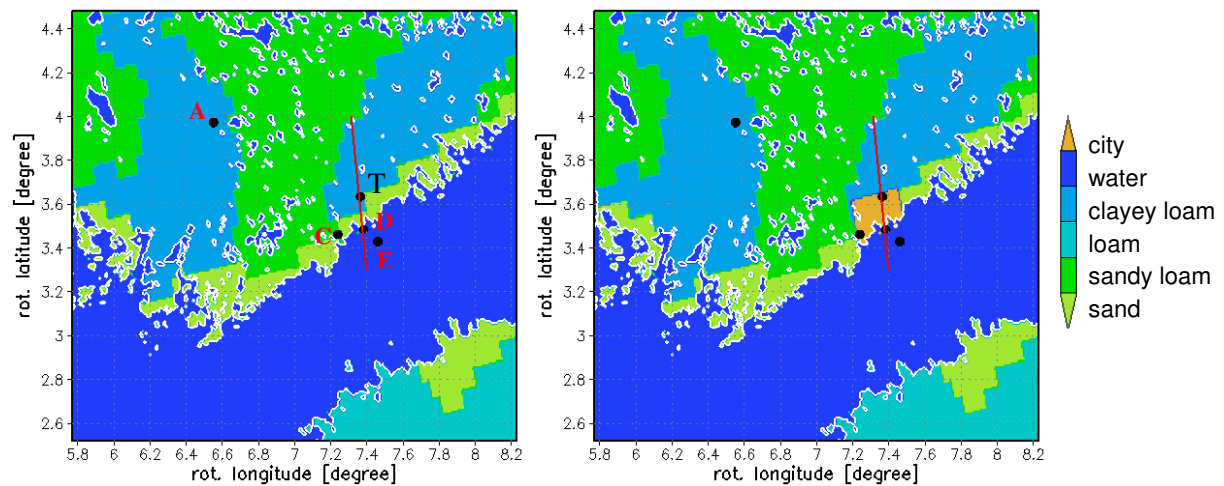


Figure 7.4 Helsinki high resolution modelling area (approx. 250km x 200km) with soil type distribution for DWD LM / LPDM. Black dots are locations of meteorological stations (A: Jokioinen, B: Vantaa, C: Kivenlahti, D: Kaisaniemi, E: Isosaari). Red line: Location of vertical cross section. Left: Operational LM soil type distribution. Right: With urban soil type "city" in the Helsinki area.

LPDM simulations were carried out for the highest model resolution of 1.1 km based on the three LM test cases in Table. A fictitious radioactive accident was set to happen at the urban meteorological station of Kaisaniemi at 60.17°N, 24.94°E. Cs-137 was released into the atmosphere over 12h at a height of 30m, with a constant rate of 4.629·10¹⁰ Bq/s amounting to 2·10¹⁵ Bq in total.

Results and discussion

For the Helsinki LPDM runs, Cs-137 release was started on 10 Apr 2002, 00 UTC +06 h and continued during the day until 10 Apr 2002, 00 UTC +18 h. Figure 7.5 and Figure 7.6 show the horizontal concentration distribution after 6h and 12h of Cs-137 emission respectively, averaged in space over the horizontal size of a grid cell and the thickness of the lowest model layer and in time over 3h of forecast. Superimposed are the streamlines derived from the spontaneous values of the horizontal velocity of the lowest model layer at the given forecast hour.

As a general feature, the plume moves parallel to the coast during the early hours of simulation and then turns inland. In Figure 7.5, streamlines already run perpendicular to the coast due to their spontaneous nature, while the plume is still spread more parallel to the coast line because it contains the information of the last three simulation hours. In Figure 7.6, the plume axis has turned inland. It can be observed that the form of the plume and the location of its maximum values are influenced by the urban external parameterisation (Figure 7.5, middle, and Figure 7.6, middle) and the existence of an anthropogenic heat source (Figure 7.5, right, and Figure 7.6, right). In the horizontal direction this can be attributed to a slight deflection of the streamlines towards the city in the early simulation hours and later to a slight convergence of the streamlines leeward of the city area caused by the urbanisation measures. The decrease of the area of maximum values in Figure 7.4 is due to the vertical extent of the plume growing with the introduction of urbanised external parameters and an anthropogenic heat source (Figure 7.7). This and the widening of the plume in Figure 7.6 suggest that the situation becomes less stable and turbulence increases with increasing LM urbanisation.

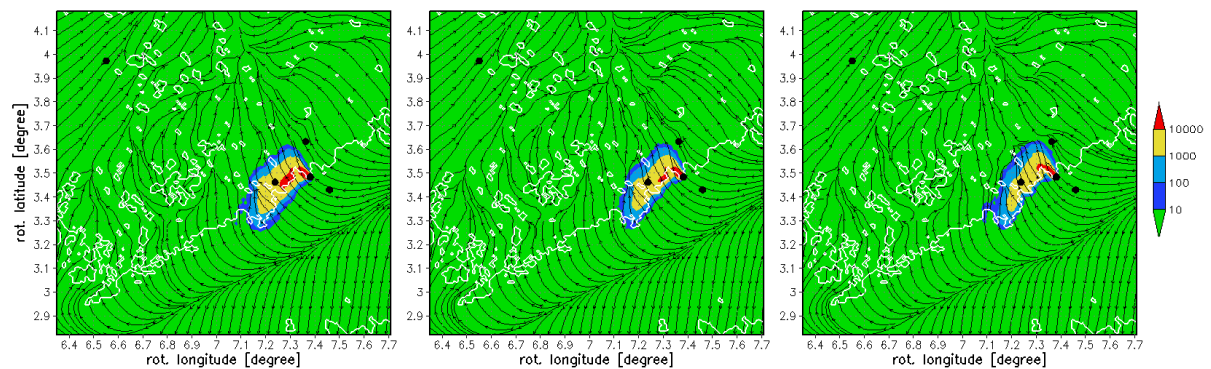


Figure 7.5 Horizontal distribution of Cs-137 concentration and streamlines of horizontal velocity at 10 Apr 2022, 00UTC+12h (after 6h of Cs-137 release) for 1.1km horizontal grid resolution, average values over lowest model layer thickness of 40.6m and 3h forecast (00UTC+09h - 00UTC+12h). Left: Case A. Middle: Case B. Right: Case C.

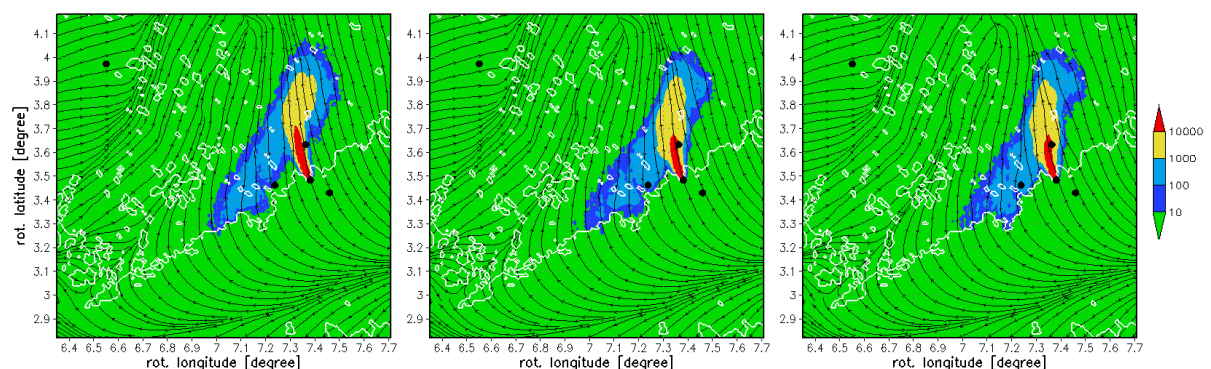


Figure 7.6 Horizontal distribution of Cs-137 concentration and streamlines of horizontal velocity at 10 Apr 2022, 00UTC+18h (after 12h of Cs-137 release) for 1.1km horizontal grid resolution, average values over lowest model layer thickness of 40.6m and 3h forecast (00UTC+15h - 00UTC+18h). Left: Case A. Middle: Case B. Right: Case C.

Figure 7.7 and Figure 7.8 show the Cs-137 distribution along the vertical cross section defined in Figure 7.3, indicating that the vertical turbulence increases and the stability weakens with urbanisation. The vertical extent of the plume becomes larger when using urbanised external parameters in the LM (Figure 7.7, middle, and Figure 7.8, middle) and grows again when the anthropogenic heat source is added (Figure 7.7, right, and Figure 7.8, right). The form of the plume cross sections suggests that introducing urbanised external parameters mainly increases the dynamical part of the turbulence via increased roughness length (dispersion of the particles more or less uniform in every direction), while the additional anthropogenic heat flux mainly affects the thermal part of the turbulence (dispersion of the particles increasingly in vertical direction). Additionally, the vertical extent of the plume may be enlarged by the increased vertical velocities observed for test cases B and C compared to test case A. The seaward propagation of parts of the plume in atmospheric levels above 200 m is most possibly induced by the upper part of a daytime land-sea circulation increasing with the introduction of the urbanisation measures into the LM.

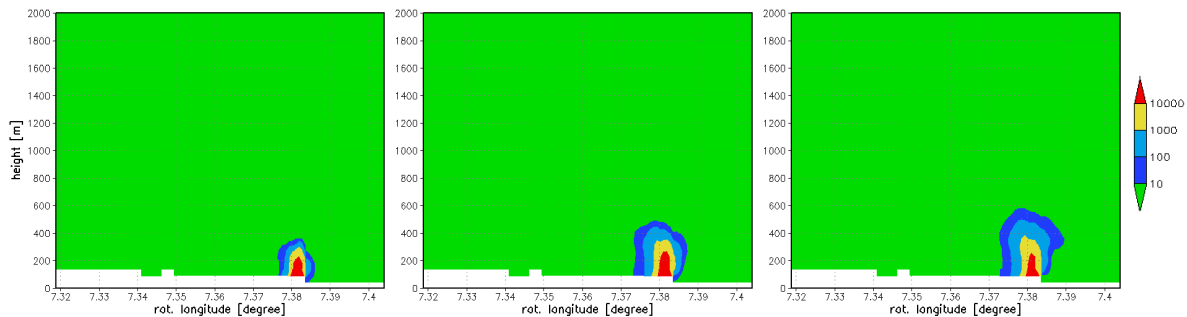


Figure 7.7 Vertical distribution of Cs-137 concentration at 10 Apr 2002, 00UTC+12h (after 6h of Cs-137 release) for 1.1km horizontal grid resolution, average values over 3h forecast (00UTC+09h - 00UTC+12h). Left: Case A. Middle: Case B. Right: Case C.

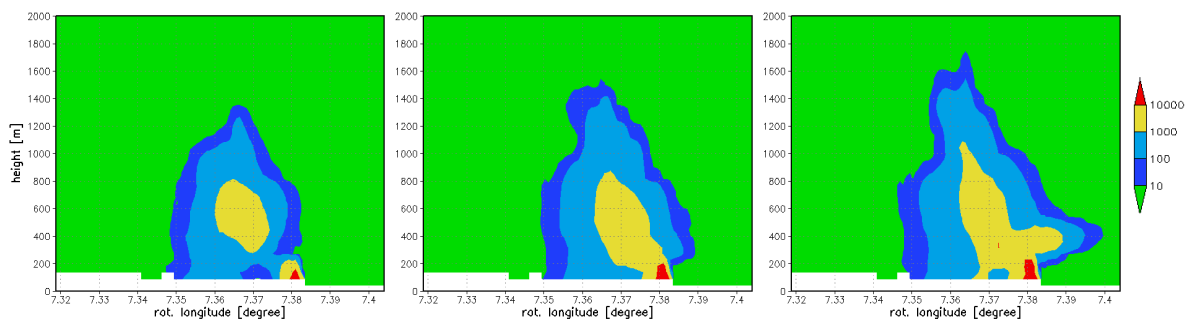


Figure 7.8 Vertical distribution of Cs-137 concentration at 10 Apr 2002, 00UTC+15h (after 9h of Cs-137 release) for 1.1km horizontal grid resolution, average values over 3h forecast (00UTC+12h - 00UTC+15h). Left: Case A, middle: Case B, right: Case C.

The time series of the Cs-137 concentration demonstrate the impact of urbanised external parameters and an anthropogenic heat source on the model results at the three stations of Kaisaniemi, Kivenlahti and Vantaa located within the urban soil type area. At Kaisaniemi (Figure 7.9, left), which represents the location of the fictitious accident, the concentration is naturally largest, but decreases with increasing LM urbanisation. This is due to the fact that the vertical extent of the concentration plume is growing with increasing turbulence and vertical wind speed, while the amount of mass available for distribution is the same for each

test case. Kivenlahti (Figure 7.9, middle), which is located west of Kaisaniemi and also close to the coast, shows peak values for the second averaging period when the plume is oriented parallel to the coast. The peak value is highest for test case A based on the operational LM version, because the streamlines in the city area are more parallel to the coast line in the early forecast hours than for the cases B and C, transporting more Cs-137 in the direction of Kivenlahti. At Vantaa (Figure 7.9, right), north of Kaisaniemi, concentrations are largest for the late forecast hours, after the plume has turned inland. The values increasing with urbanised external parameters and with an additional anthropogenic heat source reflect the change in the direction of the plume axis due to the slight convergence of the streamlines and the widening of the plume due to increased turbulent effects.

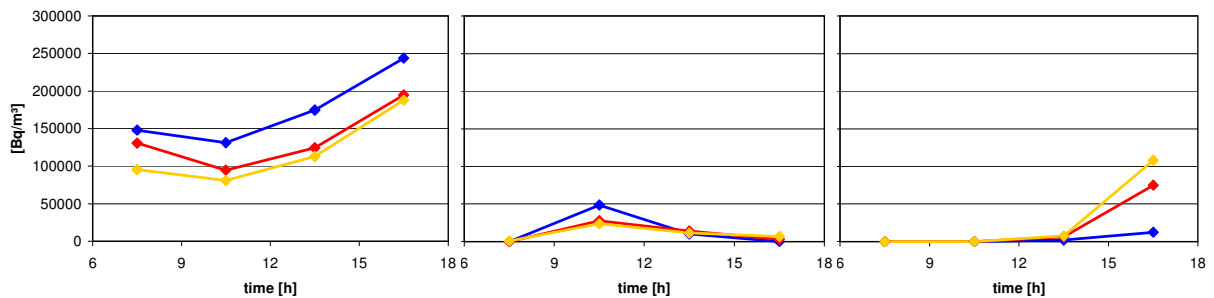


Figure 7.9 Time series of Cs-137 concentration, starting at 10 Apr 2002, 00UTC+6h. Values are averaged over lowest model layer thickness of 40.6m and 3h forecast each. Blue: Case A. Red: Case B. Yellow: Case C. Left: Kaisaniemi. Middle: Kivenlahti. Right: Vantaa.

Conclusions

The LPDM uses mainly the 3D wind vector and the turbulent kinetic energy of the LM output. In the meteorological context, LM temperature and surface flux values show the largest impact due to the urbanisation measures while the above major LPDM input values are less affected (Neunhäuserer and Fay, 2005b). Nevertheless, this study shows that with the turbulence enlarging the general dimensions of the plume and the vertical velocity or the increase in the land-sea circulation altering the form of the plume, the local impact of urbanisation measures on the concentration distribution may be large.

8. TARGET CITY COPENHAGEN - EMERGENCY MODEL SIMULATIONS

General: Information about Partner 1 (DMI and DEMA) models

For the Copenhagen Metropolitan Area and the Øresund region (including the cities of Copenhagen and Malmø), where the system will be tested for the emergency aspects (hypothetical accident or terror action), the focus, first of all, will be on radioactive materials.

The Danish Emergency Management Agency (DEMA), which is an institution under the Ministry of the Defence, is responsible for the Danish nuclear emergency preparedness. A number of national institutions and authorities contribute to the Danish nuclear preparedness, and DMI is among them. The preparedness comes into force in case of a nuclear accident posing a risk to the Danish territory and population. The aim of the preparedness is to implement the best measures to protect people against radioactivity, and to inform the general public. Hereby, injuries to the health can be avoided or reduced.

DMI is responsible for making forecasts of the transport, diffusion and deposition of a radioactive plume. DMI delivers also real time high-resolution forecast meteorological data from the DMI-HIRLAM model system to DEMA for an area covering Denmark and its surroundings. These data are used by the Accident Reporting and Guidance Operational System (ARGOS) (Hoe *et al.*, 1999, 2002) in case of accidents at nuclear installations in Denmark or surroundings. By using the Local Scale Model Chain (LSMC), developed at the Risø National Laboratory (Mikkelsen *et al.*, 1997), ARGOS can calculate forecasts of radioactive doses and concentrations. For the distances longer than 20 km the Danish Emergency Response Model of the Atmosphere (DERMA), developed at DMI (Sørensen, 1998; Baklanov *et al.*, 2005b), is also used.

The main item for this work in Fumapex is to improve urban high-resolution NWP model forecasting data for the Copenhagen Metropolitan Area and to make it available to the ARGOS emergency preparedness decision-support system. In ARGOS the data will be used for simulation of hypothetical atmospheric releases of toxic or radioactive matters (arising from e.g. an accident or a terrorist action). The scenarios include hypothetical releases of radioactivity, e.g., from the Barsebäck nuclear power plant, which is located only 20 kilometres away from the Copenhagen city centre. Assessments will be made of the implications for the emergency management and of the consequences for the citizens of Copenhagen and suburbs.

In Chapter 7 of the D8.1 FUMAPEX report (Slørdal, 2003) a general description of the presently applied ARGOS system and NWP forecasting, as well as a guideline for the forecast procedure is given.

Proceeding from the specific aspects of the Copenhagen system, focused on emergency aspects only (urban air pollution forecast items are not considered for Copenhagen as the target city in FUMAPEX), we can not make a verification and sensitivity study for the forecasting system versus air pollution monitoring data (no measurement data for accidental releases over Copenhagen). Therefore, in the next section we will perform uncertainty analysis of meteorological parameters important to emergency modelling for NWP models. Estimation of importance of uncertainty of the meteorological input to the total uncertainty of the ARGOS system will also be discussed.

8.1. Sensitivity to the DMI-HIRLAM resolution

First tests and sensitivity studies for high-resolution (1.4 km) versions of the DMI-HIRLAM modelling system were done for Copenhagen in WP4 (Amstrup, 2004; Baklanov and

Mestayer, 2004; Baklanov et al., 2005b) and also for Helsinki, Oslo, and Bologna in WP3 (Fay et al., 2004; 2005).

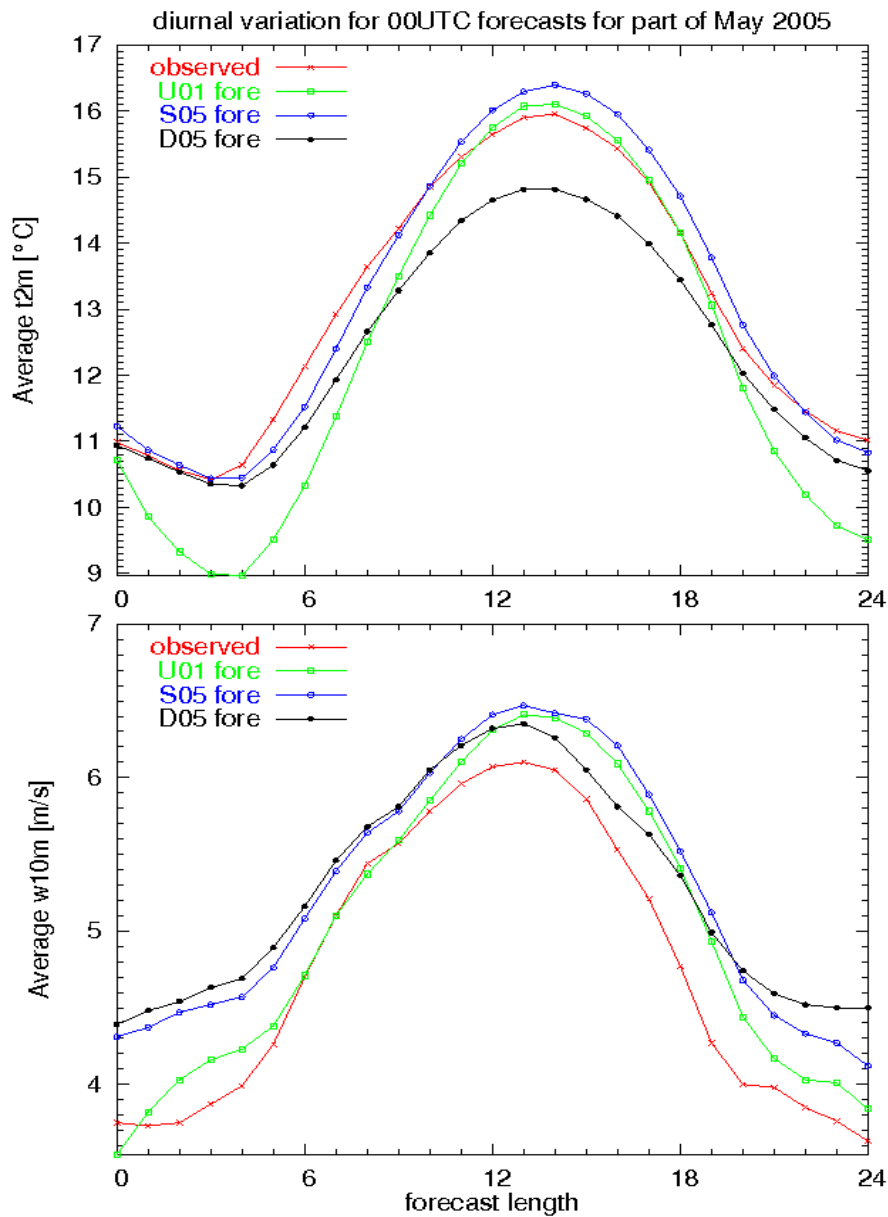


Figure 8.1. Diurnal variation during May of 2005 for 00 UTC forecasts of average temperature (in °C) at 2 m (top) and average wind velocity (in m/s) at 10 m (bottom) based on the observational data and DMI-HIRLAM-S05, -U01, and -D05 models (Mahura et al., 2005).

An overview over the different versions of DMI-HIRLAM operational NWP system used for the sensitivity studies is given in Table 8.1

Table 8.1 Different versions of the DMI-HIRLAM operational NWP system

Model Identification	G	N	E	D	T15	S05	U01 *	I01 *
Grid points (mlon)	202	194	272	182	610	496	370	118
Grid points (mlat)	190	210	282	170	568	372	260	124
No. of vertical levels	40	40	40	40	40	40	40	40
horizontal resolution	0.45°	0.15°	0.15°	0.05°	0.15°	0.05°	0.014°	0.014°
hor. res. (assimilation)	0.45°	0.45°	0.45°	-	0.45°	-	-	-
time step (dynamics)	120s	50s	50s	18s	360s	120s	60s	60s
time step (physics)	360s	300s	400s	216s	360s	120s	60s	60s
boundary age (in forec.)	6h	0h	0h	0h	6h	0h	0h	0h
boundary age (in ass.)	0h-6h	-3h-0h	-3h-0h	-3h-0h	0h-6h	0h	0h	0h
host model	ECMWF	G	G	E	ECMWF	T15	S05	S05
boundary frequency	1/(3h)	1/(1h)	1/(1h)	1/(1h)	1/(3h)	1/(1h)	1/(1h)	1/(1h)
data assimilation cycle	3h							
forecast length (long)	60h	36h	54h	36h	60h	54h	24h	24h
long forecasts per day	4	2	4	4	4	4	4	4

* – research/experimental versions

For example, in the DMI technical report (Mahura et al., 2005a) the simulation results of the DMI-HIRLAM high resolution (1.4 km) research model during spring-summer of 2005 were analysed. In this report, the high resolution model domains used in research activities of DMI are outlined; their results of land use classification and climate generation are presented. The ISBA land surface scheme is tested in more details for specific dates by modifying the parameters of roughness, albedo and anthropogenic heat fluxes over urbanized cells of domain. The outputs for models of the DMI-HIRLAM-U01 and -S05 (resolution of 5 km) vs. observational data are compared. The diurnal cycles of temperature and humidity at 2 m, wind velocity at 10 m, and mean sea level pressure are estimated based on long-term simulations. From these outputs, two specific dates of typical and low winds are also evaluated.

As shown in Fig. 8.1 (top), during May, the diurnal cycle of average temperature at 2 m is relatively well predicted by the S05 model compared with others considered. For U01, the best fit with observational data is between 11-19 UTCs, and during the rest of the day it showed the underestimation of temperature (with temperature differences of more than 1 degree during 2-5 UTCs). As seen in Fig. 8.1 (bottom), during May, the diurnal cycle of average wind velocity at 10 m was well predicted by the U01 model compared with S05. Similar situation was observed during June (figure is not shown), except that between 9 and 19 UTCs the S05 model showed better results with respect to observations. On a diurnal cycle of May, the maxima of wind velocity were observed in the middle of the day corresponding to 6.4 (6.4) vs. 6.1 m/s for the U01 (S05) models vs. observational data. The minima were observed at night corresponding to 3.5 (4.1) vs. 3.6 m/s for the U01 (S05) models vs. observational data. On a diurnal cycle of June, the maxima of wind velocity were also observed in the middle of the day corresponding to 6.1 (5.9) vs. 5.7 m/s for the U01 (S05) models vs. observational data. The minima were observed at night corresponding to 4.3 (4.8) vs. 4 m/s for the U01 (S05) models vs. observational data. It should be noted that the diurnal variation of bias and rms for forecasts in May and June (figures are not shown) was comparable, although for wind velocity the performance of the U01 model for both May and

June was better (average rms of 0.2 and 0.4 m/s for May and June, respectively). On average, the bias for both models was around 1.5-1.6 m/s during May-June.

8.2. Sensitivity to forecast duration

For the emergency preparedness in a case of an accident or terror act for the city scale we need/required, at first, to make a short-term forecast only (usually up to 6-12 hours). For larger scale hypothetical accidents or regional scale problems, the forecast duration can be increased up to 24-48 hours (in some cases even up to 60 or more hours).

Let's present the quality of the operational DMI-HIRLAM forecast for different durations or forecast lengths (see Figures 8.2 and 8.3), on example of the months from the fourth quarter of 2004 (Nielsen and Amstrup, 2005).

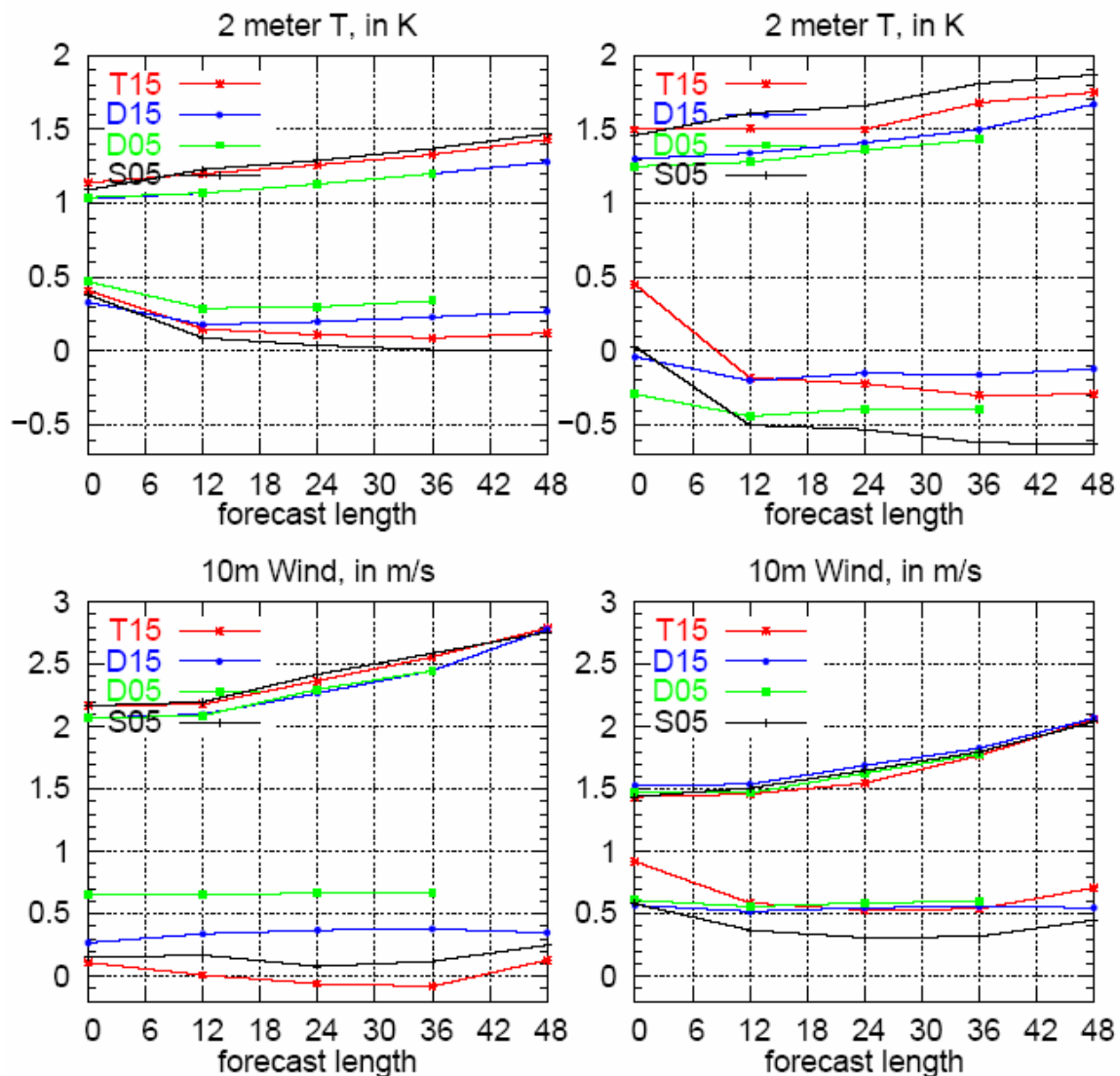


Figure 8.2. Verification results - bias (lower lines on each figure) and standard deviation (higher lines on each figure) for the Danish 18 land stations (left) and 15 coastal stations (right) for the DMI-HIRLAM-T (T15), -E (D15), -D (D05), and -S (S05) models for IV quarter of 2004 for temperature at 2 m (top) and wind at 10 m (bottom). Note, only forecasts starting at 00 and 12UTC were included in statistical analysis (Nielsen and Amstrup, 2005).

In Figure 8.2 forecasts generated by the DMI-HIRLAM versions D15 and D05 (operational prior to 14 June 2004, 15 km and 5 km resolution correspondingly) and by T15 and S05 (operational from 14 June 2004, 15 km and 5 km resolution correspondingly) are verified against 18 Danish land and 15 Danish coastal stations. The shown scores are std. dev. error (upper curves) and bias (lower curves).

T15 followed by S05 generally has the lowest std. dev. error of mslp for both land and coastal stations, particularly at 48 hour lead time. There is indication of a lower error growth rate in T15 and S05 at “long” lead times. The bias is negative in all the model versions both for land and coastal stations. S05 and T15 have the largest negative bias. For the coastal stations the std. dev. error of T2m is lowest in D05 and D15 and largest in S05. For the land stations the std. dev. error is higher than for the coastal stations, highest in S05 and T15 and smallest in D05. The T2m bias for the coastal stations is positive in all model versions with the smallest values in S05 and the highest values in D05. The bias for the land stations is ‘coldest’ in S05 and generally ‘warmest’ in D15. The coast-land amplitude of the V10m bias is largest in T15 and rather small in D15 and D05 and intermediate in S05. The V10m bias for the coastal stations is mostly positive and largest in D05. The land stations have a larger positive bias, mostly with the largest bias in T15 with values between 0.50m/s and 0.95m/s for the latter. The std. dev. errors of V10m are significantly higher for the coastal stations with the largest values in S05 and T15. For the land stations the std. dev. error is generally highest in D15 and lowest in T15, although the differences between the model versions are relatively small.

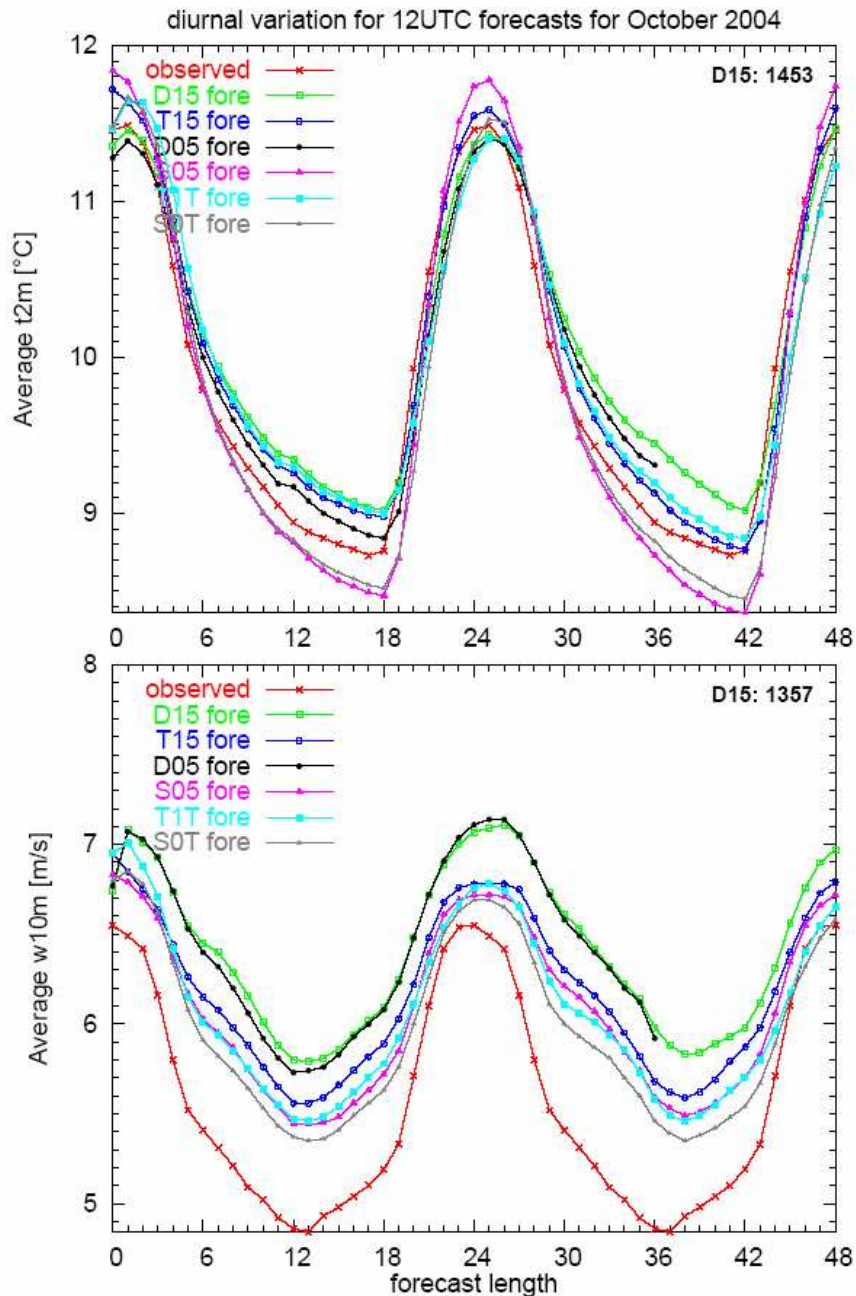


Figure 8.3. Diurnal variation of the average October temperature at 2 m (top) and wind speed at 10 m (bottom) as a function of the forecast length vs. observations. Note, only forecasts starting at 12 UTC were included in statistical analysis. The number in the upper right corner of each subfigure indicates the average number of observations used in calculation for each forecast length for D15 (Nielsen and Amstrup, 2005).

Figure 8.3 shows that the phase of the diurnal variation of T2m, V10m is generally well captured in all the shown model versions. The predicted diurnal amplitude of T2m is close to the observed or somewhat smaller throughout the quarter for all the shown model versions except S05 for October. In November and December the predicted maximum temperature is lower than observed in all the models, except G45 (operational prior to 14 June 2004, 45 km resolution). The lowest maximum temperature is predicted by S05. In October the predicted maximum temperature is higher than observed in S05 and T15, while T1T is close to the

observed value. The minimum temperature in S05 (and S0T in October) is lower than observed throughout the quarter. For the other models the minimum temperature is higher than or close to the observed in October and November, but lower than observed in December, except for G45. Throughout the quarter IV of 2004 all the models have a positive bias for wind at 10 m: largest in G45, D15, and D05 and smallest in S05. Moreover, the positive bias tends to be largest in the dark (low incoming solar radiation) hours, particularly during October and November.

8.3. Sensitivity to urban features

Several specific cases/dates during spring of 2005 were studied employing the DMI-HIRLAM high resolution model (Baklanov et al., 2005a; Mahura et al., 2005a). I.e. dates, when the dominating atmospheric transport over the Sjælland from the south-east sector was observed with the typical and low winds conditions, were studied. In these runs in the ISBA scheme (Rodriguez et al., 2003; Navascues et al., 2003) of HIRLAM, first, the roughness for cells, where the urban class is presented in the modeling domain, was increased up to 1 and 2 m. Second, the albedo was increased. Third, the contribution of anthropogenic flux ranging from 10 to 200 W/m² was incorporated into the land surface scheme. Here, as an example of such case – DMI-HIRLAM run for 30 March 2005, 00 UTC + 24 hour forecast – is shown (Figures 8.4 and 8.5) and analyzed.

The meteorological fields' simulations for the metropolitan areas were driven using the DMI-HIRLAM-S05 model (resolution of 5 km) boundary conditions. These conditions were used as input for simulation of meteorological fields for the DMI-HIRLAM research version (resolution of 1.4 km) which includes the Copenhagen (CPH) and Malmö (MAL) metropolitan areas and surroundings. Note, for each specific date 8 independent runs were performed: 1 control (no modifications in ISBA scheme) DMI-HIRLAM operational run; and modified 4 - for anthropogenic fluxes, 2 – for roughness, and 1 – for albedo.

Following the simulation results it was found that changes in **roughness** modify the structure of the surface layer wind field over urban areas. During the day time the wind velocities are lower by 1-4 m/s. For scale-roughness of 2 m, this effect became more visible and pronounced not only near CPH and MAL, but also for other less urbanized areas; during the night this effect is smaller. For roughness of 1 (2) m, the average differences in velocities are 1.8 (2.4) and 1.4 (2) m/s for CPH and MAL, respectively. For temperature, roughness change does not contribute significantly compared with wind.

Changes in **albedo** have the highest influence on the temperature field between 9-15 UTC, reaching maxima of difference in 2 and 1.8°C for CPH and MAL, respectively. But it is less than 0.5°C during the late evening – early morning period. Similarly, for wind velocities, except, that the difference between wind velocity fields is often more than two times larger for CPH vs. MAL urbanized areas.

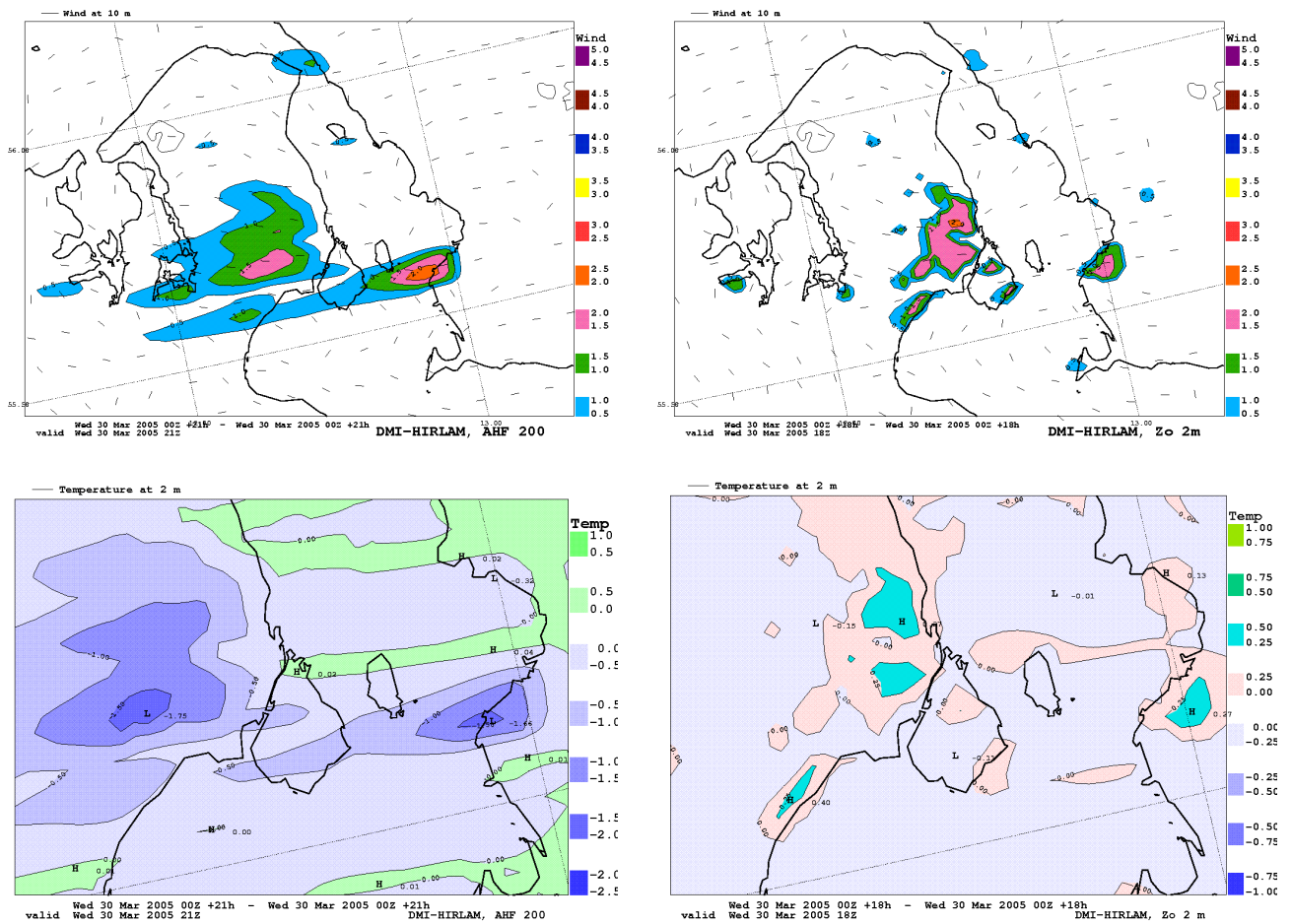


Figure 8.4 Examples of the sensitivity tests of the DMI-HIRLAM high resolution model to the urban features shown as the difference fields (runs without vs. with modifications made) for 10 meter wind velocity (upper row) and 2 meter temperature (lower row) for changes in the anthropogenic heat flux (left) and roughness (right) over the Copenhagen and Malmö metropolitan areas.

Changes in **anthropogenic heat flux** showed (starting at 16 UTC) well pronounced differences for simulated wind fields over urban cells. Then, the area is extended more toward the inland of Sjælland, and difference is rapidly increased up to 1.5 m/s by 18 UTC. During the late evening – early morning period, the difference became larger, and by 10 UTC - there is no difference visible between control and modified runs. For AHF - 200, 100, 50, and 10 W/m^2 - the highest difference (during the night time) reaches of 2.1, 1.6, 0.8, and 0.2 m/s. For temperature, for all terms AHF increased the temperature above the urban cells, except that it is smaller during 9-15 UTC with a minimum at noon. For both urbanized areas, on average (max 2.3°C), this increase is up to 1°C with a large variance. The higher is a value of AHF, the longer time is visible its influence on a diurnal cycle for latent heat flux; and this effect is more pronounced during the night time.

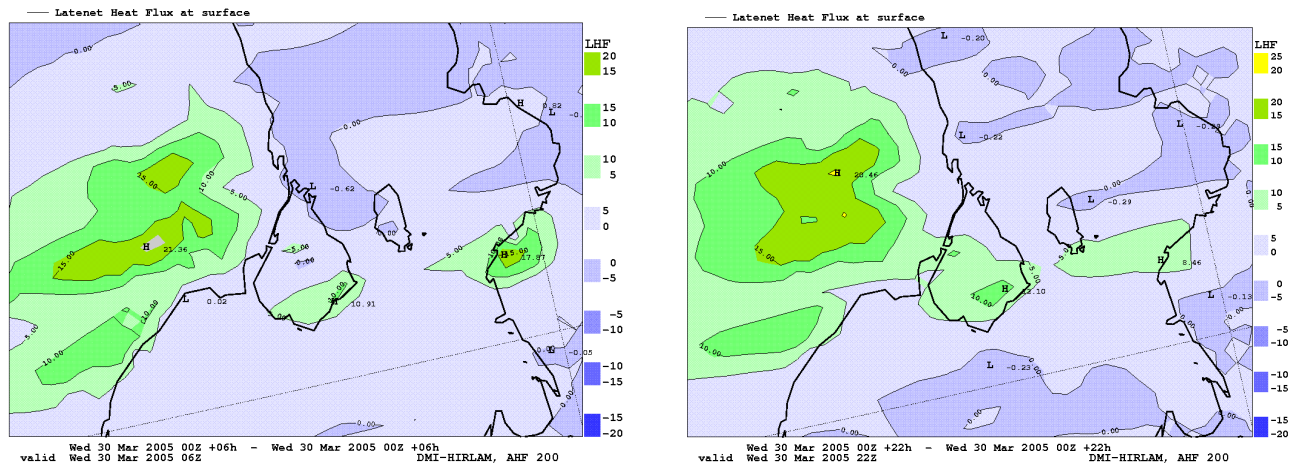


Figure 8.5 Examples of sensitivity tests of the DMI-HIRLAM high resolution model to the urban anthropogenic heat flux over the Copenhagen and Malmö metropolitan areas: the difference fields (runs without vs. with modifications made) of latent heat fluxes at 06 UTC (left) and 22 UTC (right) forecasts.

Based on these results we can see that the urban effects can be considerable in specific meteorological situations not only for large megapolices, but also for relatively small cities. The modification of the effective roughness and urban heat fluxes approach, considered in this section, gives a possibility to incorporate the main urban effects into high-resolution NWP models without a considerable increasing the computation time, which makes them suitable for operational forecast purposes. However this approach does not give a possibility to describe the urban roughness sublayer, which is a critical region where people live and where pollutants are emitted. For this purpose a new analytical model of the mean-wind and the momentum flux profiles in the urban roughness layer (Zilitinkevich and Baklanov, 2005) can be used for diagnosis of surface layer characteristics (e.g. 10 meter wind) in NWP and for lowest levels wind and turbulent input fields for dispersion modelling. Another alternative is the resolving the urban surface layer in NWP models with higher vertical resolution and specific treatments of the urban sub-layer flow and energetics (Martilli et al., 2002; Dupont et al., 2005; Baklanov et al., 2005c).

8.4. Sensitivity of dispersion models (DERMA and ARGOS) to meteorological inputs

To study the sensitivity of the dispersion models (ARGOS and DERMA) on the meteorological input data from the DMI-HIRLAM model with different resolutions and level of urbanization exercise simulations of atmospheric releases of toxic or radioactive matters (arising from e.g. an accident or a terrorist action) were used. The scenarios simulated in the FUMAPEX project include different hypothetical releases of radioactivity, e.g., from the Barsebäck nuclear power plant, a dirty bomb terror action in vicinity of the Copenhagen city, etc. (Baklanov et al., 2005b; Slørdal, 2003). One simulation example of such ARGOS exercise with a hypothetical release of radioactivity from the Barsebäck nuclear power plant with high-resolution DMI-HIRLAM data is presented in Figure 8.6.

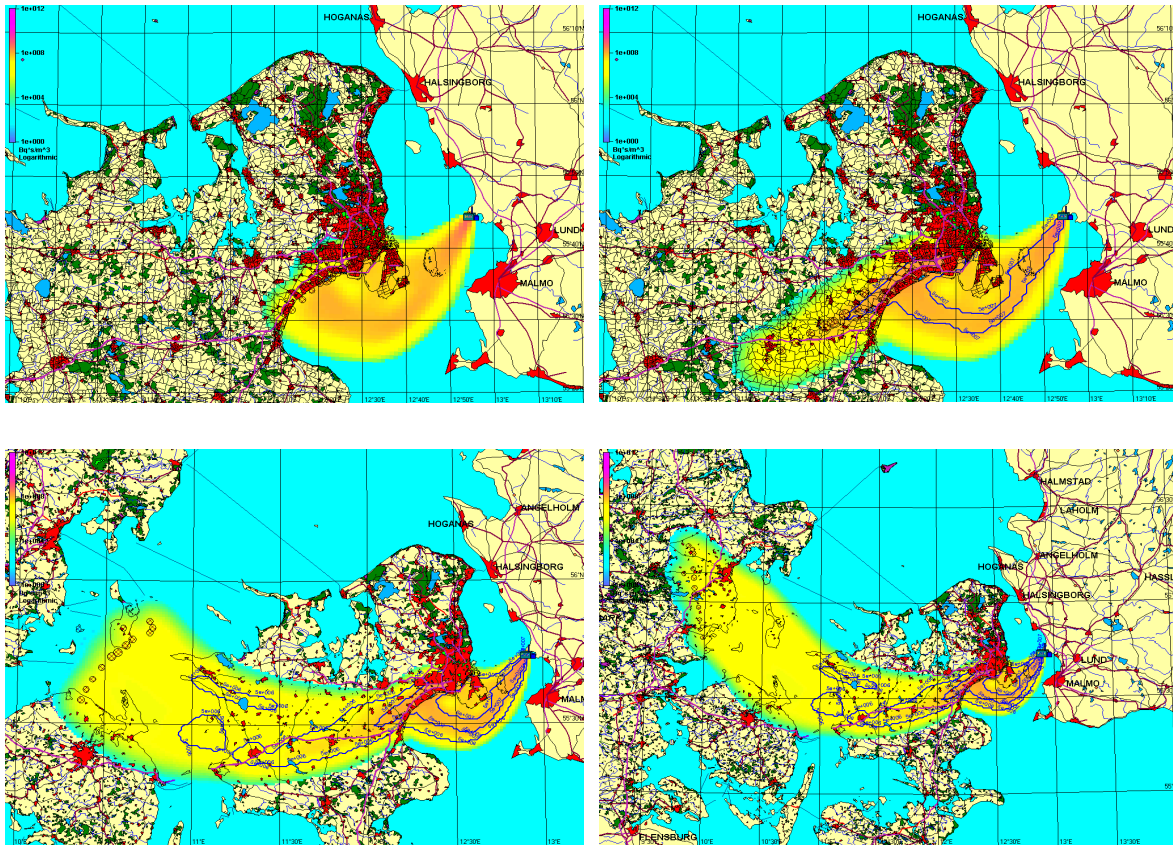


Figure 8.6 ARGOS calculation of a hypothetical release from the Barsebäck NPP for the Copenhagen metropolitan area using high-resolution DMI-HIRLAM meteorological data. Integrated Cs-137 air concentration (Bq·s/m³) in time. Graphics produced by the ARGOS decision support system, LSMC model.

In this report we will consider, as an example, a dirty bomb scenario, as described by Sohler and Hardeman (2004), with radioactive releases from different places (cities of Hillerød, Holte and Slangerup) close to the Copenhagen city. The source was Cs-137 released at a constant rate of $1e11$ Bq/s with the duration of 15 minutes or 3 hours. The information about the source term for a dirty bomb scenario is a very uncertain issue. In this sensitivity study we consider a unit release of ¹³⁷Cs as an example, it could be considered as the first stage of forecasting and further scaled later when relevant data about the release strength become available. For the meteorological situation considered, June 19, 2005 (see Figure 8.7), the hypothetical release took place, e.g. in Hillerød, longitude 12.3 deg. E and latitude 55.9 deg. N, taking place from 16:00 UTC on 19 June 2005 to 16:15 UTC. The radioactive plume was simulated by the ARGOS system and the DERMA model in forecasting and analysed modes.

The following versions of the DMI-HIRLAM model were used (see also the previous sections) for ARGOS and DERMA sensitivity study: operational T15 (15 km resolution) and S05 (5 km resolution) versions and experimental city-scale urbanised U01 version of DMI-HIRLAM with 1.4-km resolution and covering Denmark. Figure 8.7 shows the structure of wind at 10 m for the Copenhagen metropolitan area and surroundings (the Island of Sjælland) at 16 UTC on 19 June 2005 simulated by the DMI-HIRLAM-S05 model and -U01 urbanized version.

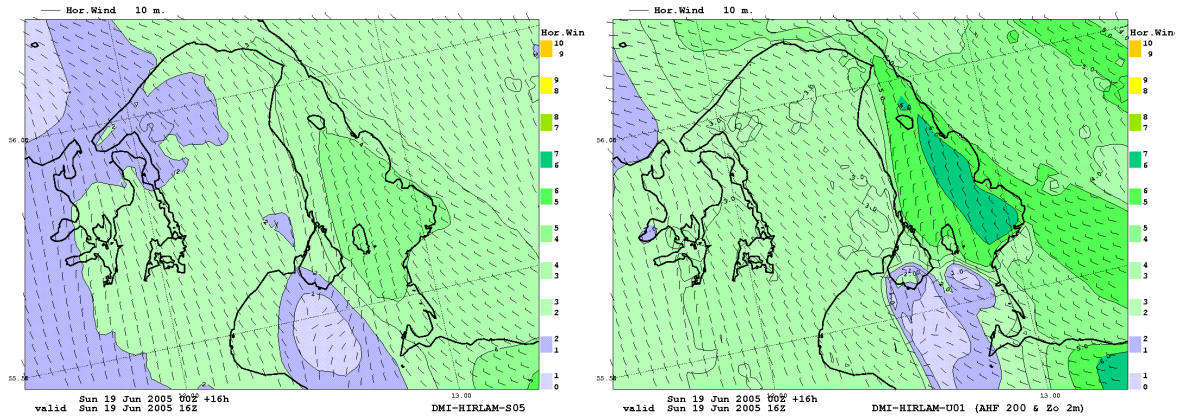
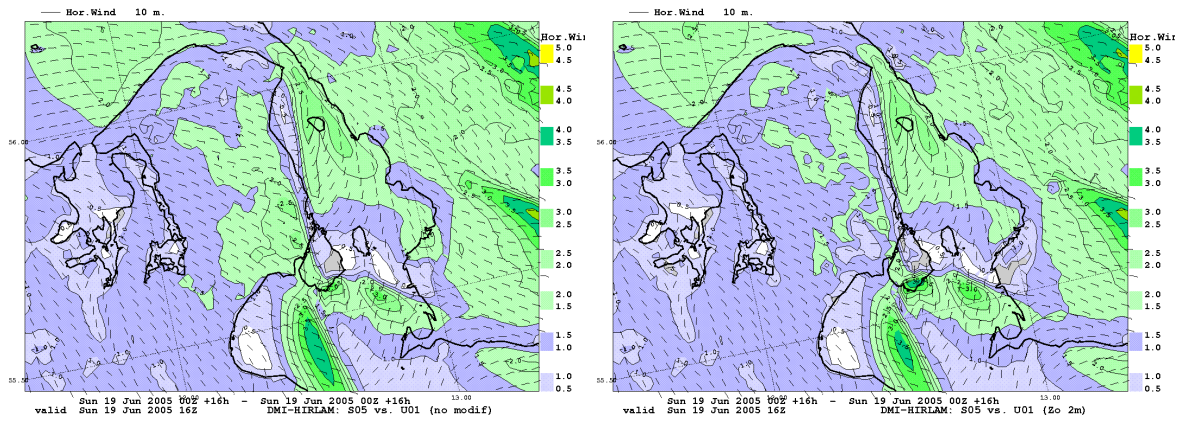
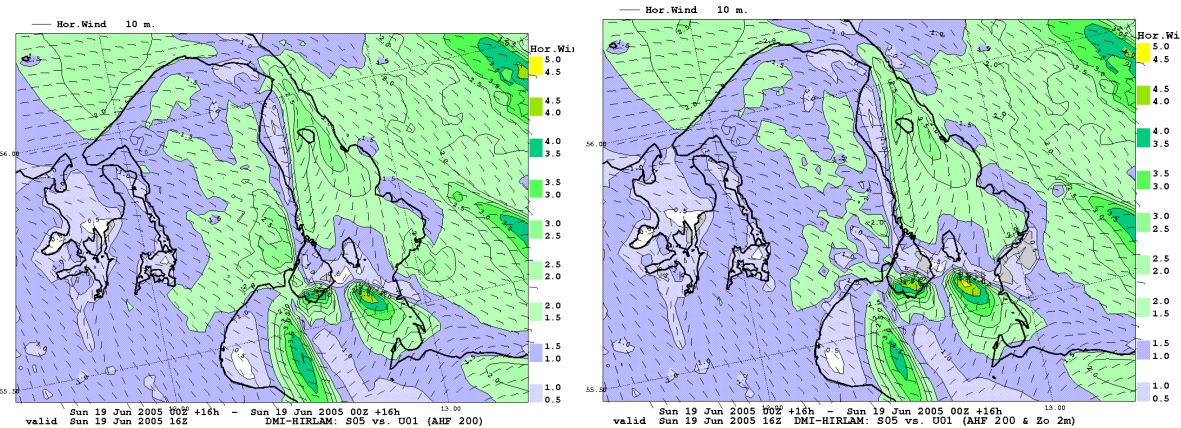


Figure 8.7 Wind fields at 10 m simulated by the DMI-HIRLAM-S05 and U01 (urbanized) models at 16 UTC on 19 June 2005.



(a)

(b)



(c)

(d)

Figure 8.8 Difference fields for the wind at 10 m simulated by the DMI-HIRLAM-S05 vs. U01 (urbanized) models at 16 UTC on 19 June 2005 for: a) no modifications in land surface scheme, b) roughness of 2 m, c) anthropogenic heat flux of 200 W/m², and d) combined effects of roughness and anthropogenic heat fluxes.

Figure 8.8 shows the difference fields between the DMI-HIRLAM-S05 vs. U01 (with modified/urbanized land surface scheme) models for wind velocity at 10 meters at 16 UTC on 19 June 2005 for several independent NWP runs performed. First, Fig. 8.8a shows the difference between the S05 vs. U01 models without any changes incorporated into the ISBA land surface scheme (LSS). Second, Figs. 8.8bcd show for the same UTC term the difference plots between the lower vs. higher resolution models for modifications made separately for roughness of 2 meters, anthropogenic heat flux of 200 W/m^2 , and combined both changes made in DMI-HIRLAM-U01 ISBA LSS. As seen from these figures: not only the higher resolution (from 5 to 1.4 km) modifies the structure of wind patterns over the studied domain, and especially over the urbanized areas, but also changes incorporated into the scheme.

In Figure 8.9 the plume from the hypothetical atmospheric release of ^{137}Cs in Hillerød, as calculated by DERMA using DMI-HIRLAM with different (1.4, 5.0 and 15-km) resolutions meteorological data, is shown for the Copenhagen metropolitan area and for Denmark.

As we can see from the maps in Figure 8.9 the plume shape and concentrations are slightly different for two operational non-urbanised versions D05 and T15, but the high-resolution urbanised version U01 gives a splitting of the plume with two local maxima and lower level of Cs-137 air concentration.

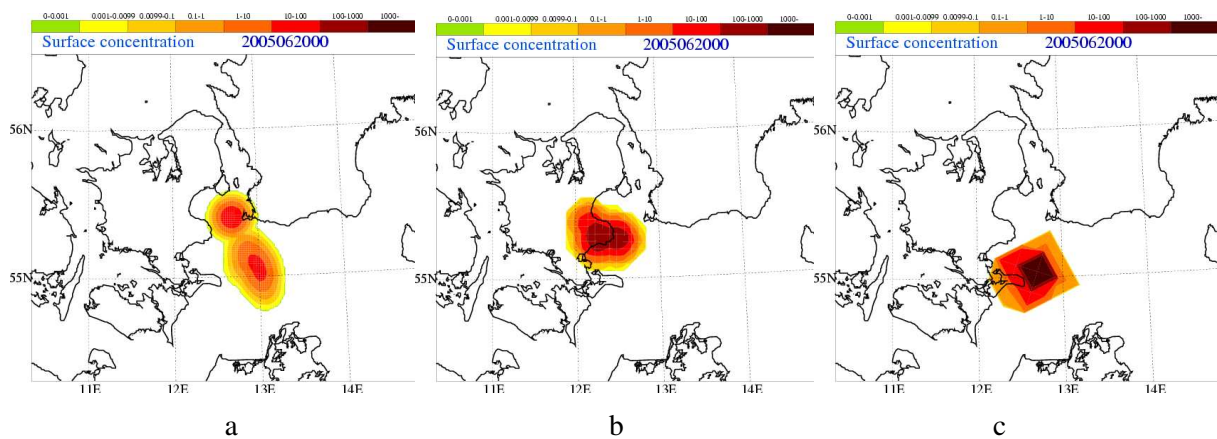


Figure 8.9 Cs-137 air concentration at 24 UTC on 19 June 2005 from the DERMA model simulations for the hypothetical atmospheric release of ^{137}Cs in Hillerød with different DMI-HIRLAM data: a) urbanised U01, b) operational D05, c) operational T15 for the Sjælland Island (incl. the Copenhagen metropolitan area) with surroundings. The star on the maps is the release site.

Three other sensitivity exercises with the releases in Slangerup (55.51N; 12.11E) and Holte (55.50N; 12.29E) are presented in Figures 8.10 – 8.12. Figure 8.10 shows the Cs-137 air concentration and total deposition patterns at 00 UTC, 20 June 2005 for the hypothetical accidental release occurred at the location of Slangerup on 16 UTC, 19 June 2005 with the duration of 15 minutes. The patterns were simulated by the DERMA model on a basis of the DMI-HIRLAM-S05 vs. U01 urbanized models. Figure 8.11 and 8.12 show the Cs-137 air concentrations and total deposition patterns at 00 UTC, 20 June 2005 for the release occurred at the location of Holte starting from 16 UTC, 19 June 2005 with the durations of 15 minutes (Fig. 8.11) and three hours (Fig. 8.12).

In Figure 8.13 the corresponding local-scale plume from the hypothetical atmospheric release of ^{137}Cs (with duration of 15 minutes) occurred at the location of Hillerød on 00 UTC, 19

June 2005, as calculated by RIMPUFF/ARGOS using meteorological data from the urbanised U01 and operational S05 and T15 DMI-HIRLAM models and visualised by ARGOS, is shown for the Copenhagen metropolitan area. 250 m resolution land orography data were used for the ARGOS simulations.

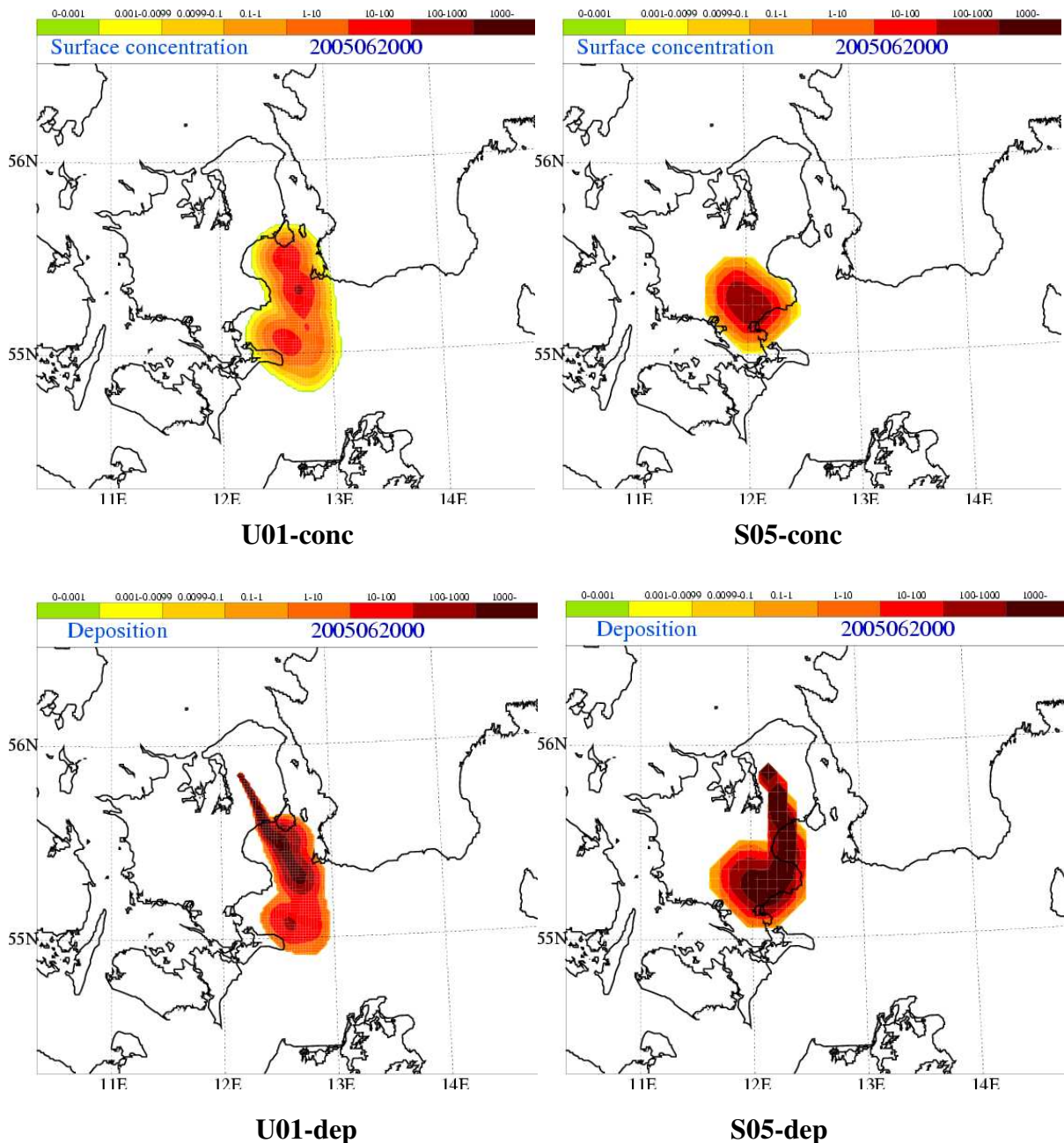


Figure 8.10 Cs-137 air concentration (top) and total deposition (bottom) patterns at 00 UTC, 20 June 2005 for the hypothetical accidental release (with duration of 15 minutes) occurred at the location of Slangerup on 16 UTC, 19 June 2005. Note, patterns were simulated by the DERMA model on a basis of the DMI-HIRLAM-S05 vs. U01 (urbanized) models (see scale for concentration and deposition in Fig. 8.9)

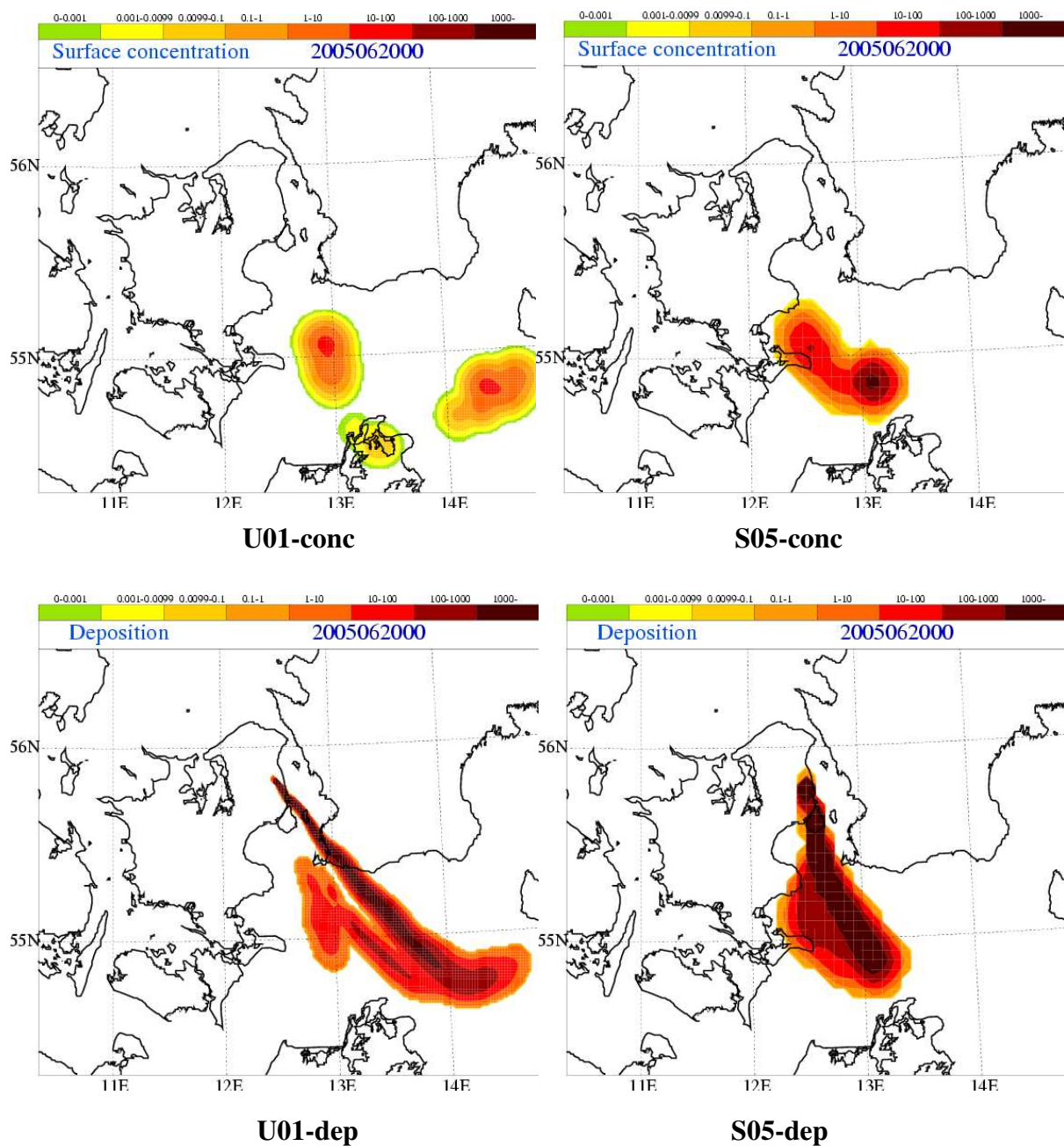


Figure 8.11 Cs-137 air concentration (top) and total deposition (bottom) patterns at 00 UTC, 20 June 2005 for the hypothetical accidental release (with duration of 15 minutes) occurred at the location of Holte on 16 UTC, 19 June 2005. Note, patterns were simulated by the DERMA model on a basis of the DMI-HIRLAM-S05 vs. U01 (urbanized) models (see scale for concentration and deposition in Fig. 8.9)

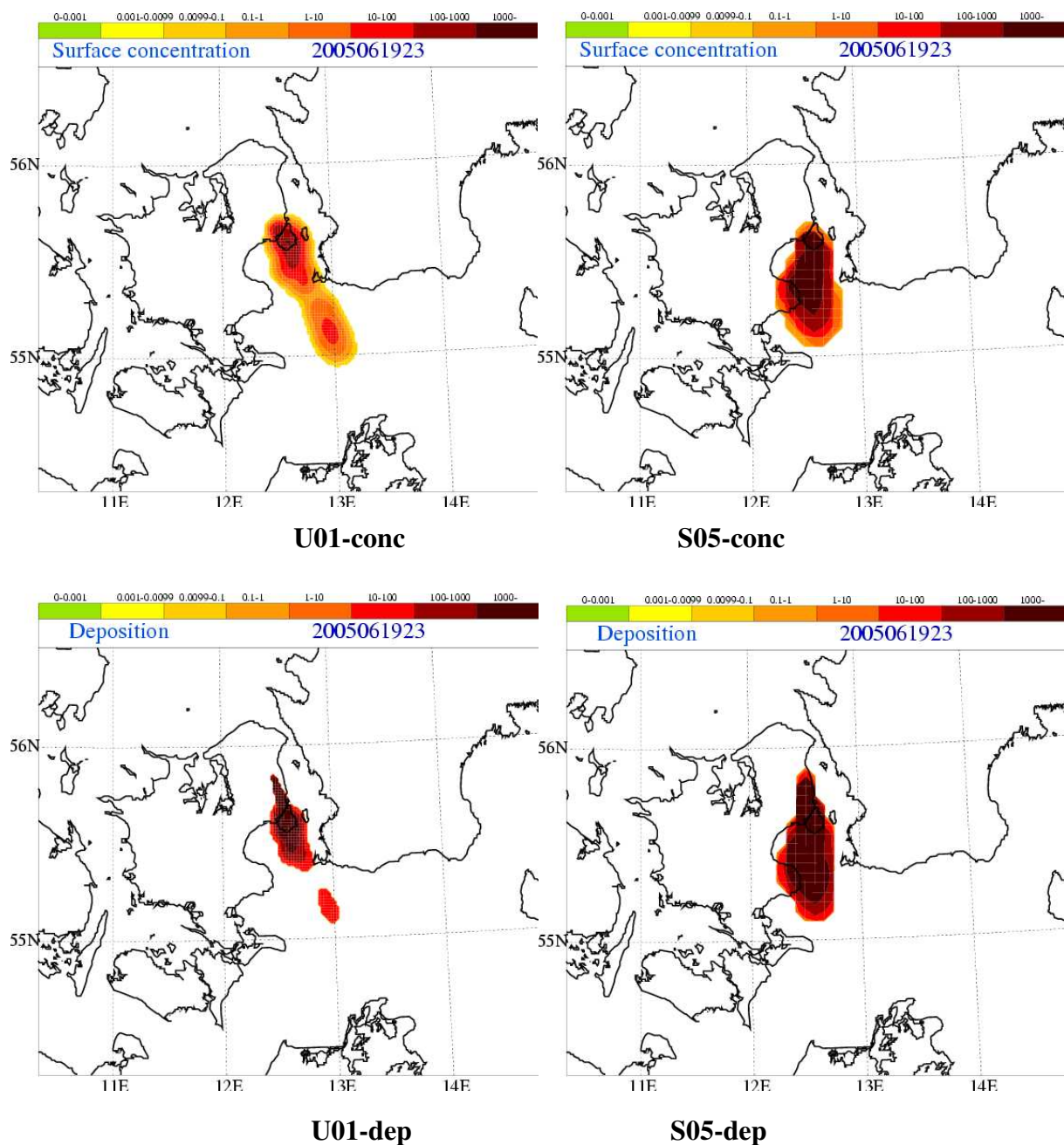


Figure 8.12 Cs-137 air concentration (top) and total deposition (bottom) patterns at 23 UTC, 19 June 2005 for the hypothetical accidental release (with duration of 3 hours) occurred at the location of Holte on 16 UTC, 19 June 2005. Note, patterns were simulated by the DERMA model on a basis of the DMI-HIRLAM-S05 vs. U01 (urbanized) models (see scale for concentration and deposition in Fig. 8.9)

Figure 8.14 shows also the differences in the ABL heights, simulated for all three versions of the DMI-HIRLAM data (urbanised U01, operational S05 and T15) and considered in the above ARGOS simulations. The urban heat island effect, considered in the urbanised version U01, on the ABL height over Copenhagen, Malmö and other Danish and Swedish cities (marked by the arrows) is very visible in Figure 8.14a. The ABL height, which is also the mixing height for the air pollutants, effects considerably on the air concentration and deposition levels of the contaminants.

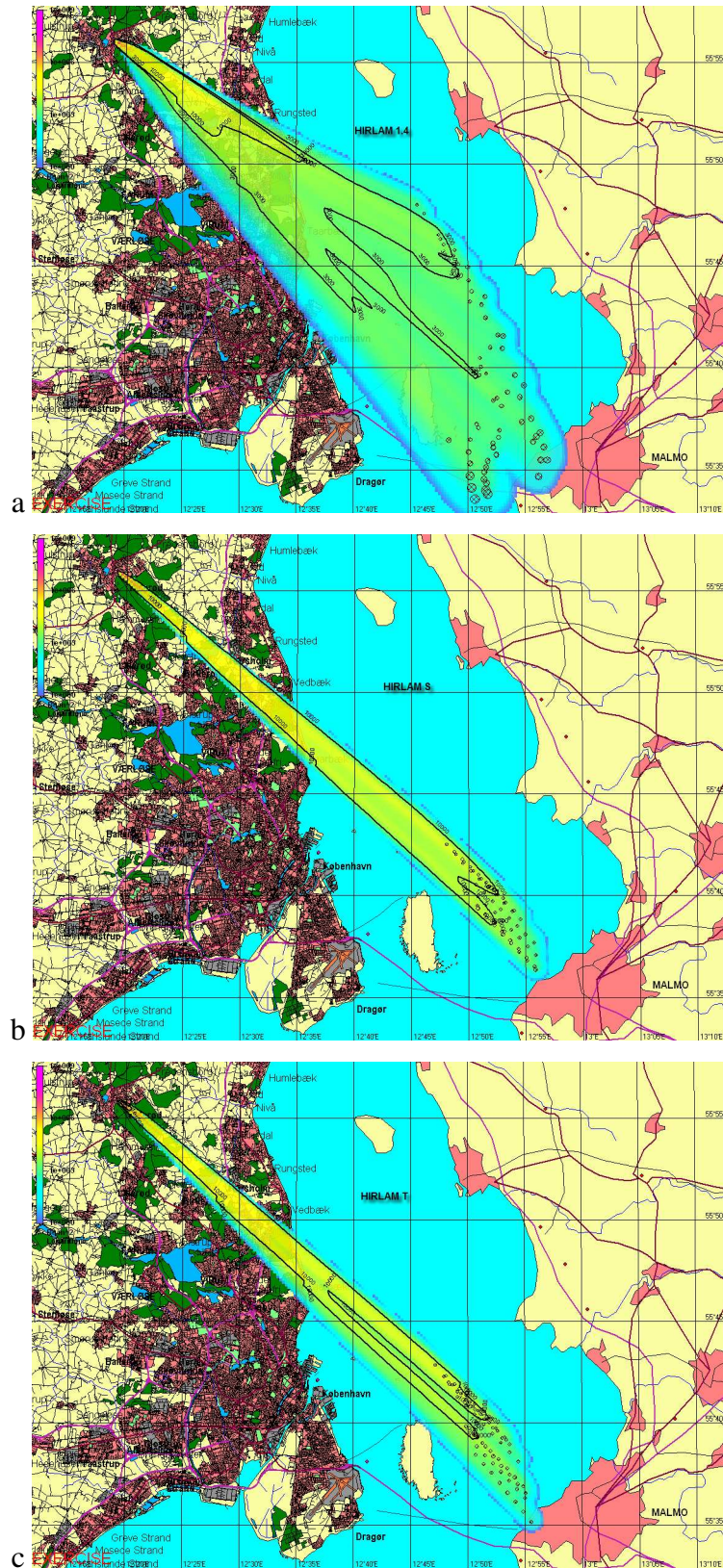


Figure 8.13 A local-scale plume from the ^{137}Cs hypothetical atmospheric release in Hillerød on 00 UTC, 19 June 2005 as calculated by RIMPUFF using DMI-HIRLAM with 1.4-km resolution and visualised by ARGOS for the Copenhagen Metropolitan Area. Cs-137 air concentration for different DMI-HIRLAM data: a) urbanised U01, b) operational D05 and c) operational T15.

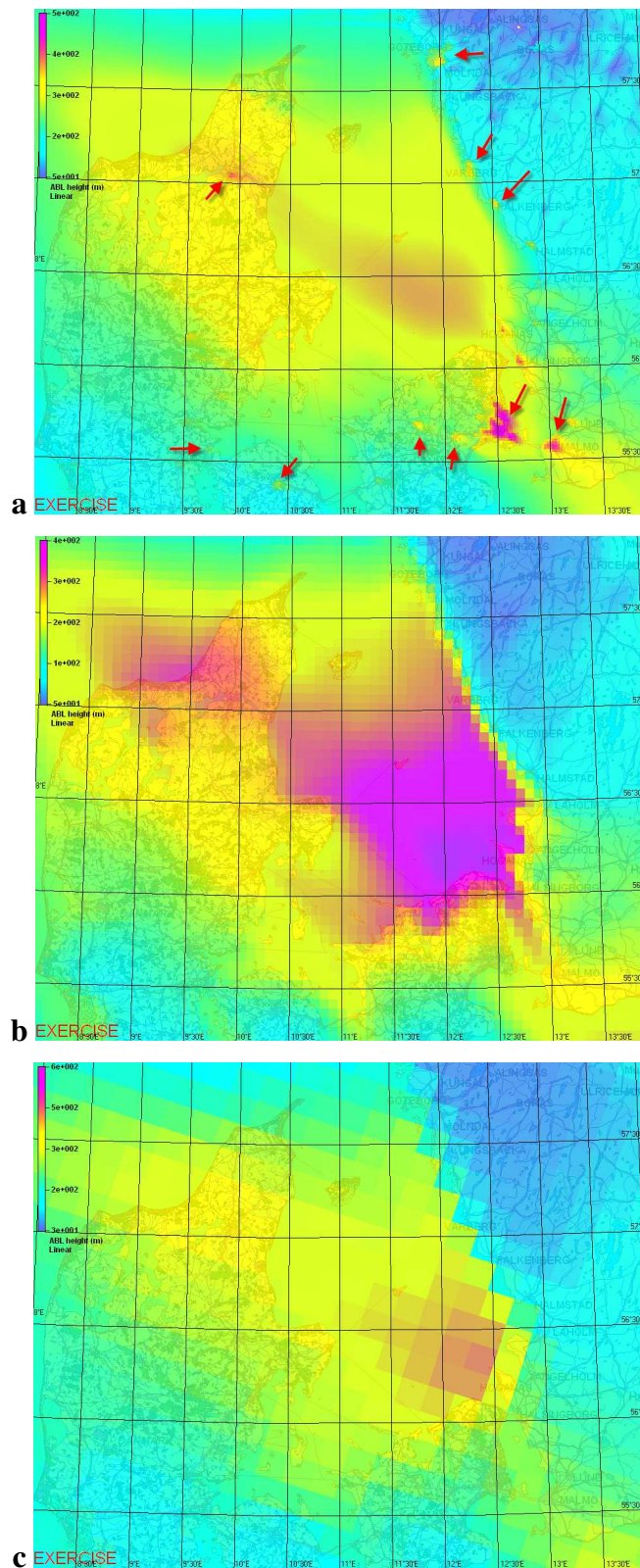


Figure 8.14 The ABL height, calculated from different DMI-HIRLAM data: a) urbanised U01, b) operational D05, c) operational T15 and visualised by ARGOS, for a large part of Denmark. Note, the scale palette is different in b and a, c figures, the arrows in a figure show the main urban areas.

Sensitivity of the meteorological data (operational non-urbanised 5-km S05, 15-km T15 and city-scale 1.4-km urbanised U01) is considerably high: the differences in the dispersion, as it is seen in Figs. 8.9-8.13, led to different level of contamination over the city areas and to different areas, contaminated by the plume.

Finally, the sensitivity of the population exposure (doses) to the urban improvements in the DMI-HIRLAM model, used for the ARGOS simulations, is presented in Table 8.2. As we can see from the table, the doses for populations of different towns and areas of Copenhagen are very different for the non-urbanised operational S05 (lower table) and for urbanised 1.4-km resolution U01 (upper table).

Table 8.2 The population doses, calculated by ARGOS for the considered hypothetical release, for the non-urbanised operational S05 (lower table) and for urbanised 1.4-km resolution U01 (upper table)

U01 1.4 km modified

Community	Collective	Potential	Expected
Lyngby-Taarbæk	4.97	0.00231	0.00224
Søllerød	3.65	0.00274	0.00267
Gentofte	3.51	0.00121	0.00118
Birkerød	2.72	0.003	0.00292
Hørsholm	1.89	0.00186	0.00181
Karlebo	1.29	0.00155	0.00151
Hillerød	1.02	0.000667	0.000648
Tårnby	0.912	0.000512	0.000497
Allerød	0.396	0.000411	0.0004
København Ø	0.00734	2.11e-006	2.05e-006
København S	0.000114	2.5e-008	2.43e-008
København C	7.07e-006	6.29e-009	6.11e-009

S05 5 km non-modified

Community	Collective	Potential	Expected
Hørsholm	10.1	0.0101	0.00978
Birkerød	7.16	0.00797	0.00774
Søllerød	7.82	0.00597	0.0058
Karlebo	1.09	0.00132	0.00128
Lyngby-Taarbæk	0.345	0.000162	0.000157
Allerød	8.43e-015	4.35e-019	3.65e-019

8.5. Evaluation of land surface scheme modifications on atmospheric transport and deposition patterns in Copenhagen metropolitan area.

In this study, which is reported separately (Mahura et al., 2005b), the spatial variability of concentration and deposition fields resulted from hypothetical accidental releases occurred in the metropolitan area of Copenhagen, Denmark was evaluated. Dependence of these on the temporal variability of meteorological variables in the lower surface layer (wind at 10 m and temperature at 2 m fields) for the High Resolution Limited Area Model (HIRLAM) Interaction Soil-Biosphere-Atmosphere (ISBA) land surface scheme as a function of parameters - roughness and anthropogenic heat flux - was estimated.

The DMI-HIRLAM-U01 research model (with a resolution of 1.4 km) was run with modified land use and climate generation files. The meteorological fields' simulations were driven using the DMI-HIRLAM-S05 model (resolution of 5 km) boundary conditions. Several specific dates – (i) low wind conditions, (ii) high precipitation, (iii) high winds, and (iv) typical conditions - were studied in details. The land surface scheme was modified for urban cells represented domain. For each specific date 4 independent runs were performed for: no modifications in scheme (control run), incorporated anthropogenic flux, urban roughness, and both latter combined. Then, the Local Scale Model Chain of ARGOS system, using modelled meteorological fields by DMI-HIRLAM-U01, was employed to simulate the atmospheric transport and deposition of hypothetical accidental releases.

The diurnal cycle of meteorological variables was analyzed comparing (difference fields at each UTC term) outputs from control run with those where changes were made. The differences in concentration and deposition fields resulted from modifications of the land surface scheme were estimated.

The influence of mentioned modifications of the land surface scheme on the DMI-HIRLAM NWP and dispersion model runs is described and summarized by Baklanov et al. (2005a,b,c) and Mahura et al. (2005a,b,c).

9. SUMMARY AND CONCLUSIONS

9.1. Summary horizontal resolution experiments

Sensitivity to horizontal resolution in NWP is investigated in studies of target cities Valencia, Turin, Helsinki, Copenhagen and Oslo with the NWP models RAMS, LM and HIRLAM. In addition the sensitivity to horizontal resolution of the photochemical model CAMx is investigated for Valencia.

Features expected to be better represented with high resolution models are the sea breeze, the orographic upslope/downslope winds and the topographic captured inversion zone.

Simulations of the 26th to 30th of July 1999 with the RAMS model 9 and 4 km give hardly noticeable differences in statistical scores. A number of different scores are computed, and all of them have almost identical values for both resolutions. This is explained by that the high resolution data are present in the coarse resolution runs when nesting is run. The time series of Appendix 1 confirm these results. Simulations with the UAQ model CAMx with 12 and 4 km show a slightly higher night time concentration of O₃ in the coarse resolution runs. It leads to increased overestimation at coastal stations. The O₃ patterns produced by high resolution CAMx runs have more variation than the ones produced with low resolution. This effect is more noticeable near high emissions areas.

Simulations of the episode 19th to 23rd of July 1999 with the RAMS model for Turin show large differences in wind fields and in correlated NO_x concentrations computed with FARM, when comparing runs with 4 km resolution against 1 km resolution. The statistical evaluation for the four meteorological stations and the four urban air quality stations shows that the 4 km runs overestimate the 10m wind speed, on the other hand NO_x levels are underestimated. . Both the positive wind speed bias and the negative NO_x bias are reduced in the 1 km runs. Meteorological and air quality parameters are not measured at the same sites, but in similar urban environment. However inspection of the horizontal wind speed and NO₂ concentration fields confirms that there is a general decrease in wind speed and increase in the NO₂ concentration, and that the patterns of both meteorological and chemical species fields better follow topography and emissions features with increasing resolution for the city area of Turin. The enhancement obtained in comparison of computed and measured NO₂ concentrations confirms that higher resolution in meteorological, physiographic and emission data are critical to obtain a satisfactory forecast of urban air quality episodes in Turin. It should be mentioned that for Turin separate experiments with highest resolution 4 km are run. The effect of increased NWP resolution is therefore significant.

Topographic variations seem to be the key factor in interpretation of sensitivity of trajectories and LPDM concentrations. In Helsinki the trajectories follow the same direction and area covered, probably due to the very small changes of topography with resolution for the flat Finnish coast. In Oslo the concentration distribution simulated with the LPDM on the basis of LM meteorological data is extremely sensible to the horizontal grid resolution. The channelling effect of the orography and the refined meteorological input data which itself depend on the orography (location of stagnation points, vertical velocity).

Trajectory simulations based on the LM runs with increasing horizontal resolution are performed for the cities of Valencia, Oslo and Helsinki. The trajectories for Valencia reflect the improved ability of higher-resolution LM to simulate the observed mesoscale sea breeze and upslope wind circulation patterns determining the characteristic Valencia ozone episodes (in the example shown, recirculation with strong upward motions and fast return to sea). That is the flow pattern suggested from observations. For Oslo the trajectories follow the main mesoscale NW-erly wind direction with increasing channelling due to increased resolution.

The channelling is less pronounced than expected, possibly because the induced stronger vertical motions at 1.1 km resolution combine with vertical wind shear to move the trajectories out of the narrower and steeper valleys of the high-resolution topography.

Further tests are needed, also concerning potential numerical effects (trajectory time step) on the simulations in complex mountain terrain.

The results of increasing the resolution and urbanizing the HIRLAM model for driving the emergency model system DERMA at DMI are

9.2. Summary vertical resolution experiments

Investigations of sensitivity to vertical resolution of NWP comprise simulations with LM - trajectory model/LPDM for Valencia, Oslo and Helsinki and MM5 - AirQUIS for Oslo.

Beforehand it was expected that increased vertical resolution would lead to better representation of the vertical structures in the stable planetary boundary layer.

Difficulties in doing clean vertical resolution studies of real cases are however noticed. The reason is that the emissions have to be localized to one level or another. Thus small changes in definition of the vertical levels might displace emission sources to levels where horizontal wind speed is very different.

The trajectories in 2.8 and 1.1 km were simulated with 35 levels (as with 7 km resolution) and with 45 levels leading only to small effects in the horizontal and vertical spread of the trajectories (Figure 7.1). This is explained with the very small changes of topography with resolution for the flat Finnish coast. Additionally, the episode day is extremely cold and stably stratified above land even during the day for that extreme inversion episode, thus reducing any potential differences.

9.3. Summary forecast length experiments

Comparison of urban air quality forecasts and meteorological forecasts on time range 0-24 hours, 24-48 hours and 48-72 hours all reveal the same feature. The forecasts are not improved by going to shorter forecast lengths. Moreover this is also the case when comparing the quality of the urban near surface meteorology though it is a well known fact that error increases with forecast length in NWP in general. The feature is demonstrated by summary verification of HIRLAM forecasts over Danish coastal and inland stations.

In the Turin case and the Oslo case the forecast quality is independent of forecast length. Also performance statistics for Valencia shows bigger variance due to which day is simulated than to the forecast length, though here there is some improvement for the shorter forecasts. This indicates that it is the meteorological and dispersion conditions themselves that are the most important factor determining the forecast quality: models are designed to solve some processes, other processes are poorly described and model development is needed.

Sensitivity to forecast length on non-observed quantities must eventually be established by analysis of systematic growth of known model errors or particular initialization problems. Initialisation problems seem to be relevant for the Oslo case. The initial conditions for the high resolution model are inherited from a lower resolution model with corresponding lower resolution in topography. Moreover initial data are extracted from the coarse model on pressure surfaces, which by convention have only a few levels in the boundary layer (1000 and 925 hPa).

Trajectory model experiments don't reveal results that are in contradiction to the above mentioned. Due to advanced data assimilation, boundary value relaxation and model-adapted interpolation scheme, spin-up and boundary errors in the LM wind fields and LM trajectories

are small, and the longer-term averaged statistical increase in wind field error with forecast time is small. In the test case, the timely onset of the sea breeze is better captured in the long forecast than the short one for 1.1 km trajectories. In general though, the longer forecast reduces differences between 7 and 1.1 km trajectories and leads to reduced localisation and probably deterioration of the 1.1 km forecast.

9.4. Summary planetary boundary layer parameterization experiments

The role of different planetary boundary layer schemes are investigated in the Oslo case. Schemes of different complexity might have different solutions for surface wind speed, surface temperature and near-surface vertical temperature gradient. However they agree remarkably on the stability and diffusion parameters. They all seem to solve their task satisfactory on a general basis.

One should also be aware that transport of heat and moisture is accomplished through the basic equations of the model as well. The grid scale advection seems to count for a part of the problem with too effective transport of heat and momentum downwards into the cold pool in the Oslo case investigated.

9.5. Summary surface data and land surface parameterization experiments

Influences of urbanisation of external parameters and addition of an anthropogenic heat source are limited to the near-surface trajectories and only on a short time scale. The reasons for this small effect on the trajectories are as follows: A direct influence of the above urbanisation measures in LM is found on many parameters (energy balance (radiation, sensible and latent heat fluxes), turbulence, T2m etc., also streamlines). Trajectories depend directly only on the grid-scale wind speeds (streamlines) and thus show a reduced effect compared to more complex models. Additionally, the trajectories start in the middle of town and experience the modified influence only for a very short time span of minutes/1h before leaving the city area. Also there are too few trajectories to capture all wind changes due to urbanisation above the city.

The LPDM uses mainly the 3D wind vector and the turbulent kinetic energy of the LM output. In the meteorological context, LM temperature and surface flux values show the largest impact due to the urbanisation measures while the above major LPDM input values are less affected. Nevertheless, there are indications that the vertical turbulence increases and the stability weakens with urbanisation and anthropogenic heat source. Introducing urbanised external parameters increases mainly the dynamical part of the turbulence via increased roughness length (dispersion of the particles more or less uniform in every direction), while the additional anthropogenic heat flux mainly affects the thermal part of the turbulence (dispersion of the particles increasingly in vertical direction).

Urbanisation of HIRLAM by increased albedo and roughness, and release of anthropogenic heat in urban grid cells has a significant impact on atmospheric concentration levels and ground deposition in the DERMA and ARGOS emergency warning systems. The increase in roughness in urban areas increases the turbulence and decreases the wind speed. The release of anthropogenic heat increases the evening and night time temperature while the increase in albedo reduces the day time temperature.

9.6. Conclusions

Increasing the horizontal resolution of the NWP model leads to sharper gradients and more extreme values in wind speed in particular. This brings the NWP forecasts closer to the scale of the UAP fields and gives an improved possibility of modelling the extreme events. However in complex terrain the increased horizontal resolution also increases the vertical

velocity along the terrain following model layers. This is a process that might lead to break up of inversions thus deteriorating the UAP forecasts. The process is not fully explained by the present work and is recommended a further study.

There is a significant tendency of deteriorating synoptic scale forecasts with forecast length in NWP in general. This will not necessarily be visible in the NWP forecasts on meso-scale. On meso-scale there are several contributions to forecasts error from e.g. insufficient parameterization of urban scale processes, resolution of surface data and urban boundary layer meteorology. This contribution might be large enough to override the error on synoptic scale. In addition UAP episodes are most frequent in situations with weak winds and little dynamic activity in general. The model's ability to describe the urban meteorology in a stationary situation will determine the error level. Short forecast lengths might suffer from spin-up problems, but this is in NWP contest a problem limited to the first 6 hours, while it might be longer for UAP models.

Introduction of urbanized external parameters and anthropogenic heat source reduces vertical stability through increased dynamical turbulence and thermal turbulence respectively. Parameterization of an anthropogenic heat source is mainly influencing the temperature fields at night time.

Chose of planetary boundary layer parameterizations are shown to have only limited impact on error level in strong inversion situations. The schemes that are tested all identify the stability regime satisfactory and estimate that vertical exchange of heat of momentum is small. This is realistic when seen in relation to the physics of these cases.

Based on the results reported here we recommend that further studies are initiated in the following fields:

- *Vertical resolution.*

The impact of increased vertical resolution need to be studied in a frame where the sensitivity on the meteorological prognosis can be separated from the contribution from altered vertical resolution of the UAQ model. Air quality models will typically be sensitive to emission levels, and these should be kept constant during the sensitivity analysis.

- *Horizontal resolution*

It is identified that there is an influence of horizontal resolution on vertical velocity through increased horizontal gradients of topography height. The vertical component of the flow along model surfaces increases. Moreover high vertical velocities are assumed to break up inversions and cold air basins. The development of vertical velocity in a non-hydrostatic vertical coordinate and steep topography needs a closer investigation.

- *Parameterizations of the planetary boundary layer*

In unstable situations the turbulent exchange of heat and momentum must be quantified by the PBL parameterization. Forecasts of wind, temperature and humidity on urban scale are shown to have errors which have small sensitive to forecast length. The reason might be that near surface meteorological conditions on local scale to some (not quantified) extent depend on the local exchange of heat and momentum.

- *Introduction of urban land surface description*

Urban land surface differ from rural surfaces in e.g. water storage capacity, conductivity, radiative properties and roughness. The effect of introducing an urban surface should be investigated on different meteorological conditions, also low latitudes and summer season.

Effects on AQ models which rely on temperature and fluxes from the meteorological input should be investigated.

- *Introduction of an anthropogenic heat source*

The anthropogenic heat is differently distributed depending on latitude and time of day and year. The anthropogenic heat sources are leakage from buildings in winter time on high latitudes and transport of heat from buildings to the urban atmosphere in summer time on lower latitudes. Further studies which take these differences into account are needed to quantify the importance of this parameter for forecasting temperature and daily temperature amplitude.

- *Representativity of observations*

A good observational description of what we attempt to describe with the models. Both meteorological and urban air quality observation network is too coarse in most of the target cities. Moreover it is difficult to separate the contribution from the NWP models and the UAQ models to the forecast quality as meteorology and air quality only exceptionally are monitored at the same locations.

ACKNOWLEDGEMENT

This report is part of work package 6 of the FUMAPEX project, which has been funded by the European Commission under the FP5 EESD programme Key Action City of Tomorrow.

REFERENCES

- Amstrup B. (2004): Validated meteorological input data provided by the larger scale models for the small scale models. *D10.5 FUMAPEX Deliverable* (DMI HIRLAM dataset). Danish Meteorological Institute, April 2004, Copenhagen, Denmark.
- Baklanov, A. and P. Mestayer (editors), (2004): Improved parameterisations of urban atmospheric sublayer and urban physiographic data classification. / A. Baklanov, E. Batchvarova, I. Calmet, A. Clappier, J.V. Chordá, J.J. Diéguez, S. Dupont, B. Fay, E. Fragkou, R. Hamdi, N. Kitwiroon, S. Leroyer, N. Long, A. Mahura, P. Mestayer, N.W. Nielsen, J.L. Palau, G. Pérez-Landa, T. Penelon, M. Rantamäki, G. Schayes and R.S. Sokhi. D4.1, 4.2 and 4.5 FUMAPEX Report, April 2004, Copenhagen, DMI, Denmark. DMI Scientific Report: #04-05, ISBN nr. 87-7478-506-0.
- Baklanov, A., A. Rasmussen, B. Fay, E. Bergen and S. Finardi (2002): Potential and shortcomings of Numerical Weather Prediction models in providing meteorological data for urban air pollution forecasting. *Water, Air, & Soil Pollution: Focus* Vol. 2, no. 5-6, 43-60.
- Baklanov A., Mahura A., Petersen C., Sattler K., N.W. Nielsen (2005a): Effects of Urbanized Areas for NWP-DMI-HIRLAM High Resolution Model Operational Runs. Manuscript submitted to *Journal of Applied Meteorology*, 10 p.
- Baklanov, A., J.H. Sørensen, S.C. Hoe and B. Amstrup (2005b): Urban meteorological modelling for nuclear emergency preparedness. *Journ. Envir. Radioactivity* (in press).
- Baklanov, A., Mestayer, P., Clappier, A., Zilitinkevich, S., Joffre, S., Mahura, A. (2005c) On the parameterisation of the urban atmospheric sublayer in meteorological models. *Atmospheric Chemistry and Physics* (submitted)
- Beljaars, A.C.M. and P. Viterbo (1998): Role of the boundary layer in a Numerical Weather Prediction Model. *In* *Clear and Cloudy Boundary Layers*, 286-304, Ed: A.A.M. Holtslag and P.G. Nuykerke, Royal Netherlands Academy of Arts and Sciences, P.O. Boz 19121, 10000 GC Amsterdam, The Netherlands, ISBN 90-6984-235-1.
- Best, M. and R. Betts (2004): The impact of climate change on our cities. The 84th AMS Annual Meeting, Joint Session 5 Climate Change and Urban Areas, Seattle, WA, 15 Jan 2004.
- Blackadar, A.K. (1976): Modelling the nocturnal boundary layer. *In* *Proceedings of the Third symposium on atmospheric turbulence, diffusion and air quality*. Boston, MA. 46-49, American Meteorological Society.
- Blackadar, A.K. (1979): Modelling pollutant transfer during daytime convection. *In* *Proceedings of the Fourth symposium on atmospheric turbulence, diffusion and air quality*. Reno NV, 443-447, American Meteorological Society.
- Bott, A. (1989): A Positive Definite Advection Scheme Obtained by Nonlinear Renormalization of the Advective Fluxes. *Mon. Wea. Rev.*, **117**, 1006-1015.
- Calori G., M. Clemente, R. De Maria, S. Finardi, F. Lollobrigida and G. Tinarelli (2005): Air quality integrated modelling in Turin urban area. *Environmental Modelling and Software*, in press.
- Calori G. and C. Silibello (2004): FARM (Flexible Air quality Regional Model) Model formulation and user manual. ARIANET Report, Milan, Italy, 59 pp.

- Cotton W.R., R.A. Pielke, R.L. Walko, G. E. Liston, C.J. Tremback, H. Jiang, R. L. McAnelly, J. Y. Harrington, M.E. Nicholls, G. G. Carrio, and J. P. McFadden (2003): RAMS 2001: Current status and future directions, *Meteorol. Atmos. Phys.* **82**, 5-29.
- Doms, G. and U. Schättler (2002): A description of the nonhydrostatic regional model LM Part I: Dynamics and numerics. COSMO and DWD, 134pp.
- Dupont, S., I. Calmet, P. G. Mestayer, and S. Leroyer (2005a): Parameterisation of the Urban Energy Budget with the SM2-U Model For The Urban Boundary Layer Simulation. *Bound.-Layer Meteorol.*, submitted
- Dupont, S., Mestayer, P. G., Guilloteau, E., Berthier, and H. Andrieu (2005b): Parameterisation of the Urban Water Budget with the Sub-Meso Soil Model, *J. Appl. Meteorol.*, submitted
- EMEP (2004): EMEP Status Report 1/04 - Transboundary acidification, eutrofication and ground level ozone in Europe, Joint MSC-W & CCC & CIAM & ICP-M&M CCE Report, August 2004, Available from www.emep.int/common_publications.html.
- Environ (2003): User's guide. Comprehensive Air Quality Model with Extensions (CAMx) Version 4.00 ENVIRON International Corporation 101 Rowland Way, Suite 220 Novato, California 94945-5010. (www.environcorp.com)
- Fay, B., L. Neunhäuserer, J. L. Palau, G. Pérez-Landa, J. Dieguez, V. Ødegaard, N. Bjergene, M. Sofiev, M. Rantamäki, I. Valkama, J. Kukkonen, A. Rasmussen, A. Baklanov (2004): Model simulations and preliminary analysis for three air pollution episodes in Helsinki. Deliverable 3.3 of the EC FUMAPEX project, Offenbach, Germany, 60pp.
- Fay, B., L. Neunhäuserer (2004a): Evaluation of high resolution simulations with the Lokalmodell of the German Weather Service for urban air pollution episodes in Helsinki and Oslo in the FUMAPEX project, 4th Annual Meeting of the European Met. Society, Nice, France, September 2004.
- Fay, B., L. Neunhäuserer (2004b): Analysis and inter-comparison of operational meteorological simulations for all target cities, D3.4 of the EC FUMAPEX project.
- Fay, B., L. Neunhäuserer, G. Bonafé, S. Jongen (2005): Analysis and inter-comparison of operational meteorological simulations for all target cities. Deliverable 3.4 of the EC FUMAPEX project, Offenbach, Germany, 80pp.
- Finardi S. (Editor), A. Baklanov, E. Batchvarova, A. Clappier, B. Fay, S. Joffre, A. Karppinen, N. Kitwiroon, L. H. Slordal, R. S. Sokhi, and A. Stein (2004): Guidelines for the construction of the interfaces from operational NWP models to different types of UAP models. Deliverable 5.1 of the EC FUMAPEX project, Milan, Italy, 47 pp
- Finardi S. (Editor), A. Baklanov, A. Clappier, B. Fay, S. Joffre, A. Karppinen, V. Ødegaard, L. H. Slordal, M. Sofiev, R. S. Sokhi, and A. Stein (2005): Improved interfaces and meteorological pre-processors for urban air pollution models. Deliverable 5.2-3 of the EC FUMAPEX project, Milan, Italy.
- Glaab, H., B. Fay, I. Jacobsen (1998): Evaluation of the emergency dispersion model at the Deutscher Wetterdienst using ETEX data. *Atmospheric Environment*, Vol. 32, No. 24, pp. 4359-4366.
- Grell, G., J. Dudhia and D. Stauffer (1994): A Description of the Fifth-Generation PENN STATE/NCAR Mesoscale Model (MM5). NCAR Technical Note, NCAR/TN-398+STR, National Center for Atmospheric Research, Boulder, Colorado, 138 pp.

- Helfand, H.M. and J.C.Labraga (1988): Design of a Nonsingular Level 2.5 Second-Order Closure Model for the Prediction of Atmospheric Turbulence. *Journal of the Atmospheric Sciences* **45**, No. 2, 113-132.
- Hoe, S., Sørensen, J.H. and Thykier-Nielsen, S. (1999): The Nuclear Decision Support System ARGOS NT and Early Warning Systems in Some Countries around the Baltic Sea. In: *Proceedings of the 7th Topical Meeting on Emergency Preparedness and Response*, September 14–17, 1999, Santa Fe, New Mexico, USA.
- Hoe, S., Müller, H., Gering, F., Thykier-Nielsen, S. and Sørensen, J.H. (2002): ARGOS 2001 a Decision Support System for Nuclear Emergencies. In: *Proceedings of the Radiation Protection and Shielding Division Topical Meeting*, April 14–17, 2002, Santa Fe, New Mexico, USA.
- Hong, S.-Y. and H.-L. Pan (1996): Non-local boundary layer vertical diffusion in a Medium-Range Forecast Model. *Monthly Weather Review* **124**, 1215-1238.
- Kinouchi, T. and J. Yoshitani (2001): Simulation of the urban heat island in Tokyo with future possible increases of anthropogenic heat, vegetation cover and water surface. *Proceedings of 2001 International Symposium on Environmental Hydraulics*, 6pp
- Kottmeier, C. and Fay, B. (1998): Trajectories in the Antarctic lower troposphere. *Jour. Geophys. Res.* **103**, D9, 10947-10959.
- Louis, J.F., M. Tiedtke and J.F. Geleyn (1982): A short history of the operational PBL-parameterization at ECMWF, Workshop on boundary layer parameterization, November 1981, ECMWF, Reading, England.
- Mahura, A., K. Sattler, C. Petersen, B. Amstrup and A. Baklanov (2005a): DMI-HIRLAM Modelling with High Resolution Setup and Simulations for Areas of Denmark. DMI Technical Report **05-12**.
- Mahura A., A. Baklanov, S. Hoe, J.H. Sorensen, C. Petersen and K. Sattler (2005b): Evaluation of Land Surface Scheme Modifications on Atmospheric Transport and Deposition Patterns in Copenhagen Metropolitan Area. *Abstract submitted to 28th NATO/CCMS International Technical Meeting on Air Pollution Modelling and Its Applications*, 15-19 May 2006, Leipzig, Germany.
- Mahura A., Baklanov A., Petersen C., Sattler K., B. Amstrup (2005c) ISBA Scheme Performance in High Resolution Modelling for Low Winds Conditions. Manuscript for HIRLAM Newsletters, 5 p.
- Martilli, A., Clappier, A., and Rotach, M. W. (2002) An Urban Surface Exchange Parameterisation for Mesoscale Models, *Boundary-Layer Meteorol.* **104**, pp 261–304.
- Martín F., M. Palacios, H. Cabal, M. Gómez, J. Domínguez, I. Sánchez, M.J. Salazar and R. Salvador (1998): Anthropogenic emission inventory around the city of Burriana (Valencia). Final Report CIEMAT no 11320-96-11-F1PE-ISP.
- Mellor G.L. and T.Yamada (1982): Development of a Turbulence Closure Model for Geophysical Fluid Problems. *Rev. Geophys. Space Phys.* **20**, 851-875.
- Mikkelsen, T., S. Thykier-Nielsen, P. Astrup, J. M. Santabárbara, J.H. Sørensen, A. Rasmussen, L. Robertson, A. Ullerstig, S. Deme, R. Martens, J. G. Bartzis and J. Päsler-Sauer (1997) MET-RODOS: A Comprehensive Atmospheric Dispersion Module. *Radiat. Prot. Dosim.* **73**, 45–56

- Millán, M.M., R.Salvador, E.Mantilla and G.Kallos (1997): Photooxidant dynamics in the Mediterranean basin in summer: Results from European research projects. *Journal of Geophysical Research* **102**, D7, 8811-8823.
- Millán, M.M., E.Mantilla, R.Salvador, A.Carratala, M.J.Sanz, L.Alonso, G.Gangoiti and M. Navazo (2000): Ozone Cycles in the Western Mediterranean Basin: Interpretation of Monitoring Data in Complex Coastal Terrain. *Journal of Applied Meteorology* Vol. **39**, 487-508.
- Navascués B., Rodríguez E., J.J. Ayuso and S.Järvenoja (2003): Analysis of surface variables and parameterization of surface processes in HIRLAM. Part II: Seasonal assimilation experiment. Norrköping. HIRLAM Technical Report **59**, 38 p.
- Neunhäuserer, L., B. Fay, A. Baklanov, N. Bjergene, J. Kukkonen, V. Ødegaard, J.L. Palau, G. Pérez Landa, M. Rantamäki, A. Rasmussen and I. Valkama (2004): Evaluation and comparison of operational NWP and mesoscale meteorological models for forecasting urban air pollution episodes - Helsinki case study. Extended abstract of 9th Int. Conf. on Harmonisation within Atmospheric Dispersion Modelling for Regulatory Purposes, June 2003, Garmisch-Partenkirchen, Germany, 5pp.
- Neunhäuserer, L. and B. Fay (2005a): Evaluation and inter-comparison of very high resolution results of different European NWP models within the FUMAPEX project. Seminar of the LM-User Group, March 2005, Langen, Germany.
- Neunhäuserer, L. and B. Fay (2005b): Towards predicting urban air pollution episodes: Introduction of urbanised parameters into the mesoscale Lokalmmodell (LM) of the German Weather Service. Shortpaper of 5th International Conference on Urban Air Quality, March 2005, Valencia, Spain, 4pp.
- Nielsen, N.W. and B. Amstrup (2005): DMI-HIRLAM Verification / Benchmarking Report for the fourth quarter of 2004. Internal report **05-03**. DMI, Copenhagen, Denmark.
- Pielke R.A., W.R.Cotton, R.L.Walko, C.J.Tremback, W.A.Lyons, L.D.Grasso, M.E. Nicholls, M.D.Moran, D.A.Wesley, T.J.Lee and J.H.Copeland (1992): A Comprehensive Meteorological Modeling System - RAMS, *Meteorol. Atmos. Phys.* **49**, 69-91.
- Rodríguez E., B. Navascués, J.J. Ayuso and S. Järvenoja (2003): Analysis of surface variables and parameterization of surface processes in HIRLAM. Part I: Approach and verification by parallel runs. Norrköping. HIRLAM Technical Report **58**, 52 pp.
- Shafran, P.C., N.L.Seaman and G.A.Gayno (2000): Evaluation of numerical predictions of boundary-layer structure during the Lake Michigan Study (LMOS). *Journal of Applied Meteorology* **39**, 412-426.
- Slördal L.H. (editor) (2003): FUMAPEX Guidelines of output from UAQIFSs as specified by end-users. FUMAPEX D8.1 report, NILU Report OR **2/2004**, Ref: U-102144, 81pp.
- Sokhi, R.S., N. Kitwiroon and L. Luhana (2003): FUMAPEX Datasets of Urban Air Pollution Models and Meteorological Pre-processors. Deliverable 2.1-2.2 of the EC FUMAPEX project, Atmospheric Science Research Group (ASRG), Science and Technology Research Centre, University of Hertfordshire, Hatfield, UK, 41pp.
- Sorteberg, A. (2001): The sensitivity of inversion strength to the formulation of the non-dimensional momentum and heat profiles. Research Report no. **117**, Norwegian Meteorological Institute, Oslo, Norway. 61pp.
- Sørensen, J.H. (1998) Sensitivity of the DERMA Long-Range Dispersion Model to Meteorological Input and Diffusion Parameters. *Atmos. Environ.* **32**, 4195-4206

Undén, P. (ed.) (2002): HIRLAM-5 Scientific Documentation. Technical report, HIRLAM, available from SMHI, S-601 76 Norrköping, SWEDEN, 132 pp. + 11 pp. appendix

Valkama, I. and J.Kukkonen (2003): Identification and classification of air pollution episodes in terms of pollutants, concentration levels and meteorological conditions. FUMAPEX report D1.2, Finnish Meteorological Institute, Helsinki, Finland, 30pp.

Zang, D.-L. and R.A. Anthes (1982): A high resolution model of the planetary boundary layer - sensitivity tests and comparisons with SESAME-79 data. *Journal of Applied Meteorology*, **21**, 1594-1609

Zilitinkevich, S., A. Baklanov, (2005): An analytical model of the mean-wind and the momentum flux profiles in the urban roughness layer. To be submitted to *Boundary-Layer Meteorol.*